CHARACTERIZATION OF VPA0450, A TYPE III SECRETED EFFECTOR PROTEIN FROM *VIBRIO PARAHAEMOLYTICUS*

APPROVED BY SUPERVISORY COMMITTEE

_____
Kim Orth, Ph.D.

_____
Nicholas Conrad, Ph.D.

_____
Lora Hooper, Ph.D.

_____
Vanessa Sperandio, Ph.D.

CHARACTERIZATION OF VPA0450, A TYPE III SECRETED EFFECTOR PROTEIN FROM *VIBRIO PARAHAEMOLYTICUS*

by

CHRISTOPHER ALLEN BROBERG

DISSERTATION

Presented to the Faculty of the Graduate School of Biomedical Sciences

The University of Texas Southwestern Medical Center at Dallas

In Partial Fulfillment of the Requirements

For the Degree of

DOCTOR OF PHILOSOPHY

The University of Texas Southwestern Medical Center at Dallas

Dallas, Texas

February, 2011

ACKNOWLEDGEMENTS

This work would not be possible without the help and support of many people. First, I would like to thank my mentor, Kim Orth, for her guidance over the past three years. Kim has a passion and drive for scientific discovery that is worth emulating. Her direction and constructive criticism have taught me how to scientifically approach a problem, properly control my experiments, interpret my data, and devise the proper next experiment. I owe much of my scientific ability to her teachings. I owe thanks to my committee members, Nicholas Conrad, Lora Hooper, and Vanessa Sperandio. We only officially met twice, but their suggestions related to this project, as well as information learned through coursework, helped to quickly move this work forward. I will always be indebted to all the members of the Orth lab for making this experience so much fun. One couldn't find a better group of people to work with. In particular, I would like to thank Melanie Yarbrough for her wisdom and sense of humor during our time sharing a bay; and Michelle Laskowski-Arce for making me feel at home when I first came to the lab, and for starting what turned out to be a great project.

My family is owed many thanks for their support through this entire process. My father Richard Broberg is the reason I first became interested in science. My fondest childhood memories often involve some form of physics or chemistry experimentation, ranging from launching model rockets to extracting natural dies to color Easter eggs. My mother, Gretchen Broberg, has always been

there for me, keeping me connected with the rest of the family when I get too busy to remember to call home. My brothers and sister, Kevin Broberg, Rich Broberg, and Lindy Donsker, have kept me grounded and provided me with much needed comic relief. Their support has been instrumental in my success as a researcher.

Most importantly, I want to thank my wife, Heather Haley, for all she has done. She has been with me through two graduate degrees, a move halfway across the country, and endless late nights and early mornings. Her encouragement to always be the best I can has pushed me to succeed. I couldn't have done it without you.

CHARACTERIZATION OF VPA0450, A TYPE III SECRETED EFFECTOR PROTEIN FROM *VIBRIO PARAHAEMOLYTICUS*

CHRISTOPHER ALLEN BROBERG

The University of Texas Southwestern Medical Center at Dallas, 2011

Supervising Professor: KIM ORTH, Ph.D.

Vibrio parahaemolyticus is a Gram-negative, halophilic bacterium first isolated over 60 years ago after a major outbreak of food poisoning in Japan. It is now recognized as a significant cause of gastroenteritis associated with the consumption of raw or undercooked seafood. The recent emergence of pandemic strains has made the study of *V. parahaemolyticus* a priority in the field of bacterial pathogenesis.

Virulence caused by *V. parahaemolyticus* has traditionally been attributed to the presence of one or more thermostable direct hemolysins. Genome

sequencing of *V. parahaemolyticus* identified two distinct Type III Secretion Systems (T3SS). T3SS1, on chromosome 1, was shown to translocate four effectors, VopQ, VopR, VopS, and VPA0450, resulting in cytotoxicity of cultured host cells. VopQ has been shown to rapidly induce autophagy upon translocation into a host cell. VopS AMPylates Rho-family guanosine triphosphatases leading to the collapse of the actin cytoskeleton and host cell rounding prior to lysis.

Herein we show that VPA0450 is a phosphatidylinositol phosphatase with homology to the inositol polyphosphate 5-phosphatase catalytic domain of the eukaryotic enzyme synaptojanin. VPA0450 was sufficient to induce membrane blebbing and the delocalization actin-binding proteins from the plasma membrane. VPA0450 contributes to cytotoxicity as strains deleted for *vpa0450* induced cell lysis less efficiently than wild-type strains. VPA0450 compromised membrane integrity by hydrolyzing the D5 phosphate from phosphotidylinositide (4,5) bisphosphate, thereby disrupting adaptor protein binding sites required for proper membrane and cytoskeleton dynamics, likely contributing to cell death by facilitating lysis. Preliminary studies have shown the C-terminus of VPA0450 is necessary for localization of this effector to the plasma membrane, possibly by binding membranes and phosphoinositides.

An improved system was developed for making chromosomal gene deletions in *V. parahemaolyticus*. New parent strains were created in which the positive regulators of each T3SS were deleted. Additional strains demonstrated

that the cytotoxicity seen during infection with T3SS1 positive strains is attributed solely to T3SS1 effectors. Infection with a strain deleted for *vopQ*, *vopS* and *vpa0450* uncovered the phenotype for VopR. Bioinformatic analysis of VopR identified effector homologs in other pathogens, homologous eukaryotic enzymes, and a catalytic triad.

TABLE OF CONTENTS

ACKNOWLEDGEMENTS IV
PREFACE VI
LIST OF PUBLICATIONS XII
LIST OF FIGURES XIII
LIST OF TABLES XV
LIST OF ABBREVIATIONS XVI

CHAPTER 1 1
LITERATURE REVIEW 1
The discovery of *Vibrio parahaemolyticus* 1
Description of *V. parahaemolyticus* 2
Emergence of Pandemic Strains 6
Diseases caused by *V. parahaemolyticus* 7
Virulence factors associated with V. parahaemolyticus 9
Swimming and swarming *11*
Thermostable Direct Hemolysins *12*
The Type III Secretion Systems of V. parahaemolyticus *15*
T3SS1 ..... *19*
Vp-PAI and T3SS2 ..... *26*
Model systems to study V. parahaemolyticus pathogenicity 29
Phosphoinositides and membrane stability 30
Membrane dynamics and blebbing in eukaryotic cells 32

CHAPTER 2 35
MATERIALS AND METHODS 35
Bacterial strains and culture conditions 35
Yeast growth conditions 35
Mammalian Cell lines and culture conditions 36
Cloning of effectors and other genes 36
Deletion of VPA0450 in POR3 strain using Lambda Red Recombinase 38
Deletion of chromosomal genes using the pDM4 suicide vector 39
Sodium dodecyl sulfate polyacrylamide gel electrophoresis (SDS-PAGE) 40
Western Blotting 40
Induction of T3SS1 and T3SS2 41
Infection of HeLa cells 41
LDH release assay 42
Transfection of tissue culture cells 42
Preparation of slides for confocal microscopy 43
Immunocytochemistry of slides 44

Confocal microscopy 44
Quantitation of blebbing or localization of GFP-tagged domains in Hela cells 45
Bioinformatic analysis 45
Purification of recombinant proteins 45
Detection of inositol polyphosphate 5-phosphatase activity using a Malachite Green microtiter-plate assay 46

CHAPTER 3 57
VIBRIO VPA0450 IS AN INOSITOL POLYPHOSPHATE 5-PHOSPHATASE 57
THAT ACCELERATES HOST CELL LYSIS 57
Introduction 57
Results 59
VPA0450 is necessary for rapid host cell lysis and is sufficient to induce host cell membrane blebbing 59
Identification of homologous bacterial effectors and a eukaryotic domain 66
VPA0450 shares catalytic and substrate coordinating residues with SPSynj IPP5C 71
The phosphatase activity of VPA0450 disrupts the interaction between the plasma membrane and the actin cytoskeleton 75
Discussion 80

CHAPTER 4 85
A NOVEL LOCALIZATION DOMAIN DIRECTS VPA0450 85
TO THE PLASMA MEMBRANE 85
Introduction 85
Results 87
VPA0450 localizes to the plasma membrane 87
Sufficiency of C-terminus to localize VPA0450 to the plasma membrane 92
Discussion 97

CHAPTER 5 99
STUDYING THE CONCERTED ACTION OF MULTIPLE T3SS EFFECTORS 99
Introduction 99
Results 101
Generation of new parent strains 101
Confirmation of VPA0450 and VopQ-induced cytotoxicity in the CAB3 strain 108
Determination of the presence of non-T3SS1 virulence factors in CAB3111
Discussion 114

CHAPTER 6 117
INITIAL CHARACTERIZATION OF VOPR, A HOPX HOMOLOG 117

Introduction 117
Results 118
Discovery of the phenotype associated with VopR 118
Identification of homologs and a VopR catalytic triad 121
Discussion 126

CHAPTER 7 129
DISCUSSION AND FUTURE DIRECTIONS 129
Introduction 129
Characterizing the multifaceted progression of T3SS1-mediated host cell death 131
Improved methods for studying T3SS effector interplay 136
Future work 137
Identify minimum domain necessary and sufficient for proper VPA0450 localization 137
Proper localization and VPA0450 activity 139
Interaction between effectors during infection 141
Identification of target and mechanism of action for VopR 142

BIBLIOGRAPHY 144

LIST OF PUBLICATIONS

Woolery AR, Luong P, **Broberg CA**, and Orth K. (2010) AMPylation: Something old is new again. *Frontiers in Cellular and Infection MicrobiologyI,* 1 (article 113). Review

Broberg CA, Zhang LL, Gonzalez H, Laskowski-Arce M, and Orth K. (2010) A *Vibrio* effector protein is an inositol phosphatase and disrupts host cell membrane integrity. *Science*, 329(5999): 1660-62. Published online 19 August 2010; 10.1126/science.1192850

Broberg CA and Clark DD. (2010) Shotgun proteomics of *Xanthobacter autotrophicus* Py2 reveals proteins specific to growth on propylene. *Arch Microbiol,* 192(11):945-57. Published online 16 Sept 2010; 10.1007/s00203-010-0623-3.

Broberg CA and Orth K. (2010) Tipping the balance with post-translational modifications. *Curr Op Microbiol,* 13(1): 34-40. Review.

Jung CM, **Broberg C**, Giuliani J, Kirk LL, and Hanne LF. (2002) Characterization of JP-7 jet fuel degradation by the bacterium *Nocardioides luteus* strain BAFB. *J Basic Microbiol*, 42(2): 127-31.

LIST OF FIGURES

FIGURE 1 *V. parahaemolyticus* exists as either a swimmer or swarmer cell. 2
FIGURE 2. Detection of *V. parahaemolyticus* in the environment increases with water temperature. 4
FIGURE 3. Dissemination of pandemic *V. parahaemolyticus* 5
FIGURE 4. Proposed evolution of *Vibrio* species. 10
FIGURE 5. Structure of TDH. 14
FIGURE 6. T3SS has structural similarities with flagellar export apparatus. 16
FIGURE 7. Organization of T3SS1 genes. 20
FIGURE 8. T3SS1 orchestrates a series of events resulting in host cell death. 22
FIGURE 9. Identification of T3SS1 secreted proteins. 23
FIGURE 10. Actin binding proteins that interact with PtdIns(4,5)P_2. 32
FIGURE 11. Detachment of the membrane from the cortex can cause bleb formation. 34
FIGURE 12. Analysis of derivatives of the POR3 strain. 60
FIGURE 13. VPA0450 expression delays cell rounding and induces transient membrane blebbing. 62
FIGURE 14. VPA0450 is required for rapid host cell lysis during infection with *V. parahaemolyticus*. 63
FIGURE 15. VPA0450 is sufficient to induce membrane blebbing. 65
FIGURE 16. VPA0450 is homologous to other uncharacterized effectors. 67
FIGURE 17. VPA0450 is homologous to the IPP5C domain of synaptojanin. 69
FIGURE 18. SPsynj IPP5C is sufficient to induce membrane blebbing. 70
FIGURE 19. VPA0450 mutants show a diminished ability to cause blebbing. 72
FIGURE 20. VPA0450 has inositol polyphosphate 5-phosphatase activity. 74
FIGURE 21. VPA0450 can delocalize a PH domain from the plasma membrane. 77
FIGURE 22. VPA0450 does not delocalize phosphatidylinositol 3-phosphate binding proteins in transfected cells. 78
FIGURE 23. VPA0450 disrupts PtdIns(4,5)P_2 at the plasma membrane. 80
FIGURE 24. The phosphatase activity of VPA0450 causes membrane blebbing and facilitates cell lysis. 84

FIGURE 25. VPA0450 C-terminus is necessary for membrane localization. 88
FIGURE 26. C-terminus is necessary to localize mCherry-VPA0450 to the plasma membrane. 89
FIGURE 27. VPA0450 C-terminus is required for full delocalization of PH(PLCδ1). 91
FIGURE 28. $VPA0450_{367-498}$ is not sufficient for membrane localization. 93
FIGURE 29. C-terminal helices of VPA0450 may be correct localization domain. 94
FIGURE 30. C-terminal helices of VPA0450 are amphipathic. 96
FIGURE 31. CAB2 induces stress fibers and cytotoxicity similar to POR2 while CAB4 is not cytotoxic to Hela cells. 105
FIGURE 32. POR3 and CAB3, but not CAB4, induce cell rounding. 107
FIGURE 33. Deletion of *vpa0450* from CAB3 accelerates rounding but delays lysis upon infection of Hela cells. 109
FIGURE 34. VPA0450 and VopQ are required for rapid host cell lysis during infection with CAB3. 110
FIGURE 35. Functional T3SS1 is required for cell Hela cell rounding during infection. 113
FIGURE 36. CAB3 cytotoxicity is mediated by T3SS1. 114
FIGURE 37. Infection with CAB3Δ*vopQS* Δ*vpa0450* uncovers the VopR phenotype. 119
FIGURE 38. VopR does not directly contribute to cytotoxicity during infection. 121
FIGURE 39. VopR has homology to multiple bacterial effectors and eukaryotic domains. 122
FIGURE 40. Mutation of putative catalytic residues abrogates the activity of VopR. 124
FIGURE 41. VopR is lethal to yeast. 126
FIGURE 42. T3SS1 orchestrates a multifaceted host cell death. 131

LIST OF TABLES

TABLE 1. *V. parahaemolyticus* strains used to study effectors are derived from the RimD2210633 clinical isolate..... 19

TABLE 2. T3SS1 effectors target diverse substrates to drive cytotoxicity 23

TABLE 3. The actin cortex, Ras signaling, and innate immunity are modulated by T3SS2 effectors..... 27

TABLE 4. Bacterial and Yeast Strains 47

TABLE 5. Constructs..... 48

TABLE 6. Primers 52

TABLE 7. Characteristics of established and new *V. parahaemolyticus* parent strains 103

LIST OF ABBREVIATIONS

(*In alphabetical order*)

2xYT	2 times yeast tryptone
ADP	Adenosine diphosphate
AMP	Adenosine monophosphate
Amp	Ampicillin
ATP	Adenosine triphosphate
BLAST	Basic local alignment search tool
BSA	Bovine serum albumin
CFU	Colony forming unit
Cm	Chloramphenicol
CNF1	Cytotoxic necrotizing factor 1
CTX	Cholera toxin
DMEM	Dulbecco's modified Eagle media
DMSO	Dimethyl sulfoxide
EPC	Epithelioma papulosum cyprini
ERK	Extracellular signal-regulated kinase
ERM	Ezrin, radixin, moesin family of proteins
FERM	Free (activated) ezrin, radixin, moesin family of proteins
Fic	Filamentation induced by cyclic AMP
FYVE	Fab1, YOTB, Vac1 and EEA1-associated zinc finger domain
Gen	Gentamycin
GFP	Green fluorescent protein
GMP	Guanosine monophosphate
GTP	Guanosine triphosphate
GTPase	Guanosine triphosphatase
H-NS	Heat-stable nucleoid structuring protein

HRP	Horseradish peroxidase
IL-8	Interleukin-8
IPP5C	Inositol polyphosphate 5-phosphatase
IPTG	Isopropyl β-D-1-thiogalactopyranoside
JNK	C-Jun N-terminal kinase
Kan	Kanamycin
KP	Kanagawa phenomenon
LB	Luria Bertani
LC3	Microtubule- associated protein1 light chain 3
LDH	Lactate dehydrogenase
MAPK	Mitogen activated protein kinase
MKK	Mitogen activated protein kinase kinase
MLB	Marine Luria Bertani
MMM	Minimal marine media
MOI	Multiplicity of infection
NEB	New England Biolabs
OP	Opaque
PARP	Poly ADP ribose polymerase
PBS	Phosphate buffered saline
PCR	Polymerase chain reaction
PH	Pleckstrin homology
PI3K	Phosphatidylinositol 3-kinase
PLCδ1	Phospholipase Cδ1
PNGase	Peptide: N-glycanase
PRM	Proline rich motif
PRR	Proline rich region
PS	phosphatidylserine
PtdIns	Phosphoinositide

PtdIns(3,4,5)P_3	Phosphoinositide 3,4,5-triphosphate
PtdIns(3,4)P_2	Phosphoinositide 3,4-bisphosphate
PtdIns(3)P	Phosphoinositide 3-phosphate
PtdIns(4,5)P_2	Phosphoinositide 4,5-bisphosphate
PtdIns(4)P	Phosphoinositide 4-phosphate
RT-PCR	Reverse transcriptase-polymerase chain reaction
SCV	*Salmonella* containing vesicle
SDS-PAGE	Sodium dodecyl sulfate-polyacrylamide gel electrophoresis
Spsynj	*Schizosaccharomyces pombe* synaptojanin 1
T3SS	Type III secretion system
T3SS1	T3SS on chromosome 1
T3SS2	T3SS on chromosome 2
T6SS	Type VI secretion system
TBST	Tris-buffered saline with Tween 20
TDH	Thermostable direct hemolysin
Tet	Tetracycline
Tgase	Transglutaminase
TLH	Thermo labile hemolysin
TR	Translucent
TRH	TDH-related hemolysin
Vop	*Vibrio* outer protein
Vp-PAI	*Vibrio* parahaemolyticus pathogenicity island I
WASP	Wiskott Aldrich syndrome protein
WAVE	WASP family Verprolin-homologous protein
WH2	Wiskott-Aldrich homology 2
YC	Yeast complete media
YC-D	Yeast complete media with dextrose
YC-G/R	Yeast complete media with galactose and raffinose
Yop	*Yersinia* outer protein

CHAPTER 1
LITERATURE REVIEW

The discovery of *Vibrio parahaemolyticus*

In the fall of 1950 in the southern suburbs of Osaka, Japan, an outbreak of acute gastroenteritis sickened 272 individuals. Twenty of these people ultimately died. While the source of the illness was believed to be *shirasu*, a small partially dried sardine, the etiologic agent was unknown. An intense investigation began, with filtered homogenates from *shirasu* passed through a guinea pig model to eliminate poisoning by chemicals as a possible cause of the disease. When the test animals developed peritonitis, the homogenates were inoculated to various growth media. Along with other known bacterial organisms, two species of unidentified gram-negative rods were also isolated. Unable to separate these organisms by isolation streaking, they were inoculated intraperitoneally into mice. When disease symptoms developed several hours later, ascitic fluid was collected and streaked onto blood agar. One of the organisms was identified as *Proteus morganii*. The other organism was previously unclassified, and was named *Pasteurella parahaemolytica*. Further testing showed that this organism alone was pathogenic to mice, and could be isolated from the stool samples of afflicted individuals from the original outbreak (50, 57, 83, 86). *P. parahaemolytica* was

reclassified as *Vibrio parahaemolyticus* when it was found that it grew preferentially on high salt media (57).

Description of *V. parahaemolyticus*

V. parahaemolyticus is a Gram-negative, halophilic, mesophilic, small rod that may have a single curve to its shape (27, 111). It exists as either a swimmer cell with a single polar flagella, or a swarmer cell covered in lateral flagella (discussed below) (76) (Figure 1). Depending on environmental conditions, *V. parahaemolyticus* can produce a capsule, with over 70 different K antigens detected (86).

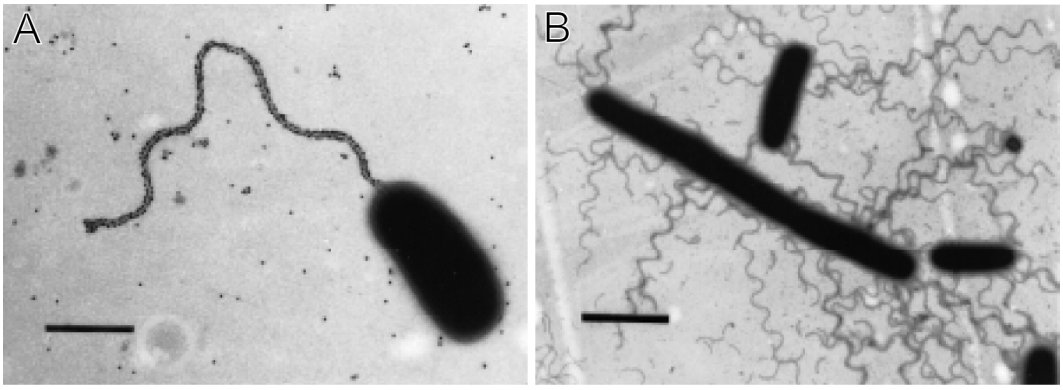

FIGURE 1 *V. parahaemolyticus* exists as either a swimmer or swarmer cell.
V. parahaemolyticus constitutively produces a single polar flagella in its swimmer form (**A**), but can switch to a swarmer cell (**B**) in which cells produce multiple peritrichous flagella and may not septate. Error bars (**A**) 1μm and (**B**) 3μm. Adapted from (76).

V. parahaemolyticus is found free living in brackish and estuarine waters, and requires salinity for survival (4). In winter months when water temperatures are unfavorable, *V. parahaemolyticus* may be undetectable. It has been proposed that the organism survives in marine sediment, and is reintroduced to the water column when temperatures rise to favorable levels. In locations when water temperatures do not decrease below 15 °C, *V. parahaemolyticus* may be detected year round (111), with the number of organisms detected increasing as water temperatures rise (Figure 2) (55). *V. parahaemolyticus* is disseminated throughout the world, and has been detected in coastal waters as far north as the southern coast of Alaska (Figure 3) (27, 122).

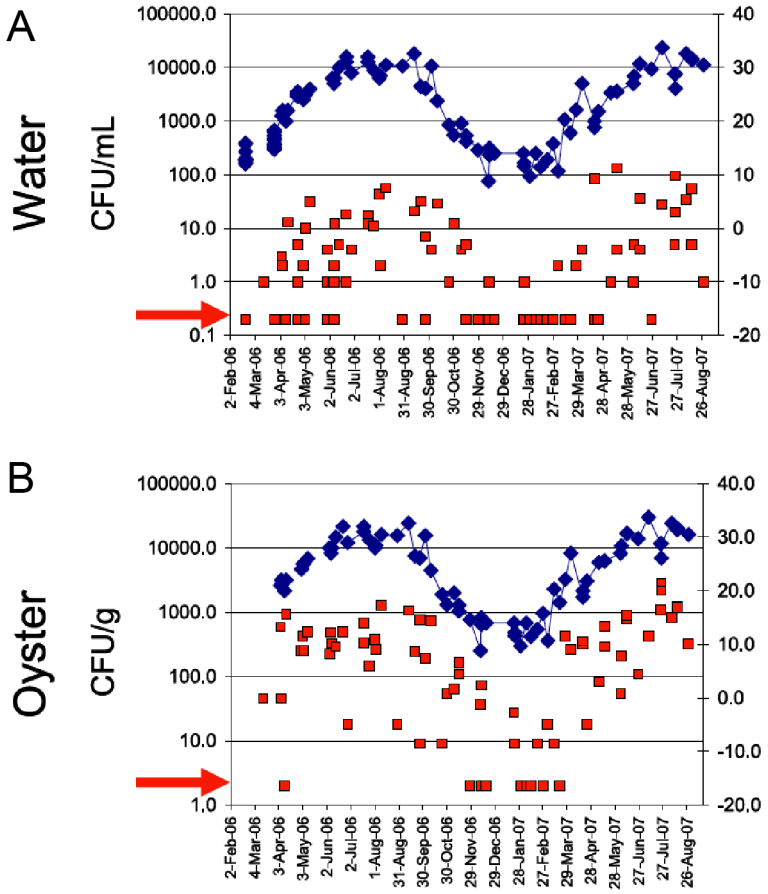

FIGURE 2. Detection of *V. parahaemolyticus* in the environment increases with water temperature.

The density of *V. parahaemolyticus* (red squares and left axis) cultured from (**A**) water and (**B**) oysters is plotted with surface water temperature (°C, blue diamonds and right axis) over 18 months. Red arrows denote limit of detection. Adapted from (55).

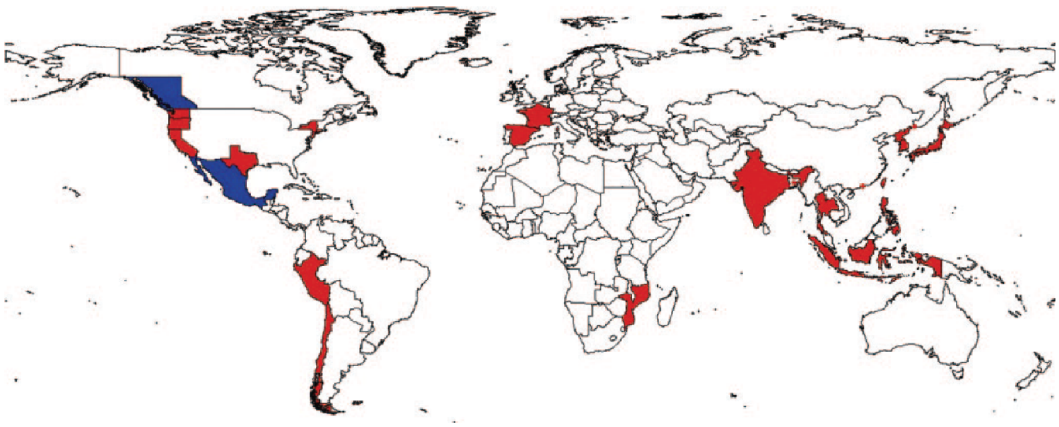

FIGURE 3. Dissemination of pandemic *V. parahaemolyticus*.
Areas where the O3:K6 pandemic serovar of *V. parahaemolyticus*, or it variants, are shown in red. Blue regions denote locations where *V. parahaemolyticus* has been detected in the environment, or cases of disease have occurred, but the serovar was not determined. Adapted from (86)

Emergence of Pandemic Strains

V. parahaemolyticus accounts for 20-30% of all food poisoning cases (2), and is the leading cause of foodborne illness, in Japan. The high rate of infection is attributed to the overall high seafood diet, as well as the common practice of eating seafood raw (6). Gastroenteritis caused by *V. parahaemolyticus* is generally associated with the consumption of raw or undercooked seafood, including fish, crab and other crustaceans, and mollusks. As *V. parahaemolyticus* is sensitive to heat, cooking generally kills the bacterium rendering contaminated food safe to eat (132).

In the United States, the first case of gastroenteritis caused by *V. parahaemolyticus* occurred in 1971 in Maryland and was associated with contaminated crabmeat (81). *V. parahaemolyticus* is the primary cause of US *Vibrio*-associated foodborne illness (65, 132) with oysters as the most common source of *V. parahaemolyticus* gastroenteritis (84).

As a consequence of their feeding mechanism, the concentration of *V. parahaemolyticus* in filter feeders such as oysters results in levels of bacteria up to 100-fold higher than surrounding waters (83). Additionally, up to 100% of oysters may be contaminated with *V. parahaemolyticus* and/or *V. vulnificus* during summer months increasing the chances of infection (83). As water temperatures increase in late spring and into summer, the level of *V. parahaemolyticus* detected in water, sediment and oysters also rises (Figure 2)

(55). Additionally, the ability to detect *V. parahaemolyticus* in an increasing range of coastal waters may coincide with an average increase in ocean temperatures as a consequence of global warming (27, 77).

An increase in non-cholera *Vibrio* infections since the mid 1990s has been associated with the detection of a new clonal group, which includes three new serotypes: O3:K6, O4:K68, and O1:K untypeable (83). Since 1996, the most common serotype of *V. parahaemolyticus* has been O3:K6. While non-pandemic variants for this serotype were detected in Japan as early as 1983, illness caused by this strain was first observed in a Japanese traveler returning from Indonesia in 1995. An outbreak of diarrheal disease then occurred in Calcutta, India in February, 1996 with 50-80% of isolates confirmed as O3:K6 (86). *V. parahaemolyticus* has now been detected in North and South America, Europe, Africa, and Asia (27) with outbreaks of disease occurring worldwide (Figure 3). The RimD 2210633 strain of *V. parahaemolyticus*, of the O3:K6 serotype, will be the focus of this study.

Diseases caused by *V. parahaemolyticus*

Infection with *V. parahaemolyticus* can cause three distinct medical conditions. Acute gastroenteritis presents with abdominal cramping, diarrhea, nausea, vomiting, low-grade fever, headache, and occasional bloody diarrhea

different than that seen in other enteric infections. Infection occurs 4 hours to four days after consumption of contaminated food, and lasts three days. The illness is self-resolving in immunocompetent individuals and can be sufficiently treated with oral rehydration alone (86, 132).

Wound infection is common among fishermen and is generally acquired when small wounds occur in or around seawater (49). This form of *V. parahaemolyticus* infection is sometimes limited to cellulitis, but may progress to necrotizing fasciitis, an uncommon infection of soft tissues characterized by a rapid spread of the bacteria with associated inflammation and necrosis of tissues (116).

Septicemia occurs when *V. parahaemolyticus* enters the blood stream of the patient and is disseminated throughout the body. Systemic immune activation leads to inflammation and increased vascular permeability. This can result in hypovolemic shock, multisystem organ failure and death (113). The subpopulation of patients most at risk for septicemia includes those with underlying medical conditions including liver disease, diabetes, cancer, and recent gastric surgery (132). Immunocompromised individuals, and those with liver failure due to liver cirrhosis or hepatitis virus infection, seem to be at greatest risk of septicemia (9, 49)

Virulence factors associated with V. parahaemolyticus

Genomic analysis has demonstrated that a common *Vibrio* progenitor gave rise to *V. parahaemolyticus*, *V. cholerae*, and the other *Vibrio* species. The acquisition of a Type III Secretion System (T3SS) similar to that found in *Yersinia* species and herein referred to as T3SS1, was the basis of a *V. parahaemolyticus* ancestor. The acquisition by some strains of a second Type III Secretion System (T3SS2), and Thermostable Direct Hemolysin (TDH) and TDH related hemolysin (TRH) genes has lead to a number of *V. parahaemolyticus* species with varying degrees of pathogenicity. This evolution is separate from that of *V. cholerae*, which also acquired T3SS2, as well the phage-encoded cholera toxin (CTX) in some strains, but does not possess T3SS1 (Figure 4) (90). In addition to Type III Secretion and TDH genes, *V. parahaemolyticus* possesses flagella for swimming and swarming, as well as the ability to produce a capsule, both factors that likely aid in environmental survival as well as colonization of the human host. Gene loci for two separate Type VI Secretion Systems (T6SS1 and 2) have been identified. Type VI secretion is present in many Gram-negative pathogens, and may be involved in modulation of eukaryotic signaling (20). However, activation of these genes is not altered under T3SS-inducing conditions meant to mimic the environment encountered within a human host (42). As such, these systems in *V. parahaemolyticus* may be used for competition in the environment and will not be discussed further here.

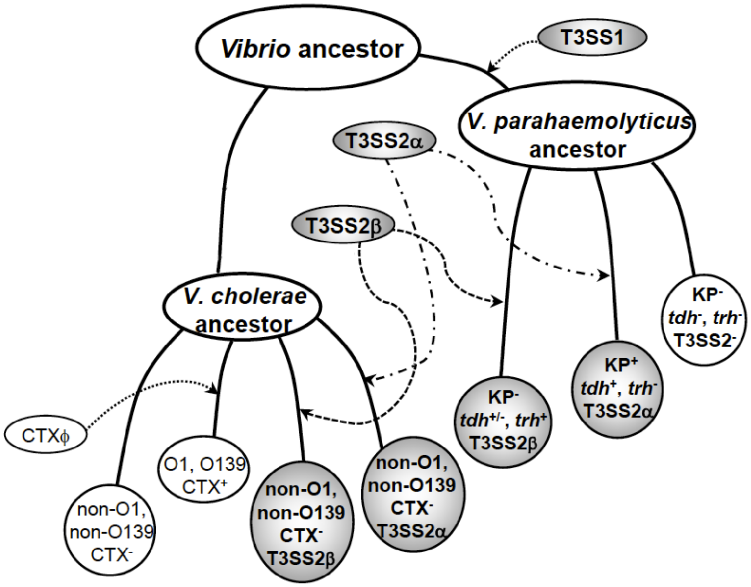

FIGURE 4. Proposed evolution of *Vibrio* species.
Genetic analysis indicates that *V. parahaemolyticus* was formed from a common *Vibrio* progenitor upon the acquisition of T3SS1, and that various serovars are a result of the acquisition of TDH, TRH and/or T3SS2. This evolution was independent of *V. cholerae*, although the progenitor is shared. Adapted from (90)

Swimming and swarming

A common virulence factor associated with many intestinal pathogens is the presence of one or more flagella. *V. parahaemolyticus* possesses two different types of flagella with distinct functions. A polar flagellum is constitutively expressed and is used for swimming (58). The whip of the flagellum is made of six different flagellin proteins, and is sheathed which may aid in attachment. The energy to rotate this flagellum is provided by a sodium motive force, which is advantageous in salt water with an average pH of 8. *V. parahaemolyticus* expressing this single flagellum is capable of swimming at speeds up to 60 μm/s (76).

A decrease in rotation speed as a consequence of increased viscosity, or growth under iron-limiting conditions, induces a switch to a swarmer cell type and the production of a number of non-sheathed peritrichous flagella (76). Lateral flagella allow the bacteria to swarm over solid or semi-solid substrates (7, 8, 109). These flagella are different than the single polar flagellum in that they are unsheathed, made from a single flagellin protein, and are powered by the proton motive force (Figure 1) (76).

The switch from swimmer to swarmer is highly regulated. The activation of OpaR, a *V. harveyii* LuxR homolog and the regulator of capsule production, blocks production of the lateral flagella (*laf*) genes, which are necessary for lateral flagella production (54). Inactivation of OpaR switches the cell from opaque (OP)

to the translucent (TR) form which lacks a capsule and can swarm effectively over surfaces or through viscous liquids (93). ScrG and ScrC, both GGDEF and EAL-domain containing proteins, regulate c-di-GMP levels in the cell, with increased c-di-GMP leading to lateral flagella synthesis and swarming. ScrG can also block CpsA synthesis, which is necessary for capsule synthesis, as well as decrease biofilm formation and adherence to surfaces (35, 59). A decrease in c-di-GMP may also enhance expression of other virulence factors, including T3SS proteins (41).

Thermostable Direct Hemolysins

Nearly all *V. parahaemolyticus* strains isolated from clinical samples possess β-hemolytic activity attributed to TDH or TRH (127). Termed the Kanagawa phenomenon (KP), these isolates are able to lyse human erythrocytes when plated on a high-salt media called Wagatsuma agar (88).

V. parahaemolyticus RimD 2210633 possesses two copies of the TDH toxin, *vpa1314* (*tdhA*) and *vpa1378* (*tdhS*) (71). TDH is a reversible amyloid toxin (37) that has been shown to associate with cholesterol and sphingolipid-enriched lipid rafts. Disruption of these lipid microdomains abrogated cytotoxicity in nucleated cells, but not hemolytic activity against erythrocytes, indicating two potential activities for this toxin (75). The determination of the x-ray crystallographic structure showed TDH forms a homotetramer with a central pore

23 Å in diameter (Figure 5). This relatively large pore size helps explain previously observed low ion selectivity, allowing both water and ions to flow through a membrane with a TDH tetramer embedded with little impedance (129). This alteration in ion flux from affected cells in the intestine may be the mechanism for the diarrhea observed during infection (51). While TDH was considered to be a major virulence factor for *V. parahaemolyticus* pathogenesis, deletion of both *tdhA* and *tdhS* did not affect cytotoxicity towards cultured Hela cells, and still showed partial fluid accumulation in a rabbit ileal loop model indicating the effects of other virulence factors (67, 70, 95). The cell death of cultured cells infected with TDH-deficient strains was later correlated with functional T3SSs (94).

The KP test is commonly used to identify pathogenic *V. parahaemolyticus* in seafood as well as patient samples. The reproducibility of the KP test is dependent on pH, media salinity, and erythrocyte type. As such, identification of pathogenic serovars by this method is not always accurate. Identification of the *tdh* gene in samples has been shown to more accurately predict virulence, as it is a genetic test rather than a phenotypic test (52). The *tdh* gene is encoded and co-regulated with T3SS2 genes (42). The identification of TDH may actually serve to identify *V. parahaemolyticus* strains with T3SS2, the expression of which may be a significant factor in determining is a serovar can cause pandemic outbreaks of disease.

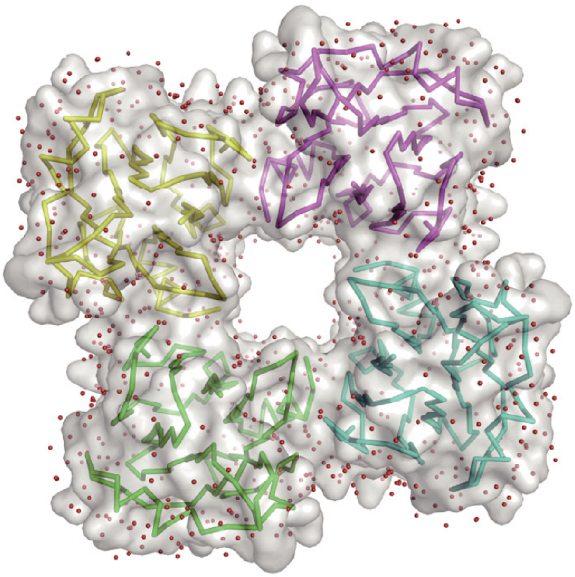

FIGURE 5. Structure of TDH.
When TDH is embedded in a membrane it forms a homotetramer with a large central pore that is predicted to allow water and ions to flow from the targeted host cell with low impedence. Adapted from (129)

The Type III Secretion Systems of V. parahaemolyticus

The T3SS is a bacterial organelle evolved to deliver proteins, termed effectors, directly into the cytoplasm of a eukaryotic cell (39). Made up of 20-30 proteins, the secretion apparatus consists of a basal body that spans both the inner and outer bacterial membranes, a needle that acts as a conduit between the bacterial and eukaryotic cells, and a translocon pore that is inserted into the eukaryotic cell membrane (33, 40, 73). Structurally, the apparatus bears resemblance to a flagellar system from which it may have evolved (Figure 6). Some secretion apparatus proteins have homology to flagellar export proteins, with core transmembrane proteins showing the highest level of conservation (73).

The T3SS allows bacteria to translocate effectors from their cytoplasm directly to the cytoplasm, or cytoplasmic face of the host cell membrane, without release of the effectors to the cytoplasm (23). The specific complement of effectors within a pathogen determines not only its lifestyle, but also the disease that it causes. *Yersinia pestis*, the causative agent of plague, encodes six effectors that prevent phagocytosis and cripple innate immune signaling, with the bacterium remaining extracellular throughout the disease process (123). In contrast, *Salmonella* species encode two different T3SSs. The first system induces phagocytosis of the bacterium through activation of signaling cascades that regulate actin polymerization. Once inside the host cell, the second system down-regulates actin polymerization and alters the lipid composition of the phagosome

to prevent phagosome-lysosome fusion, maintaining the bacteria within a vacuole (72, 105).

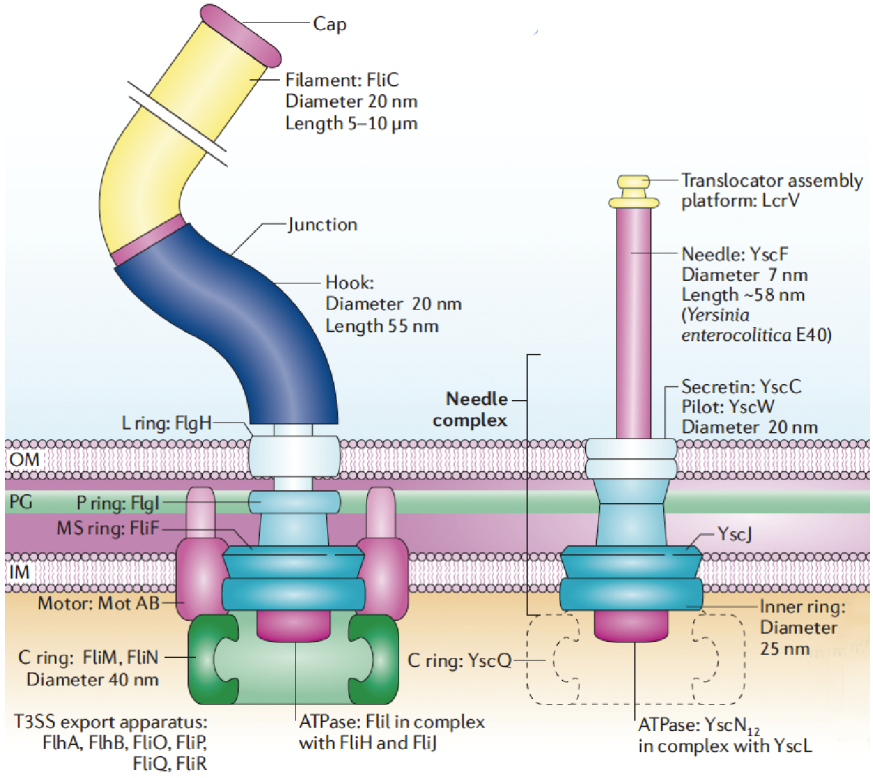

FIGURE 6. T3SS has structural similarities with flagellar export apparatus. The T3SS may have evolved from a flagella system, and has high homology to the core export proteins of the flagellar export apparatus. Adapted from (23)

There are over 100 different characterized effector proteins (3). While their activities and targets vary, effectors identified thus far tend to manipulate a limited set of eukaryotic systems. Common targets of T3S effectors include the actin cytoskeleton, innate immune signaling, and autophagy. These systems can be turned up- or down-regulated depending on the specific needs of the pathogen (14, 67, 85, 89, 124, 131).

For translocation, effectors must first be delivered to the secretion system. It is generally accepted that the first 20-50 amino acids of an effector encodes a secretion signal and followed by a chaperone-binding region up to 100 amino acids in length (1, 39). However, no consensus for the secretion signal has been uncovered (3, 104, 119). It has been hypothesized that delivery may be mediated by primary or secondary structure of the effector N-terminus, by the chaperone itself, or through the mRNA encoding the effector (3). Synonymous substitutions that alter the mRNA sequence but not the amino acid sequence, as well as frame shift mutations in the 5' portion of effector mRNA molecules, have both been shown to decrease translocation of some effectors. (110). The same mRNA alteration strategies have also been shown to support an N-terminal protein signal for translocation (68). A peptide secretion signal model is supported by studies where protein synthesis was blocked by chloramphenicol, but secretion was not immediately abrogated. Additionally, effectors could be blocked from translocation by tagging the N-terminus with ubiquitin. Removal of the ubiquitin

with UBP1 allowed for immediate translocation (98). It is possible that it is a combination of peptide sequence and effector: chaperone complex that is required for recognition and translocation of effectors.

Translocation occurs in an ATP-dependent manner. Effectors, generally bound to chaperones in a quiescent, partially folded state, are unfolded and threaded through the needle. The chaperone remains in the bacterial cytoplasm (1, 3, 39). Upon entering the host cell cytoplasm, the effectors refold into an active state where they manipulate eukaryotic signaling cascades to facilitate infection and disrupt the host immune response (38).

Genomic sequencing of *V. parahaemolyticus* RimD 2210633 revealed two pathogenicity islands, one on each of the two chromosomes (71). The first island encodes T3SS1 and some of its cognate effectors (91, 93). Vp-PAI, the second island, encodes T3SS2, some of its effectors, as well as the TDH genes. Both islands have a number of uncharacterized hypothetical proteins (42, 60, 71, 91). Based on G+C content, T3SS1 was ancestrally acquired, while T3SS2 was obtained through a relatively recent lateral gene transfer (71). The presence of two T3SS2 gene clusters (T3SS2α and T3SS2β) in different *V. parahaemolyticus* strains indicates this acquisition has occurred at least twice (90).

Several *V. parahaemolyticus* strains were created from RimD 2210633 to enable the study of each T3SS and the characterization of these hypothetical proteins. The POR1 strain maintains both functional T3SSs, but is deleted for

tdhAS. POR2 is constructed from the POR1 background, and has a deletion of *vcrD1*, an inner membrane structural ring for T3SS1 that prevents formation of the T3SS1 needle. POR2 secretes only from T3SS2. POR3 is similar to POR2, but has a deletion of *vcrD2* instead of *vcrD1*, and can secrete only from T3SS1 (Table 1) (95).

TABLE 1. *V. parahaemolyticus* strains used to study effectors are derived from the RimD2210633 clinical isolate

	TDH	T3SS1	T3SS2
RimD 2210633	+	+	+
POR1	-	+	+
POR2	-	-	+
POR3	-	+	-

T3SS1

T3SS1 is present in all *V. parahaemolyticus* strains and is a defining characteristic of this species (90). This system causes cytotoxicity in cultured human cells, but does not appear to contribute to enterotoxicity during infection as determined by a rabbit ileal loop model (14, 67, 70, 95). T3SS1 is similar to the Yersinia *ysc* T3SS based on the number of genes, gene identity, and order (Figure

7) (71, 82, 91). Growing liquid cultures at 37 °C in low calcium media induces T3SS1, similar to induction of the *Yersinia* secretion system.

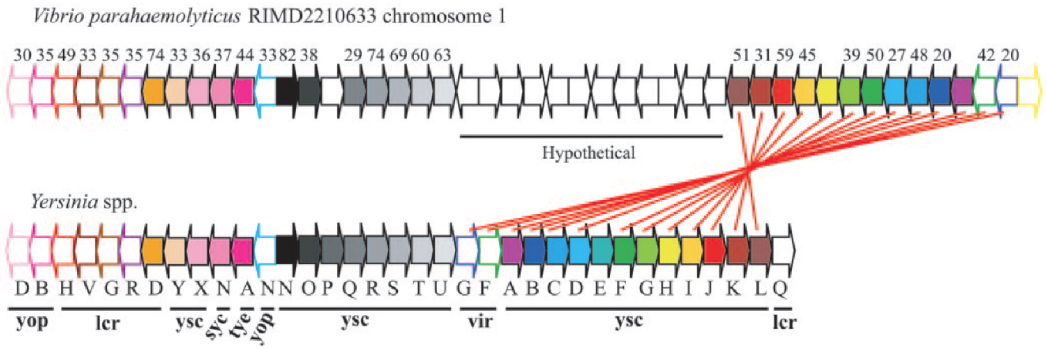

FIGURE 7. Organization of T3SS1 genes.
V. parahaemolyticus T3SS1 genes are similar in size, orientation and organization to the *Yersinia* T3SS, with the addition of 12 non-homologous hypothetical genes. Adapted from (95)

Transcription of the T3SS1 genes is regulated by three interacting proteins (ExsC, ExsD, and ExsE) that control the activity of ExsA, a member of the AraC family of transcriptional activators. Under non-inducing conditions, ExsA is bound to ExsD, and anti-activator, and rendered inactive. ExsE, a substrate for T3SS1, is bound to its chaperone ExsC, also an anti-anti-activator of the system. When low calcium conditions are encountered ExsE is secreted releasing ExsC, which binds to ExsD. By sequestering ExsD, ExsA is released

and is able to activate transcription of T3SS1 genes. This regulatory system requires low-level expression of T3SS1 genes to allow for the initial secretion of ExsE (62). This may be accomplished through leaky regulation of the T3SS1 genes, or additional regulatory systems that allow for some expression under inhibitory conditions. Preliminary evidence indicates the Heat-stable Nucleoid Structuring protein (H-NS), common in Gram-negative bacteria and known for genome-wide repression of protein expression by binding to curved DNA normally found at active sites of transcription and blocking transcriptional machinery (32) may negatively regulate T3SS1, but it is not currently understood how this protein fits into the regulatory cascade (62).

While the regulation of T3SS1 is just now being elucidated, the characterization of two T3SS1 effectors, VopQ and VopS (discussed below), support a model for induction of autophagy, followed by cell rounding, and then cell lysis. Rapid induction of autophagy by VopQ causes the target cell to digest itself and prevents phagocytosis of the infecting *V. parahaemolyticus*. The collapse of the actin cytoskeleton by VopS leads to cell rounding and shrinkage. Finally, cells lyse and release their contents (Figure 8) (16).

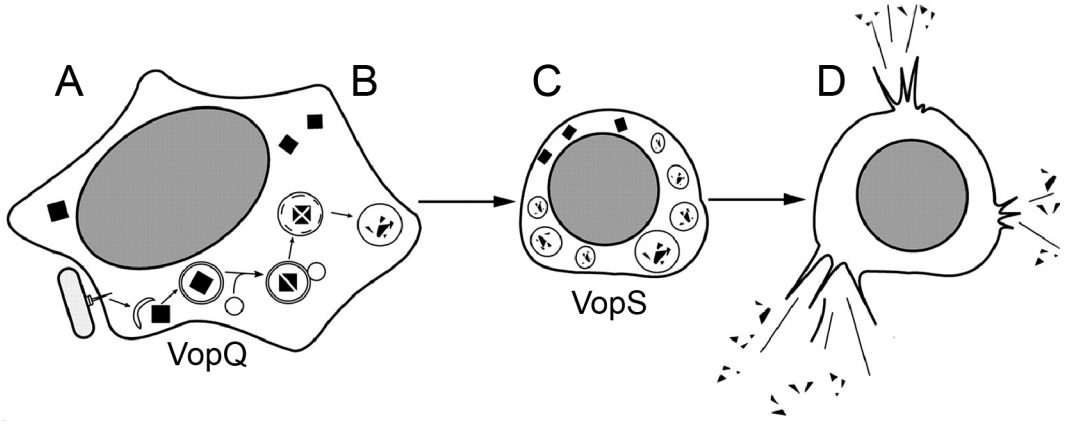

FIGURE 8. T3SS1 orchestrates a series of events resulting in host cell death. (**A**) *V. parahaemolyticus* uses T3SS1 to inject effectors into the cytoplasm of a host cell. (**B**) VopQ mediates the rapid induction of autophagy. (**C**) VopS then AMPylates Rho-family GTPases ultimately causing a collapse of the actin cortex and cell rounding. (**D**) Rounding is followed by cell lysis and release of cellular contents. Adapted from (16).

An *in silico* screen for chaperone proteins previously identified four potential T3SS1 effectors (Table 2). VP1680, VP1683, and VP1686, now referred to as VopQ, VopR and VopS, respectively, are located within the T3SS1 gene locus. VPA0450 is unlinked to T3SS1, and is located on the second chromosome (93). Secretion of VopQ, VopS, and VPA0450 was confirmed by secretion assay using POR1 grown under inducing conditions. VopR was not detected as it has a pI outside the range of the 2-D gel used to separate the secreted proteins prior to mass spectrometer analysis (Figure 9) (91).

TABLE 2. T3SS1 effectors target diverse substrates to drive cytotoxicity

Effector	Domain	Activity	Cellular consequence
VopQ (VP1680)	Unique to VopQ	Unknown target or mechanism	Induces autophagy
VopR (VP1683)	TGase/Papain-like protease fold	Unknown target or mechanism	Cellular rounding
VopS (VP1686)	Fic domain	AMPylates Rho-family GTPases	Collapse of the actin cytoskeleton
VPA0450	Inositol polyphosphate 5-phosphatase	Removes D5 phosphate from PtdIns(4,5)P2	Destabilization of plasma membrane

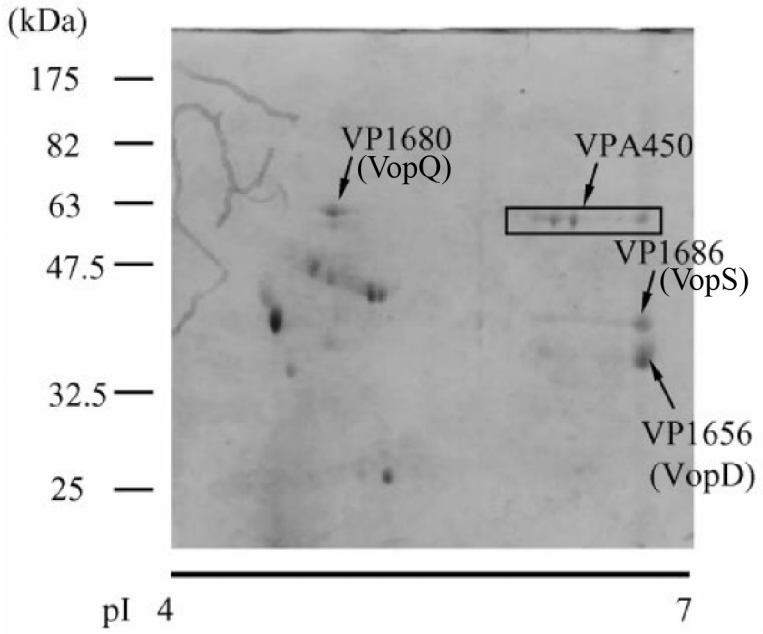

FIGURE 9. Identification of T3SS1 secreted proteins.
2-D gel electrophoresis followed by mass spectrometer analysis of proteins secreted by *V. parahaemolyticus* identified VP1680 (VopQ), VP1686 (VopS) and VPA0450 as potential T3SS1 effectors. VopD is a component of the translocon. Adapted from (91).

Burdette, *et al*., showed in previous work that VopQ (VP1680) induced PI3-kinase independent autophagy upon infection with POR3, or transfection of *vopQ*, into Hela cells. Microinjection of rVopQ into Hela cells induced autophagy in less than five minutes as measured by conversion of LC3-I to LC3-II and formation of LC3-GFP punctae. VopQ was necessary for rapid host cell lysis during infection as cells infected with a Δ*vopQ* strain of *V. parahaemolyticus* lysed 3 hours slower than those infected with a wild type strain. In addition to inducing autophagy, VopQ was able to block phagocytosis of *V. parahaemolyticus* by RAW 264.7 macrophages, possibly through the sequestration of necessary membrane components (14). Recent studies have identified VopQ as an activator of the JNK, p38 and ERK MAPK pathways in human intestinal epithelial cell cultures. MAPK activation resulted in secretion of IL-8, and was necessary for full cytotoxicity (74, 108). The target of VopQ and mechanism for this activation were not determined, leaving the question of whether or not autophagy activation is the intended purpose of VopQ or an off-target effect. The molecular target and mechanism of action for VopQ are still under investigation.

The target and mechanism of action for VopR (VP1683) has not been determined. The initial characterization of this effector is discussed in Chapter 6.

VopS (VP1686) is responsible for the rounding of cells and cytoplasmic dispersion of actin seen during infection of Hela cells with POR3. VopS indirectly

targets the actin cytoskeleton by AMPylating Rho-family GTPases (131). The Fic domain within VopS mediates the direct transfer of adenosine monophosphate from ATP to the switch 1 region of these small G-proteins, preventing their binding to downstream effectors. This blocks the signaling cascade regulating the actin cytoskeleton, leading to its collapse (69, 128).

VPA0450 has now been shown to be a phosphatidylinositide phosphatase homologous to the inositol polyphosphate 5-phosphatase (IPP5C) domain of the eukaryotic protein synaptojanin. By disrupting the homeostasis of inositides at the plasma membrane, VPA0450 is sufficient to induce membrane blebbing. The activity of VPA0450, and its contribution to host cell lysis, is discussed in detail in Chapter 4.

T3SS1 initially was proposed to kill cells by apoptosis based on Annexin V staining of phosphotidylserine (PS) after three hours of infection with *V. parahaemolyticus* POR3 (91). Our work has demonstrated that LDH is released in as little as two hours, indicating the Annexin V staining was likely due to cell permeability rather than the flipping of PS to the outer leaflet of the plasma membrane (15). Additionally, POR3 failed to activate caspases or cleave poly ADP ribose polymerase (PARP), both indicators of apoptosis activation (16). An additional study has indicated cell death proceeds by oncosis based on the uptake of a membrane impermeable dye as well as protection of cells from cytotoxicity by PEG3350, an osmoprotectant (135). These studies were performed with *V.*

parahaemolyticus NY-4 which, as an O3:K6 serovar, harbors a gene encoding TDH (132). The *tdh* gene would need to be deleted and the osmoprotection assay repeated before oncosis could be identified as a mechanism of cell death during *Vibrio* infection. Apoptosis has been shown to occur in Epithelioma papulosum cyprini (EPC) cells from a carp fish during infection with a *Vibrio alginolyticus* strain that harbors the VopQ homolog Va1680 (134). It is possible that this fish cell line, or fish in general, do not have the target of VopQ, and the cells default to apoptosis when not directed to induce autophagy.

Vp-PAI and T3SS2

T3SS2 is found primarily in clinical isolates, and is associated with pandemic strains of *V. parahaemolyticus* and large outbreaks of disease (95). Strains without T3SS2 are generally considered to lack pathogenic potential (17). T3SS2 is unlike any other specific T3SS, but has closest homology to the Hrp1 system also found in *Pseudomonas syringae* (23, 95). The activity of T3SS2 has been associated with enterotoxicity in the rabbit ileal loop model (95), as well as disruption of tight junction integrity in cultured cell monolayers (17, 70). While TDH is co-regulated with T3SS2, it is not necessary for the pathogenic effects observed in these model systems (17, 42, 60, 70).

Induction of Vp-PAI gene expression occurs upon contact with bile acids. Specific components of crude bile, including deoxycholate, taurodeoxycholate,

and glycodeoxycholate, were able to induce a number of genes, most residing within Vp-PAI (42). The transcriptional regulators, and putative environmental sensors, were identified as the ToxR homologs VtrA (VPA1332) and VtrB (VPA1348). Both of these proteins contain an N-terminal OmpR-like winged helix-turn-helix DNA binding domain, as well as predicted single transmembrane regions. Epistasis studies demonstrated that VtrA initated expression of VtrB. VtrB, in turn, activated transcription of *tdhAS*, T3SS2 structural genes, and effectors including VopL, VopA, VopC, and VopT (Table 3) (60).

TABLE 3. The actin cortex, Ras signaling, and innate immunity are modulated by T3SS2 effectors.

Effector	Domain	Activity	Cellular consequence
VopL (VPA1370)	WH2 and PRR	Nucleation of actin polymerization	Alteration of cell shape, possible loss of tight junction integrity
VopA (VPA1346)	Acetyltransferase	Inhibition of MAPK signaling	Lack of innate immune activation and cytokine production
VopT (VPA1327)	ADP-Ribosyltransferase	ADP-ribosylation of Ras	Induction of cytotoxicity
VopC (VPA1321)	Cytotoxic Necrotizing Factor-1 homolog	Deamidation of Rho GTPases, making them constitutively active (hypothesized)	Disregulation of actin network, inhibition of apoptosis (hypothesized)

VopL (VPA1370) was identified as a protein containing three Wiskott-Aldrich homology 2 (WH2) domains. The WH2 domains are able to bind actin monomers and are thought to position them for elongation of an actin filament. Transfection of VopL into Hela cells resulted in the formation of stress fibers independent of Rho-family GTPase activity (67). A homolog from *V. cholerae*, VopF, has similar domain architecture but induces aberrant actin protrusions on the cell surface (114). Biochemical analysis showed that rVopL was sufficient to nucleate actin polymerization independent of other cellular factors (67).

VopA (VPA1346, also referred to as VopP) was characterized as a YopJ homolog that blocks MAPK signaling by acetylating a conserved lysine residue on MAPKKs, preventing phosphorylation and blocking activation of the pathway and cytokine induction. VopA differs from YopJ in that it only targets the MAPK pathway, whereas YopJ also blocks NF-κB signaling (117, 118).

VopT (VPA1327) has homology to the ADP-ribosyltransferase domain of the *Pseudomonas aeruginosa* effectors ExoS and ExoT. It has been shown to transfer ADP-ribose to Ras, a small monomeric GTPase. This activity is partially responsible for the cytotoxicity seen during infection of Caco-2 monolayers with *V. parahaemolyticus* (61).

VopC (VPA1321) has homology to cytotoxic necrotizing factor 1 (CNF1) an exotoxin found in some pathogenic *E. coli* strains. CNF1 has been shown to

specifically activate Rho, Rac and Cdc42 by deamidating a glutamine residue in the switch 2 region of each enzyme, preventing hydrolysis of GTP. This causes induction of numerous actin-dependent phenotypes, as well as modification of the mitochondrial network, and inhibition of apoptosis (80). A functional analysis of VopC to determine if it shares catalytic activity with CNF1 has not been performed. As such the activity and phenotypic consequences of VopC translocation into host cells is undetermined.

Model systems to study V. parahaemolyticus pathogenicity

To date, much of the work characterizing how *V. parahaemolyticus* causes disease has been reductionist in its approach. Many, but not all, toxins and effectors have been identified and characterized. While this has yielded significant and valuable data, how these various bacterial factors work together is also of importance. Disease mediated by *V. parahaemolyticus* does not occur through the isolated actions of individual effectors. Rather, effectors and toxins work in concert to orchestrate a disease progression that is difficult to study.

To facilitate the study of the T3SSs as a whole, in conjunction with the effects of TDH, multiple animal models have been developed. Intraperitoneal injection of V. parahaemolyticus into mice has demonstrated that both T3SS1 and TDH contribute to lethality during systemic infection, while T3SS2 is necessary for fluid accumulation in the rabbit ligated ileal loop (48). These findings are

supported by a study in which piglets infected orogastrically with a *V. parahaemolyticus* NY-4 strain expressing only T3SS2 resulted in acute, self-limited diarrhea similar to that seen in humans. A different strain with only T3SS1 failed to produce symptoms. When these same strains were used in a lung-inhalation model in mice, The T3SS1-expressing strain caused 80-100% mortality in 12 hours, while the T3SS2-expressing strain did not cause death of the test subjects (97). These results suggest a role for T3SS2 effectors in causing the initial infection and diarrheal disease, while T3SS1 may be required for survival from immune clearance once out of the intestine and into deeper tissues. Continued development of relevant model systems will continue to improve our understanding of how each T3SS contributes to disease.

Phosphoinositides and membrane stability

A BLAST search of the amino acid sequence for VPA0450 places this protein within the endonuclease/exonuclease/phosphatase family of enzymes with specific homology to multiple phosphatidylinositol 4,5-bisphosphate 5-phosphatases. This raises the question of how an effector can manipulate the inositide network, and specifically phosphatidylinositol 4,5-bisphosphate (PtdIns(4,5)P_2), to facilitate pathogenesis.

Phosphoinositides (PtdIns) are central to the regulation of a number of diverse cellular processes due to the diversity of species that can be generated

through reversible phosphorylation events. PtdIns(4,5)P_2 regulates endo- and exocytosis, phagocytosis, cell motility, ion transport, cell adhesion and multiple signal transduction events. PtdIns(4)P and PtdIns(4,5)P_2 represent the bulk of the PtdIns lipids present in mammalian cells (30). Detection of PtdIns(4,5)P_2 using GFP-tagged PH domains specific for this lipid show that it resides primarily in the plasma membrane and some vesicular structures (5).

At the plasma membrane, PtdIns(4,5)P_2 binds to and activates proteins that promote actin polymerization, including WAVE, WASP, talin, and FERM proteins while inhibiting actin depolymerizing proteins such as profilin, gelsolin capping protein, and cofilin (Figure 10) (102, 125). A number of studies have demonstrated that sequestration or hydrolysis of PtdIns(4,5)P_2 leads to actin cytoskeleton defects including depolymerization (100, 102).

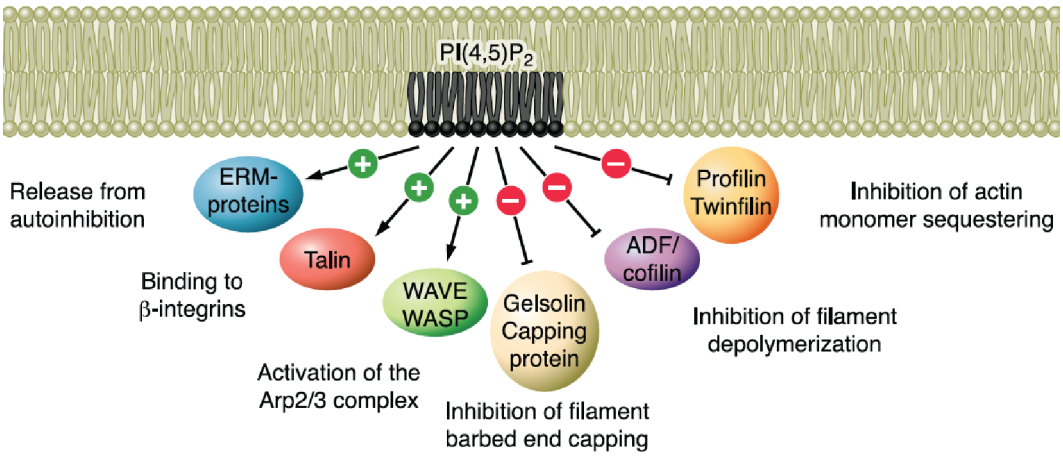

FIGURE 10. Actin binding proteins that interact with PtdIns(4,5)P_2. PtdIns(4,5)P_2 positively regulates ERM proteins, talin, WAVE and WASP to promote actin polymerization, and blocks activation of the actin inhibiting proteins gelsolin, ADF/cofilin and profilin. Adapted from (102).

Membrane dynamics and blebbing in eukaryotic cells

The loss of PtdIns(4,5)P_2, and the associated integrity of the actin cytoskeleton, can have drastic consequences for a cell. PtdIns(4,5)P_2 binds to proteins that act as adaptors linking the plasma membrane to the cytoskeleton (22, 30). The result of this loss of PtdIns(4,5)P_2 is the formation of dynamic membrane blebs.

Dynamic membrane blebbing is a normal process in eukaryotic cells associated with cytokinesis, cell spreading, and locomotion. Dynamic blebs are visually indistinguishable from blebs formed during apoptosis, but are smaller and more structured than the static blebs formed during necrosis (22). Blebs normally

form as a result of a localized loss of actin integrity or through loss of connection of the plasma membrane with the actin cytoskeleton. Once the plasma membrane is freed from the structure of the cytoskeleton, the hydrostatic pressure of the cytoplasm pushes the membrane outward, forming a bleb (Figure 11) (21). The actin cortex reforms under the bleb membrane, halting bleb expansion. Attachment of the myosin cortex to the newly formed actin cortex, followed by actomyosin contractility, retracts the bleb (34).

VPA0450, by targeting PtdIns(4,5)P_2, is able to affect the stability of the actin cortex and plasma membrane. Other pathogens have been shown to target inositides to maintain an intracellular vacuole for bacterial survival (72), but not as a mechanism to drive lysis of the targeted host cell. The characterization of VPA0450 will provide insights into *V. parahaemolyticus* pathogenesis, as well as further our understanding of PtdIns-mediated membrane dynamics.

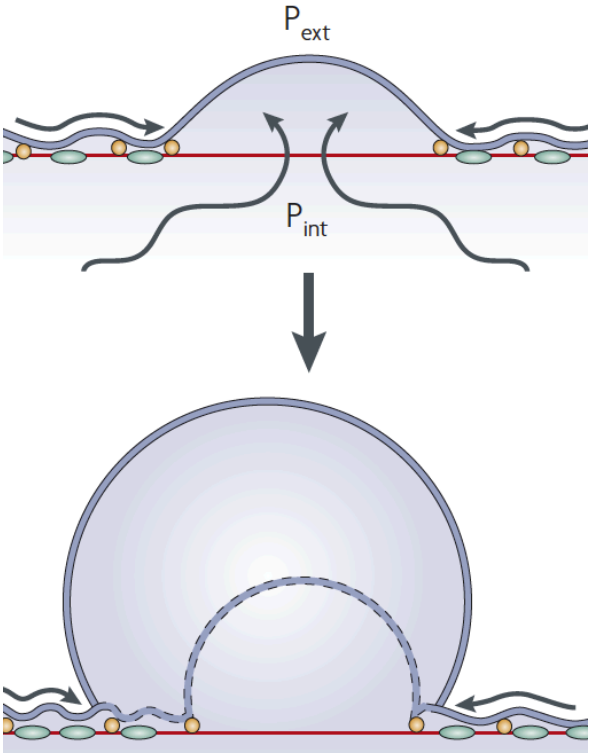

FIGURE 11. Detachment of the membrane from the cortex can cause bleb formation.
A local disconnection of cortex-actin linkers (yellow) between the plasma membrane (purple) from the actin cortex (red) allows the higher hydrostatic pressure of the cytoplasm to push the membrane outward, forming a bleb. Adapted from (21).

CHAPTER 2
MATERIALS AND METHODS

Bacterial strains and culture conditions

Strains used in this study are described in Table 4. Antibiotics were added to media to maintain plasmids when needed. *V. parahaemolyticus* strains were grown at 30°C on minimal marine media (MMM) agar plates (77mM K_2HPO_4, 35mM KH_2PO_4, 20mM NH_4Cl, 5mM $MgSO_4$, 5mM K_2SO_4, 2% NaCl, 0.4% galactose and 1.5% agar) for 24 to 48 hours, then stored at room temperature. Liquid cultures of *V. parahaemolyticus* were grown in marine LB (MLB, 1% tryptone, 0.5% yeast extract, 3% NaCl) at 30 °C unless noted otherwise.

E. coli DH5α, Sm10 and BL21/DE3 were maintained at 37 °C on Luria-Bertani (LB) agar plates (1 % tryptone, 0.5 % yeast extract, 1 % NaCl and 1.5 % agar). After growth, *E. coli* plates were sealed with parafilm and stored at 4°C. Liquid cultures were grown on a shaking platform in 2xYT (1.6 % tryptone, 1 % yeast extract and 0.5 % NaCl).

Yeast growth conditions

Yeast BY4741 harboring pRS413 vectors was maintained on yeast complete (YC) media (1.2g yeast nitrogen base (YNB), 5 g ammonium sulfate, 10 g succinic acid, 6 g sodium hydroxide, 0.75 g amino acid mix minus hisitdine and

15 g agar per liter) with 2 % dextrose. Induction of genes under the Gal promoter was done on YC with 2 % galactose and 1 % raffinose.

Mammalian Cell lines and culture conditions

Hela cells were maintained in DMEM containing 4.5g/L glucose (Invitrogen) supplemented with 10% heat inactivated FBS (Sigma), 1mM sodium pyruvate, 100U/ml penicillin, 100μg/ml streptomycin, 2mM L-glutamine (Invitrogen), and 5% CO_2 at 37°C. Cultures were split 1:8 every three days, and frozen stocks kept in 90% heat-inactivated FBS and 10% DMSO in liquid nitrogen.

Cloning of effectors and other genes

Constructs generated for this dissertation are listed in Table 5. For each construct, the gene of interest was amplified using Vent polymerase (NEB) and primers listed in Table 6 in 50 μl reactions. PCR products were confirmed by running a 2 μl aliquot on an agarose gel, then were purified using a PCR purification kit (Fermentas). PCR product and vector DNA were digested with the appropriate restriction enzymes (NEB). Each digest was separated by agarose gel electrophoresis, and DNA purified by gel extraction (Fermentas). Digested plasmid and insert were ligated with T4 DNA ligase (NEB) and transformed into chemically competent DH5α *E. coli* or electrocompetent Sm10 *E. coli*. Bacteria

harboring the plasmid of interest were selected by plating on antibiotic-containing media. Resulting colonies were screened by colony PCR, grown overnight in 2xYT broth with the appropriate antibiotic, and plasmid purified with a mini-prep kit (Invitrogen). All cloned vectors were confirmed by restriction analysis followed by sequencing.

For initial identification of the VPA0450 phenotype, the effector was amplified by PCR from *V. parahaemolyticus* genomic DNA and cloned into pcDNA3-flag, resulting in a full-length VPA0450 construct with a C-terminal flag tag for eukaryotic expression.

VPA0450, with 700 base pairs of upstream sequence containing the endogenous transcriptional and translational start sequences, was cloned into pSP72. The Stratagene QuikChange mutagenesis kit was then used to make a silent mutation within the VPA0450 coding sequence to remove an internal HindIII restriction site. The resulting vector was used as a template for future cloning of all VPA0450 constructs. VopR, SPsynj IPP5C and other genes of interest were likewise cloned into the appropriate expression vector followed by site directed mutagenesis when needed.

For eukaryotic expression studies, VPA0450-flag was cloned into pSFFV. Potential catalytic residues were mutated to alanine using the QuikChange kit on the wild type vector. VPA0450 and the 700bp sequence were cloned into pLafR for complementation of the knockout strain

Deletion of VPA0450 in POR3 strain using Lambda Red Recombinase

The POR3Δ*vpa0450* deletion strain was made using a method adapted from Datsenko and Wanner (28). Briefly, the 1kb upstream and downstream flanking sequenced of VPA0450 were cloned on either side of a chloramphenicol (Cm) resistance cassette in the suicide plasmid pLafR (provided by Dr. Linda McCarter). This construct was conjugated into POR3 by triparental mating with *E. coli* DH5α carrying the pLafR vector, and a second *E. coli* carrying pRK2013, encoding the *tra* genes for plasmid transmission. Transconjugates were selected on minimal media containing 3% NaCl and 20μg/ml tetracycline. After several passages to allow for allelic exchange of the Cm^R cassette for the VPA0450 gene, pLafR was eliminated by conjugation with the incompatible plasmid pH1JI. Positive deletion strains (Gen^R, Cm^R) were confirmed by PCR and sequencing. POR3Δ*vpa*0450 was then cured of the pH1JI plasmid by repeated passaging on media without gentamicin at 37°C. The knockout was complemented by conjugating pLafR containing the VPA0450 gene and 700bp of upstream sequence to include the endogenous promoter and RBS into POR3Δ*vpa0450*, and selecting on minimal media containing 3% NaCl and 20μg/ml tetracycline. Complementation was confirmed by PCR and sequencing. To confirm expression of *vpa0450* in the complement POR3Δ*vpa0450*+VPA0450-H356A were induced for type III secretion (see below). cDNA was made from isolated total RNA and

both were used as templates for PCR amplification of *vpa0450* segments. PCR reactions were separated on an agarose gel and stained with ethidium bromide.

Deletion of chromosomal genes using the pDM4 suicide vector

Unmarked, isogenic gene deletions were made using pDM4, a suicide vector containing a λ-pir dependent origin of replication, chloramphenical-resistance marker, and SacBR counter-selection genes. All pDM4 vectors were maintained in SM10 *E. coli*, which is lysogenized with λ-phage and as such is competent for pDM4 replication. For each gene deletion, 1 kb upstream and downstream flanking sequence of the gene to be deleted was cloned into pDM4, with a single restriction site linking the two regions. This construct was mated into the *V. parahaemolyticus* recipient strain and transconjugates selected by then plating onto MMM agar with 25 μg/ml chloramphenical (MMM + Cm_{25}). Fifty individual colonies were selected and patched onto a second MMM + Cm_{25} plate. After growing up overnight, ten patches were streaked for isolation on MMM with 15 % sucrose agar plates. Fifty of the resulting colonies were patched to both a MMM + Cm25 plate, and an additional MMM with 15 % sucrose plate. Colonies that grew on the sucrose containing plate, but not the chloramphenical plate, were restreaked to MMM agar, and inoculated into MLB broth overnight. Genomic DNA was isolated from the overnight cultures, and screened by PCR using the outside primers for the original 1 kb flanking regions. Strains that had

the target gene deleted yield a 2 kb product. The PCR products from these tentative positives was purified using a PCR purification kit (Fermentas), and sequenced using a primer ~200 bp upstream of the target gene, oriented such that it would sequence across where the deleted gene had been located. Frozen stocks were made of confirmed positives for later use. For multiple gene deletion strains, individual genes were sequentially deleted.

Sodium dodecyl sulfate polyacrylamide gel electrophoresis (SDS-PAGE)

Samples were diluted into 6x SDS-PAGE sample buffer (250mM Tris at pH 6.8, 50% glycerol, 10% sodium dodecyl sulfate, 500mM β-mercaptoethanol, and 0.5% bromophenol blue) and boiled 5-10 minutes. SDS-PAGE gels were cast according to the protocol in Molecular Cloning (103). Proteins were separated in SDS-PAGE buffer (250mM Tris Base, 2M glycine, and 0.1% SDS) for 20 minutes at 200 volts, followed by 60 minutes at 150 volts for. After separation, proteins were transferred to PVDF membrane (Millipore) in transfer buffer (125mM Tris base pH 7.6, 100mM glycine, and 20% methanol) for 80 minutes at 100 volts.

Western Blotting

After transfer, membranes were blocked in 5% milk in TBST, and then probed with rabbit effector specific antibody, M2 mouse anti-flag monoclonal

antibody (Sigma) or JL-8 mouse anti-GFP monoclonal antibody in 5% milk in TBST. Membranes were washed three times in TBST then probed with HRP-conjugated secondary antibody in 5% milk in TBST. After three additional washes, HRP activity was detected on film using an ECL+ chemiluminescence detection kit (GE Health Sciences) according to manufacturer's instructions.

Induction of T3SS1 and T3SS2

To induce T3SS1, *V. parahaemolyticus* strains were grown overnight in 2xYT at 30°C with appropriated antibiotic selection. Overnight cultures were diluted 1:10 into pre-warmed high glucose DMEM (Gibco) and incubated at 37°C. For infection studies, cell cultures were grown until an A_{600} of 1.0±0.1 was reached. For secretion assays, cultures were grown for 3-4 hours. Induction of T3SS2 follows the same protocol, except overnight cultures are diluted into MLB with 0.04 % crude bile (Sigma).

Infection of HeLa cells

Hela cells were plated on sterile coverslips in 6-well dishes at $2.5x10^5$ per well and grown for 24 hours then infected with induced POR3, POR3Δ*vpa0450*, POR3Δ*vpa0450* +VPA0450 and POR3Δ*vpa0450*+VPA0450-H356A in triplicate for each time point at an MOI of 10. At indicated time points, cells were fixed in 3.2% paraformaldehyde in 1x PBS for at least 1 hour, but no longer than 24 hours,

at 4°C, then stained and viewed as described.

LDH release assay

Hela cells were plated in 24-well dishes at $1.5x10^5$ per well, grown for 24 hours, and then washed with DMEM without phenol red or any additions. Media was removed from each culture well and replaced with 1 ml DMEM containing the appropriate induced *V. parahaemolyticus* strain at an MOI of 10. Wells were infected in triplicate for each time point unless indicated. Samples were tested using a colorimetric cytotoxicity detection kit (Takara Bio) according to manufacture's instructions, and absorbances read on a FLUOStar Optima plate reader (BMG Labtech). Data was complied using Excel and graphed with Prism GraphPad.

Transfection of tissue culture cells

For transfection experiments, $2x10^5$ Hela cells were seeded on sterile coverslips in 6-well dishes and grown for 24 hours. Cells were transfected with FuGENE HD (Roche) transfection reagent using 2 μg total DNA per well. To examine phenotype for each gene of interest, each well was transfected with 200 ng pEGFP-N1 as a transfection marker and 200 ng plasmid expressing the bacterial effector or other gene to be tested. To test localization of PH and FYVE domains, cells were transfected as above with 50 ng of pEGFP-PH(PCLδ1) or

pEGFP-2xFYVE in place of pEGFP-N1. Empty pSFFV vector was added for a total of 2 μg DNA/well. Eighteen hours after transfection, cells were fixed, stained, and cover slips mounted as described.

To confirm expression of effectors, Hela cells were plated without cover slips in 6-well dishes and transfected as described. Plates were put on ice and cells scraped to loosen adherent cells. Media was pipeted into pre-chilled eppi-tubes and centrifuged at high speed for 10 minutes at 4 °C to pellet all cells. Supernatants were removed, and 200 μl 6x SDS loading buffer added. Pellets were resuspended by pipeting, then boiled for 10 minutes. The resultant cell digests were separation by SDS-PAGE and transferred to PDVF membrane for immunoblot analysis.

Preparation of slides for confocal microscopy

After fixation, cells were permeablized for 3 minutes at room temperature in 0.1 % Triton X-100 in PBS. Nuclei were stained with Hoechst 33342 (1:1000 of a 10 mg/ml dilution, Sigma) and actin was stained with rhodamine phalloidin or Alexa 488 phalloidin (1:100, Invitrogen) followed by two washes with PBS. Cover slips were mounted to slides in 10 % glycerol with propyl gallate and sealed with clear nail polish.

Immunocytochemistry of slides

Cells were seeded onto sterile cover slips in 6-well dishes and infected or transfected as described. At indicated time points, cells were fixed in methanol for 10 minutes at -20 °C followed immediately by permeabilization with acetone for 1 minute at -20 °C. After washing with PBS, cover slips were blocked in a solution of 3 % BSA and 0.3 M glycine in PBS for 30 minutes, rinsed with PBS, then incubated overnight at 4 °C with M2 mouse anti-flag monoclonal antibody (Sigma) to detect transfected flag-tagged constructs, or mouse anti-PtdIns(4,5)P_2 monoclonal antibody (Assay Designs) to detect PtdIns(4,5)P_2 localization during infection. Coverslips were then washed three times with PBS and incubated with Alexa-fluor 594-conjugated donkey anti-mouse antibody in 3 % BSA and 1x PBS at room temperature in the dark for 1 hour. Cover slips were washed three additional times with PBS, then mounted and viewed as described.

Confocal microscopy

Transfected and infected Hela cells were visualized on a Zeiss LSM510 laser scanning confocal microscope. Images were converted and Z-stacks compiled using ImageJ and Adobe Photoshop software. Only linear adjustments were made to contrast and brightness.

Quantitation of blebbing or localization of GFP-tagged domains in Hela cells

Transfected Hela cells were visualized using the epifluorescence function of a Zeiss LSM510 laser scanning confocal microscope. Quantification of blebbing, and localization of PH(PLCδ1)-GFP and 2xFYVE-GFP, were performed by counting at least 300 transfected cells per slide, from three independent experiments per condition. The number of cells showing the described phenotype was reported as a percentage of the total number of transfected cells observed.

Bioinformatic analysis

Homologs of VPA0450 were identified by using the PSI-BLAST algorithm (www.ncbi.nlm.nih.com/blast). Pertinent hits were aligned using PROMALS (prodata.swmed.edu/promals) (96).

Purification of recombinant proteins

pGex-Tev-VPA0450, pGex-Tev-VPA0450-H356A and pET22b-SPsynj IPP5C were transformed into BL21(DE3) cells. Single colonies were grown in 2xYT to an OD_{600} of 0.8 and then induced with 0.4 mM IPTG for 16 hours at room temperature. Harvested cells were lysed using an Emulsiflex C-5 cell homogenizer (Avastin). His-tagged SPsynj IPP5C was purified using Ni^{2+} affinity beads (Qiagen) and standard purification protocols. GST-tagged VPA0450 and

VPA0450-H356A were purified using glutathione agarose beads (Sigma). His-Tev protease was added to protein bound GST-beads and the mixture incubated overnight. Flow through was collected and further cleaned by FPLC using HiTrap Q HP ion exchange (GE) and HiLoad Superdex75 (GE) gel filtration columns. Purity of each protein was determined by separation on SDS-PAGE gels and Coomassie blue staining.

Detection of inositol polyphosphate 5-phosphatase activity using a Malachite Green microtiter-plate assay

The inositol polyphosphate 5-phosphatase enzymatic activity of VPA0450 was determined by a Malachite Green assay (18, 45, 115) using synthetic phosphatidylinositol polyphosphates (Echelon) as substrates. Enzyme reactions were carried out on 96-well plates in a final volume of 20 µl. The enzyme, substrate and reaction buffer with Mg^{2+} were incubated for 15 min at 30 ºC at pH 7.0. Reactions were terminated by adding 40 µl of a cold solution of malachite green chloride (Sigma) and ammonium molybdate (Sigma). After 15 min of incubation at room temperature to let the color develop, 60 µl of 7.8 % H_2SO_4 was added to reduce the background color. After additional incubation at room temperature for 30 min, absorbance at 620 nm was measured using a FLUOstar OPTIMA plate reader (BMG Labtech) and the amount of released phosphate was calculated based on a KH_2PO_4 (Sigma) inorganic phosphate standard curve.

TABLE 4. Bacterial and Yeast Strains

E. coli

Strain	Description	Reference
DH5α	Used for cloning; F- *φ80lacZΔM15* Δ(*lacZYA*-argF)U169 *recA1 endA1 hsdR17*(rk-, mk+) *phoA supE44 thi-1 gyrA96 relA1* λ-	Invitrogen
Sm10	Used for cloning of pDM4 vectors, produces the λ-pir protein *thi*-1 *thr*-1 *leu*B6 *sup*E44 *ton*A21 *lac*Y1 *rec*A2::RP4-2-*Tc*::*Mu Kn*^{R}	A gift from D. Call
BL12(DE3)	Used for recombinant protein expression; F- *omp*T *hsd*SB(rB–, mB–) *gal dcm* (DE3)	Novagen

V. parahaemolyticus

Strain	Description	Reference
POR1	RIMD2210633 Δ*tdhA* Δ*tdhS*; Amp^R, Kan^R	A gift from T. Honda (95)
POR2	POR1Δ*vcrD1*; Amp^R, Kan^R	A gift from T. Honda (95)
POR3	POR1Δ*vcrD2*; Amp^R, Kan^R	A gift from T. Honda (95)
POR3Δ*vpa0450*	POR3 Δvpa0450; Amp^R, Kan^R, Cm^R	This study
POR3Δ*vpa0450* + VPA0450	POR3 Δvpa0450 + pLafR *vpa0450*; Amp^R, Kan^R, Cm^R, Tet^R	This study
POR3Δ*vpa0450* + VPA0450 H356A	POR3 Δvpa0450 + pLafR *vpa0450* H356A; Amp^R, Kan^R, Cm^R, Tet^R	This study
POR3Δ*vopR*	POR3 Δ*vp1683*; Amp^R, Kan^R, Cm^R	This study
POR3Δ*vopR* + VopR	POR3 Δ*vp1683* + pLafR *vp1683*; Amp^R, Kan^R, Cm^R, Tet^R	This study
CAB2	POR1Δ*exsA* (*vp1699*); Amp^R, Kan^R	This study
CAB3	POR1 Δ*vtrA* (*vpa1332*); Amp^R, Kan^R	This study
CAB3Δ*vpa0450*	CAB3 Δ*vpa0450*; Amp^R, Kan^R	This study
CAB3Δ*vopQ*	CAB3 Δ*vp1680*; Amp^R, Kan^R	This study
CAB3Δ*vopR*	CAB3 Δ*vp1683*; Amp^R, Kan^R	This study
CAB3Δ*vopQS* Δ*vpa0450*	CAB3 Δ*vp1680* Δ*vp1683* Δ*vp1686* Δ*vpa0450*; Amp^R, Kan^R	This study
CAB3Δ*vcrD1*	CAB3 Δ*1662*; Amp^R, Kan^R	This study
CAB3Δ*vscN1*	CAB3 Δ*1668*; Amp^R, Kan^R	This study
CAB4	POR1 Δ*vtrA* (*vpa1332*) Δ*exsA* (*vp1699*); Amp^R, Kan^R	This study

S. cerevisiae

BY4741	*Mat**a** his3Δ1 leu2Δ0 met15Δ0 ura3Δ0*	Research Genetics

TABLE 5. Constructs

Eukaryotic Expression Vectors

Plasmid	Description	Reference
pcDNA3.1-flag	Mammalian expression vector; Amp^R, Neo^R; P_{CMV} promoter	Invitrogen
pcDNA3 VPA0450-flag	Mammalian expression vector; Amp^R; VPA0450 cloned into BamHI and XhoI sited of pcDNA3-flag using primers MLA1 and MLA2	This study
pSFFV	Mammalian expression vector; Amp^R, Neo^R; pcDNA3 backbone with intron to increase expression	K. Orth (92)
pSFFV VPA0450-flag	Mammalian expression vector; Amp^R, Neo^R; VPA0450-flag cloned into pSFFV backbone using primers CB117 and CB128	This study
pSFFV VPA0450 a1098g	Mammalian expression vector; Amp^R, Neo^R; silent point mutation to remove internal HindIII site of pSFFV VPA0450-flag using primers CB96 and CB97	This study
pSFFV VPA0450-flag N104A	Mammalian expression vector; Amp^R, Neo^R; N104A mutant of pSFFV VPA0450-flag using primers CB88 and CB89	This study
pSFFV VPA0450-flag E136A	Mammalian expression vector; Amp^R, Neo^R; E136A mutant of pSFFV VPA0450-flag using primers MLA5 and MLA6	This study
pSFFV VPA0450-flag D261A	Mammalian expression vector; Amp^R, Neo^R; D261A mutant of pSFFV VPA0450-flag using primers CB102 and CB103	This study
pSFFV VPA0450-flag R265A	Mammalian expression vector; Amp^R, Neo^R; R265A mutant of pSFFV VPA0450-flag using primers CB94 and CB95	This study
pSFFV VPA0450-flag D355A	Mammalian expression vector; Amp^R, Neo^R; D355A mutant of pSFFV VPA0450-flag using primers MLA7 and MLA8	This study
pSFFV VPA0450-flag H356A	Mammalian expression vector; Amp^R, Neo^R; H356A mutant of pSFFV VPA0450-flag using primers CB86 and CB87	This study
pSFFV VPA0450-flag Δ367-475	Mammalian expression vector; Amp^R, Neo^R; 367-476 deletion mutant of pSFFV VPA0450-flag using primers CB132 and CB133	This study
pSFFV SPSynj1 IPP5C-flag	Mammalian expression vector; Amp^R, Neo^R; SPSynj1 IPP5C-flag cloned into pSFFV backbone using primers CB144 and CB145	This study
pEGFP-N1	Vector for expression of GFP in mammalin cells; Km^R;	ClonTech

pEGFP-C1 2xFYVE	Mammalian expression vector; Km^R; two copies of the FYVE domain from EEA1 with GFP fused to the N-terminus	A gift from N. Alto
pEGFP-N1 PH(PLC-δ1)	Mammalian expression vector; Km^R; PH domain from PLCδ1 with GFP fused to C-terminus	A gift from H. Yin
pSFFV VopR-flag	Mammalian expression vector; Amp^R, Neo^R; VopR-flag cloned into pSFFV backbone using primers MLA11 and MLA10	This study
pSFFV VopR-flag-C223A	Mammalian expression vector; Amp^R, Neo^R; C223A mutant of pSFFV VopR-flag using primers CB36 and CB37	This study
pSFFV VopR-flag-H261A	Mammalian expression vector; Amp^R, Neo^R; H261A mutant of pSFFV VopR-flag using primers CB40 and CB41	This study
pSFFV VopR-flag-D288A	Mammalian expression vector; Amp^R, Neo^R; D288AA mutant of pSFFV VopR-flag using primers CB42 and CB43	This study
pRS413 P_{Gal}	Yeast expression vector with galactose-inducible promoter	NEB
pRS413 P_{Gal} VopR	Yeast expression vector; Amp^R, *HIS3*; VopR cloned into pRS413 P_{Gal} backbone using primers MLA9 and MLA10	This study
pRS413 P_{Gal} VopR-C222A	Yeast expression vector; Amp^R, *HIS3*; C222A mutant of pRS413 P_{Gal} VopR using primers CB38 and CB39	This study
pRS413 P_{Gal} VopR-C223A	Yeast expression vector; Amp^R, *HIS3*; C223A mutant of pRS413 P_{Gal} VopR using primers CB36 and CB37	This study
pRS413 P_{Gal} VopR-H261A	Yeast expression vector; Amp^R, *HIS3*; H261A mutant of pRS413 P_{Gal} VopR using primers CB40 and CB41	This study
pRS413 P_{Gal} VopR-D288A	Yeast expression vector; Amp^R, *HIS3*; D288A mutant of pRS413 P_{Gal} VopR using primers CB42 and CB43	This study

Subcloning Vectors

Plasmid	**Description**	**Reference**
pSP72	Small vector for mutagenesis and subcloning of VPA0450 into other vectors; Amp^R	Promega
pSP72 (-700bp)-VPA0450	VPA0450 with ~700bp of upstream sequence cloned into pSP72 backbone using primers CB197 and CB198	This study
pSP72 (-700bp)-VPA0450 a1098g	silent adenosine to guanosine point mutation to remove internal HindIII site of pSP72 (-700)-VPA0450 using primers CB96 and CB97	This study

Plasmids for generating knockout strains

Plasmid	Description	Reference
pLafR	Cosmid vector used for generating marked isogenic chromosomal gene deletions in *V. parahaemolyticus*; Tet^R; IncO	A gift from L McCarter (36)
pLafR *vpa0450*	*vpa0450* with 1kb upstream and downstream flanking genomic DNA cloned into the HindIII and BamHI sites in pLafR	This study
pLafR *vpa0450*-flag	Wild type complementation vector; VPA0450-flag cloned into pLafR using primers CB197 and CB198	This study
pLafR *vpa0450*-flag H356A	Wild type complementation vector; VPA0450-flag H356A cloned into pLafR using primers CB197 and CB198	This study
pLafR *vpa0450*::cm^R	Knockout construct after λred recombination replacement of *vpa0450* with *cat*	This study
pLafR *vp1683*	*Vp1683* with 1kb upstream and downstream flanking genomic DNA cloned into the BamHI and PstI sites in pLafR using primers MLA12 and MLA13	
pLafR *vp1683*::cm^R	Knockout construct after λred recombination replacement of *vp1683* with *cat*	This study
pKD3	Plasmid with chloramphenicol acetyl transferase (*cat*) resistance marker used as PCR template for gene to replace *vpa0450* in pLafR *vpa0450* and create pLafR *vpa0450*::cm^R	A gift from L McCarter (28)
pPH1JI	Plasmid used to kick out pLafR after conjugation, and resolve merodiploid state; IncP, Gen^R, Sm^R, Spc^R, Tra^+, mob^+	A gift from L McCarter (47)
pRK2013	RK2 *tra* donor for conjugating pLAfR and pDM4 vectors into *V. parahaemolyticus*; Km^R	A gift from L McCarter (31)
pDM4	Plasmid used for generating unmarked isogenic chromosomal gene deletions in *V. parahaemolyticus*; λ-pir dependent OriR6K replication origin, Cm^R, $SacBR^+$	A gift from D. Call (136)
pDM4 ±1kb (VPA0450)	1kb upstream and downstream flanking genomic DNA of *vpa0450* cloned into the SalI, SpeI and BglII sites, respectively, of pDM4 using primers CB234, CB235, CB236 and CB237	This study
pDM4 ±1kb (VopQ)	1kb upstream and downstream flanking genomic DNA of *vp1680* cloned into the ApaI, SphI and SacI sites, respectively, of pDM4 using primers CB242, CB243, CB297 and CB298	This study

pDM4 ±0.7kb (VopR)	1kb upstream and downstream flanking genomic DNA of *vp1683* cloned into the SpeI, SphI and SacI sites, respectively, of pDM4 using primers CB246, CB247, CB248 and CB249	This study
pDM4 ±1kb (VopS)	1kb upstream and downstream flanking genomic DNA of *vp1686* cloned into the SalI, BglII and SacI sites, respectively, of pDM4 using primers CB299, CB300, CB252 and CB253	This study
pDM4 ±1kb (VcrD1)	1kb upstream and downstream flanking genomic DNA of *vp1662* cloned into the SpeI, BglII and SacI sites, respectively, of pDM4 using primers CB301, CB302, CB303 and CB304	This study
pDM4 ±1kb (VscN1)	1kb upstream and downstream flanking genomic DNA of *vp1668* cloned into the SalI, SpeI and SphI sites, respectively, of pDM4 using primers CB305, CB306, CB307 and CB308	This study

Plasmids for Recombinant Protein Expression

Plasmid	**Description**	**Reference**
pGEXrTEV	Protein expression vector; translational fusion of N-terminal glutathione S-transferase (GST) with TEV cleavage site for removal of purification tag; Amp^R	
pGEXrTEV VPA0450	Protein expression vector; GST tagged VPA0450 with TEV site for cleavage and removal of purification tag made using primers MLA1 and MLA4	This study
pGEXrTEV VPA0450-H356A	H356A mutant of pGEXrTEV VPA0450-flag using primers CB86 and CB87	This study
pET22b SPSynj1 IPP5C	Inositol polyphosphate 5-phosphatase catalytic domain cloned from Schizosaccharomyces pombe synaptojanin1 into the protein expression vector pET22b; Amp^R	A gift from J. Hurley

TABLE 6. Primers

Cloning Primers

Code	Name	Site	Tag	Sequence [a,b,c,d,f]	Tm (°C)
MLA1	F-VPA0450 BamHI-AUG-004	BamHI		GATC GGATCC ATG TCG ACA ATT CAA ATT AAT AG	58
MLA2	R-VPA0450 1491-XhoI no stop	XhoI	Flag	GATC CTCGAG TTA AAG ATT TGC CAC GAA TTG TTT AT	60
CB117	F-VPA0450 Hind3-AUG-004	HindIII		GATC AAGCTT ATG TCG ACA ATT CAA ATT AAT AG	58
CB128	R-VPA0450 1491-Flag-(UAA)-NotI	NotI	Flag-*	GATCGATC GCGGCCGC TTA CTT GTC ATC GTC GTC CTT GTA GTC AAG ATT TGC CAC GAA TTG TTT AT	60
MLA4	R-VPA0450 1491-UAA-NotI			GATCGATC GCGGCCGC TTA AAG ATT TGC CAC GAA TTG TTT AT	60
CB197	F-VPA0450 -700bp-HindIII	HindIII		GATC AAGCTT CAT GAG CCA TGA ATA AAA GAT G	58
CB198	R-VPA0450 1491-Flag-UAA-BamHI	BamHI		GATC GGATCC CTA CTT GTC ATC GTC GTC CTT GTA GTC AAG ATT TGC CAC GAA TTG TTT ATT	62
CB144	F-SPSynj1 IPP5Pase HindIII-AUG-1624	HindIII		GATC AAGCTT C ACC ATG AAC CAT GAG CTG AGA AAA AGA G	62
CB145	R-SPSynj1 IPP5Pase 2640-flag-UAA-NotI	NotI	Flag-*	GATCGATC GCGGCCGC TTA CTT GTC ATC GTC GTC CTT GTA GTC AGA AGT CTG ACT AGC ATC TC	58
CB179	F-Km^R NheI-ATG-004	NheI		GATC GCTAGC ATG AGC CAT ATT CAA CGG GA	58
CB180	R-Km^R 813-UAA-SacII	SacII		GATC CCGCGG TTA GAA AAA CTC ATC GAG CAT C	60
CB234	F-VPA0450 SalI-(-1kb)	SalI		GATC GTCGAC CAT AAC CAC AGC CGC CGC	60
CB235	R-VPA0450 SpeI-(-1kb)	SpeI		GATC ACTAGT AAA ATA AAC TCA TTT CTA AAC ATG	58
CB236	F-VPA0450 SpeI-(+1kb)	SpeI		GATC ACTAGT CCA CAG AGC CGT ATT TAT CT	60
CB237	R-VPA0450 BglII-(+1kb)	BglII		GATC AGATCT GTC GGT TAT AGC CAA GCG G	60
CB242	F-VopQ ApaI-(-1kb)	ApaI		GATC GGGCCC CAT TTG CTT TCG CTG CCG C	56
CB243	R-VopQ SphI-(-1kb)	SphI		GATC GCATGC AAC TCC CTC CTA CAC ACG C	60
CB297	F-VopQ SphI-(+1kb)	SphI		GATC GCATGC CTT TTT GCT TAT TGC ATC GAC	58
CB298	R-VopQ SacI-(+1kb)	SacI		GATC GAGCTC CTC AAC CAG TGA TGA CCG TG	62
CB246	F-VopR SpeI-(-1kb)	SpeI		GATC ACTAGT CTT AGC GCA CGA AAT AAC TC	58

CB247	R-VopR SphI-(-1kb)	SphI		GATC GCATGC GTA AAA ACC TTA AAC TTG AAT AAA C	62
CB248	F-VopR SphI-(+1kb)	SphI		GATC GCATGC TCG AGG CTT GTA CGT TGA TTT	60
CB249	R-VopR SacI-(+1kb)	SacI		GATC GAGCTC AAC TCC CTC CTA CAC ACG C	60
CB299	F-VopS SalI-(-1kb)	SalI		GATC GTCGAC GTC GTC TTA GAC GCG GTG	58
CB300	R-VopS BglII-(-1kb)	BglII		GATC AGATCT GTA GAG AAT TGG TTA GCA TCC	58
CB252	F-VopS BglII-(+1kb)	BglII		GATC AGATCT CTT AGC GCA CGA AAT AAC TC	58
CB253	R-VopS SacI-(+1kb)	SacI		GATC GAGCTC AGA TTT TTC AAA TTG CCG AGC	58
CB301	F-VP1662 (-1kb) SpeI	SpeI		GATC ACTAGT TGC AGT TGA GCT TTG AGC AAA G	64
CB302	R-VP1662 (-1kb) BglII	BglII		GATC AGATCT TAT GTA AAG ATT GCA GAT AGC G	60
CB303	F-VP1662 (+1kb) BglII	BglII		GATC AGATCT TGA ACG CAG CAC TTG TAC AAT C	64
CB304	R-VP1662 (+1kb) SacI	SacI		GATC GAGCTC TCT CTT TCA ATT GAG TCA GCG	60
CB305	F-VP1668 (-1kb) SalI	SalI		GATC GTCGAC TTA ACG TTT TGA GTT TTT GCA TG	60
CB306	R-VP1668 (-1kb) SpeI	SpeI		GATC ACTAGT TGT AAA AAA TAT GCG CAA TGA TTG	62
CB307	F-VP1668 (+1kb) SpeI	SpeI		GATC ACTAGT TCG AAC GAT TAT TAG AAA TTA AG	60
CB308	R-VP1668 (+1kb) SphI	SphI		GATC GCATGC TTA GCA GCC GCG AGT TCG	58
CB342	F-SPSyj1 IPP5Pase HindIII-AUG-1624	HindIII		GATC AAGCTT ATG AAC CAT GAG CTG AGA AAA AGA G	62
CB343	R-SPSynj1 IPP5C 2640-NotI no stop	NotI		GATCGATC GCGGCCGC AGA AGT CTG ACT AGC ATC TC	60
CB344	F-VPA0450 alpha8-10 NotI-1nt-1102	NotI		GATCGATC GCGGCCGC A TTT TCT CAA AAG TTG ATT GAA AAC	60
CB345	R-VPA0450 alpha8-10 1491-Flag-UAA-XbaI	XbaI	Flag-*	GATC TCTAGA TTA CTT GTC ATC GTC GTC CTT GTA GTC AAG ATT TGC CAC GAA TTG TTT ATT	62
CB346	F-VPA0450 delta a8-10 KpnI-004	KpnI		GATC GGTACC TCG ACA ATT CAA ATT AAT AGT CAA C	64
CB349	R-VPA0450 delta Ca8-10 1491-Flag-XbaI no stop	XbaI	Flag	GATC TCTAGA CTT GTC ATC GTC GTC CTT GTA GTC AAG ATT TGC CAC GAA TTG TTT ATT	62
MLA9	F-VopR BamHI-AUG-004	BamHI		A TCG GGA TCC ATG GTT AAT ATC AAT ACG TCA C	56
MLA10	R-VopR 975-Flag-EcoRI-*	EcoRI	Flag-*	A TCG GAA TTC TTA CTT GTC ATC GTC GTC CTT GTA GTC ACC AAG TTT GTG GCT ATC G	62

MLA11	F-VopR HindIII-AUG-004	HindIII		A TCG AAG CTT ATG GTT AAT ATC AAT ACG TCA C	56
MLA12	F-VopR BamHI-(-1kb)	BamHI		CTA GGA TCC GTA CCA AAT GTA GAA CGC GAT TAC	68
MLA13	R-VopR PstI-(+1kb)	PstI		GTT CTG CAG CGG TAG CCT GAC GGA CTG AC	66

Mutagenesis primers

Code	Name	Sequence [e,f]
CB86	F-VPA0450 H356A	T TTT GAG AAT GTC AGC GAC GCT AAG CCA GTG CAG TCA ACG
CB87	R-VPA0450 H356A	CGT TGA CTG CAC TGG CTT AGC GTC GCT GAC ATT CTC AAA A
CB88	F-VPA0450 N104A	G GTC CTG ACG TTA ACG TAC GCC CAA GCC AAC CAA AAG ATG
CB89	R-VPA0450 N104A	CAT CTT TTG GTT GGC TTG GGC GTA CGT TAA CGT CAG GAC C
CB94	F-VPA0450 R265A	G ATC ACT GGC GAT CTC AAT GAA GCT GAG AAG CGC GTT GCT GAA GG
CB95	R-VPA0450 R265A	CC TTC AGC AAC GCG CTT CTC AGC TTC ATT GAG ATC GCC AGT GAT C
CB102	F-VPA0450 D261A	AG TT CTG ATC ACT GGC GCT CTC AAT GAA CGT GAG A
CB103	R-VPA0450 D261A	T CTC ACG TTC ATT GAG AGC GCC AGT GAT CAG AAC T
MLA5	F-VPA0450 E136A	CTT ATT TGC CGA ACA AGA ATC GCT ATT GCT TGC TAA CGA CCT AGA
MLA6	R-VPA0450 E136A	TCT AGG TCG TTA GCA AGC AAT AGC GAT TCT TGT TCG GCA AAT AAG
MLA7	F-VPA0450 D355A	GAT GGT TTT GAG AAT GTC AGC GCT CAT AAG CCA GTG CAG TCA ACG
MLA8	R-VPA0450 D355A	CGT TGA CTG CAC TGG CTT ATG AGC GCT GAC ATT CTC AAA ACC ATC
CB96	F-VPA0450 nt a1098g silent	CAG TCA ACG TTC GAA GTC AGG AGC TTT TCT CAA AAG TTG AT
CB97	R-VPA0450 nt a1098g silent	AT CAA CTT TTG AGA AAA GCT CCT GAC TTC GAA CGT TGA CTG
CB132	F-VPA0450 delta nt 1102-1425	CA ACG TTC GAA GTC AGG AGC-GAA AAA TAC GAA CAG CTA AG
CB133	R-VPA0450 delta nt 1102-1425	CT TAG CTG TTC GTA TTT TTC-GCT CCT GAC TTC GAA CGT TG
CB175	F-pBAD 980-NheI-981	C AAT AAT ATT GAA AAA GGA AGA GTG CTA GCA TGA GTA TTC AAC ATT TC
CB176	R-pBAD 981-NheI-980	GA AAT GTT GAA TAC TCA TGC TAG CAC TCT TCC TTT TTC AAT ATT ATT G
CB177	F-pBAD 1841-SacII-1842	CT CAC TGA TTA AGC ATT GGT AAC CGC GGC TGT CAG ACC AAG TTT ACT C

CB178	R-pBAD 1842-SacII-1841	G AGT AAA CTT GGT CTG ACA GCC GCG GTT ACC AAT GCT TAA TCA GTG AG
CB260	F-pBAD-KnR add XbaI at AraC *	C AAT TGT CTG ATT CGT TAC CAA TCT AGA TTA TGA CAA CTT GAC GGC TAC
CB261	R-pBAD-KnR add XbaI at AraC *	GTA GCC GTC AAG TTG TCA TAA TCT AGA TTG GTA ACG AAT CAG ACA ATT G
CB36	F-VopR C223A	CAA AAT GCC AAG GCA GGT TGC GCT ACC ACA TTT GCT TTC GCT GCC
CB37	R-VopR-C223A	GGC AGC GAA AGC AAA TGT GGT AGC GCA ACC TGC CTT GGC ATT TTG
CB38	F-VopR C222A	CAA AAT GCC AAG GCA GGT GCC TGT ACC ACA TTT GCT TTC GCT GCC
CB39	R-VopR-C222A	GGC AGC GAA AGC AAA TGT GGT ACA GGC ACC TGC CTT GGC ATT TTG
CB40	F-VopR H261A	G TTT AAA AAA GGC CAT TCT GGC ACG GCC CTT TAT GTA TTG GTA GG
CB41	R-VopR-H261A	CC TAC CAA TAC ATA AAG GGC CGT GCC AGA ATG GCC TTT TTT AAA C
CB42	F-VopR D288A	CA TGG AAT AAA GAC GTA AAA ATC GTC GCT CCT TGG GCG GCG TCA G
CB43	R-VopR-D288A	C TGA CGC CGC CCA AGG AGC GAC GAT TTT TAC GTC TTT ATT CCA TG

Sequencing Primers

Code	**Name**	**Sequence** [f]	**Tm (°C)**
CB92	F-VPA0450 647-667	CTTTGGAGATCAATGGACAAC	60
CB93	R-VPA0450 828-809	CAGCACATCAGAGGCTTCAG	62
CB131	R-VPA0450 sequencing 128-107	CTGTATTCTTTACCAAATACAG	60
CB142	T7 promoter sequencing	GAAATTAATACGACTCACTATAG	60
CB161	F-VPA0450 sequencing 1292-1312	CGAGCTTTATTATCGGTAAAG	58
CB164	F-pLafR ~170bp upstream of MCS	GGGCATTCTTGGCATAGTG	60
CB181	F-pBAD 811-828 seq for KnR cassette	CCCGCCATAAACTGCCAG	58
CB182	R-pBAD 2005-1986 seq for KnR cassette	CCTTTGATCTTTTCTACGGG	58
CB194	F-SPSynj1 IPP5Pase 418-436	GCTGTTGCCATCCGATTTG	58
CB195	R-SPSynj1 IPP5Pase 638-618	GGTACGACTTCTTCATATGTC	60
CB267	F-VPA0450 seq (~210bp upstream of gene)	GACAGCCGCAGACTGACC	60
CB268	F-VopQ seq (~200bp upstream of gene)	CCGAATGGTCGACAACTTG	58

CB269	F-VopS seq (~200bp upstream of gene)	CCAGCCGTTTACTGGGAC	58
CB289	F VopR seq (~200bp upstream of gene)	GGGCGGAGTGCAGTT TTG	58
CB317	F-VP1662 - 200bp upstream for Seq	CTCGCGGTCGCGTGTTTG	60
CB318	F-VP1668 - 200bp upstream for Seq	CTATCTGACTATTGATAATACTC	60
CB364	F-pSFFV upstream of HindIII	CTCCCGTTGCGGTGCTG	58
CB361	R-pSFFV 230bp downstream of ApaI	CATGCCTGCTATTGTCTTCC	58
CB362	F-pSurf 100bp upstream of T7 promoter	CATTGACGCAAATGGGCGG	60
CB363	R-pSurf downstream of MCS	CCAGAATAGAATGACACCTAC	60
CB34	F-VopR 349-368	GACACCTCGTCTTCCAAAAC	60
CB35	R-VopR 679-659	CAAATGTGGTACAGCAACCTG	62
MLA14	F-VopR 408-430	CAAAGACAACCTTCAAAAGCTGG	66
MLA15	R-VopR 560-540	GTCGCTCTTTGATCTTGCGCG	62

[a]Blue corresponds to restriction enzyme recognition sequence
[b]Red corresponds to stop codon
[c]Green corresponds to start codon
[d]Brown corresponds to tag sequence
[e]Purple corresponds to mutated residues
[f]All primers listed 5' to 3'

CHAPTER 3

VIBRIO VPA0450 IS AN INOSITOL POLYPHOSPHATE 5-PHOSPHATASE THAT ACCELERATES HOST CELL LYSIS

Introduction

Vibrio parahaemolyticus is a Gram-negative, halophilic bacterium normally found in marine and estuarine environments (27). Originally isolated from patients during a severe gastroenteritis outbreak in Osaka, Japan in 1950 (57), *V. parahaemolyticus* is now recognized as major causative agent of gastroenteritis associated with the consumption of undercooked or raw seafood and shellfish (132). Infection with *V. parahaemolyticus* is generally self-limiting in immunocompetent patients, but may cause wound infections, fulminant necrotizing fasciitis, and often leads to death in patients with pre-existing liver pathology (27, 83, 86, 99).

Initial characterization of *V. parahaemolyticus* focused on TDH as the cause of pathogenesis. However, strains with both TDH genes deleted showed significant cytotoxicity in a tissue culture model of infection, indicating the presence of additional virulence factors (95). Sequencing of the *V. parahaemolyticus* RimD 2210633 genome identified two Type III Secretion Systems (T3SS) (71). T3SS1, on chromosome 1, is found in all *V. parahaemolyticus* strains, and is associated with cytotoxicity of cultured cells, while T3SS2, on chromosome 2, is found in clinical isolates and is associated

with enterotoxicity and fluid accumulation in a rabbit ligated ileal loop model (90, 95). We have previously characterized the T3SS2 effectors VopL and VopA/P. VopL was shown to be a potent nucleator of actin polymerization leading to stress fiber formation and alteration of cell shape (67). VopA/P was demonstrated to be an acetyltransferase targeting MKK and blocking activation of all of the MAPK signaling pathways, thereby crippling the activation of the innate immune response (117, 118). However, *V. parahaemolyticus* mutants unable to form the T3SS2 needle and translocate these and other T3SS2-specific effectors are still cytotoxic to cultured cells, indicating T3SS1 might contribute to pathogenesis.

Four T3SS1 effectors have been predicted or characterized. VopQ, VopR and VopS are encoded on chromosome 1, with their genes located within T3SS1 structural gene genomic island (16, 91). A fourth T3SS1 secreted protein, VPA0450, is located on chromosome 2 (91). We have shown that VopQ is necessary and sufficient to activate PI3K-independent autophagy by an as yet unknown mechanism (14). VopS AMPylates the switch 1 region of Rho-family GTPases, blocking interaction of these GTPases with their downstream signaling molecules. This inhibits the signaling that regulates the actin cytoskeleton, eventually leading to its collapse and the rounding of affected host cells (131). VopR currently does not have a known target or mechanism of action.

In this chapter, the cellular and biochemical activity of VPA0450 is described. We identify VPA0450 to be an inositol polyphosphate 5-phosphatase

that specifically targets a plasma membrane lipid leading to the acceleration of host cell lysis. The rapid death of targeted host cells may benefit *V. parahaemolyticus* by enabling entry of the bacteria from the lumen of the gut into underlying tissues, or through the avoidance of immune clearance.

Results

VPA0450 is necessary for rapid host cell lysis and is sufficient to induce host cell membrane blebbing

The contribution of individual effectors can often be determined by creating a deletion of the gene of interest for use in infection experiments. We generated a marked, isogenic deletion of *vpa0450* in the POR3 genetic background (POR3Δ*vpa0450*), as well as a strain complemented *in trans* with *vpa0450* (POR3Δ*vpa0450* + VPA0450). RT-PCR of a 250 bp segment of *vpa0450* was used to demonstrate deletion and complementation of *vpa0450*. Transcript for VPA0450 can be detected in the wild type POR3, and the complemented POR3Δ*vpa0450* + VPA0450 strain, but not in the deletion strain (POR3Δ*vpa0450*), indicating a successful knockout (Figure 12).

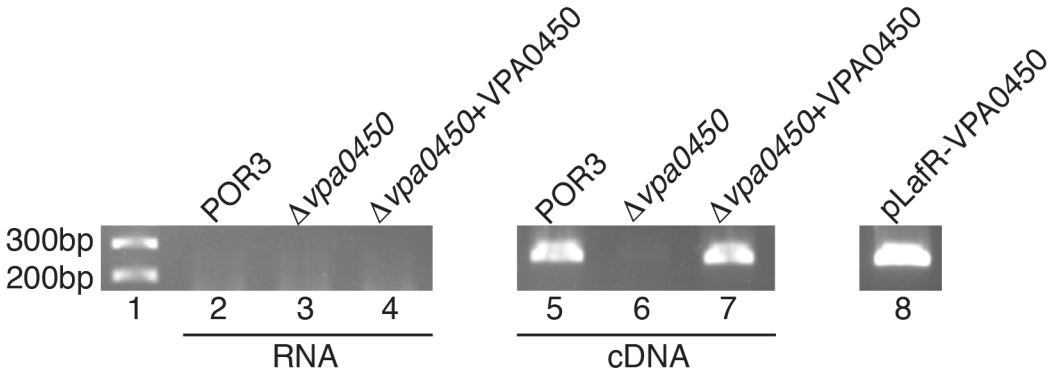

FIGURE 12. Analysis of derivatives of the POR3 strain.
POR3, POR3Δ*vpa0450*, and POR3Δ*vpa0450* + VPA0450 were induced for type III secretion, and total RNA purified. RNA was used either directly in a PCR reaction (lanes 2-4), or to synthesize cDNA templates for PCR amplification using reverse transcriptase PCR (lanes 5-7). Amplification of the 250bp segment indicates transcription of the *vpa0450* gene in the POR3 parental strain and the POR3Δ*vpa0450* + VPA0450 complemented strain, but not in the POR3Δ*vpa0450* knockout. Lane one shows the 200bp and 300bp segments of the DNA ladder, pLafR-VPA0450, used to complement the deletion strain, was included as a positive control for the PCR reaction and for size comparison.

Hela cells were infected with each of these strains to determine the contribution of VPA0450 to cytotoxicity. We found that the strain lacking VPA0450 (POR3Δ*vpa0450*) caused cell rounding faster than the POR3 parental strain or the complemented strain (POR3Δ*vpa0450* + VPA0450) (Figure 13A-C). Additionally, the POR3 and complemented strains induced transient blebbing of the host cell membrane (Figure 13D, F-H). Membrane blebs were not seen in cells infected with POR3Δ*vpa0450* (Figure 13E). Analysis of LDH release from infected cells revealed that POR3Δ*vpa0450* delayed cell lysis by approximately

one hour when compared to the POR3 and complemented strains. (Figure 14). Thus, the presence of VPA0450 contributed to the blebbing phenotype during the early stages of infection and to rapid cell lysis in the later stages.

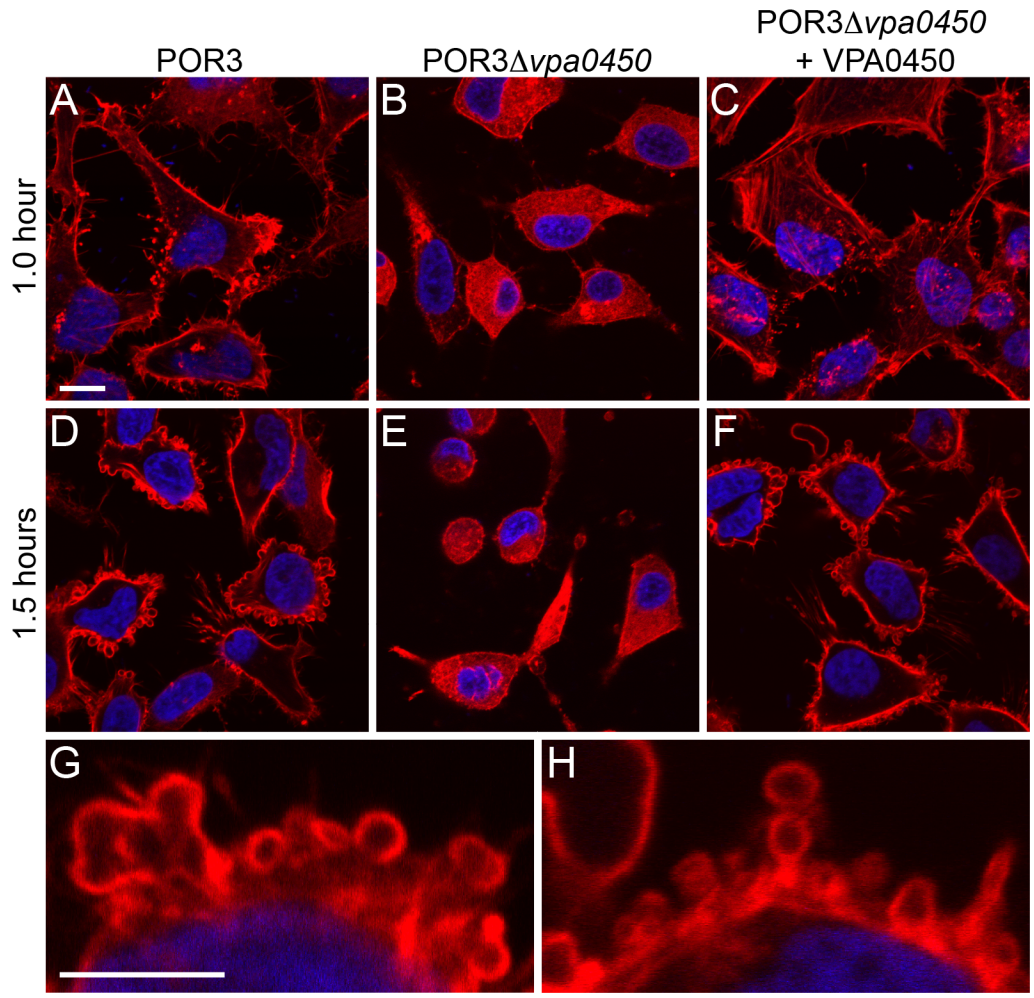

FIGURE 13. VPA0450 expression delays cell rounding and induces transient membrane blebbing.
HeLa cells infected with POR3, POR3Δ*vpa0450*, or POR3Δ*vpa0450* + VPA0450 were visualized by confocal microscopy at (**A** to **C**) 1 hour and (**D** to **F**)1.5 hours. Blebbing is shown in detail from POR3 (**G**) and POR3Δ*vpa0450* + VPA0450 (**H**) infection at 1.5 hours. Scale bars, 20 μm. Actin was stained with rhodamine-phalloidin (red), and nuclei were stained with Hoechst (blue).

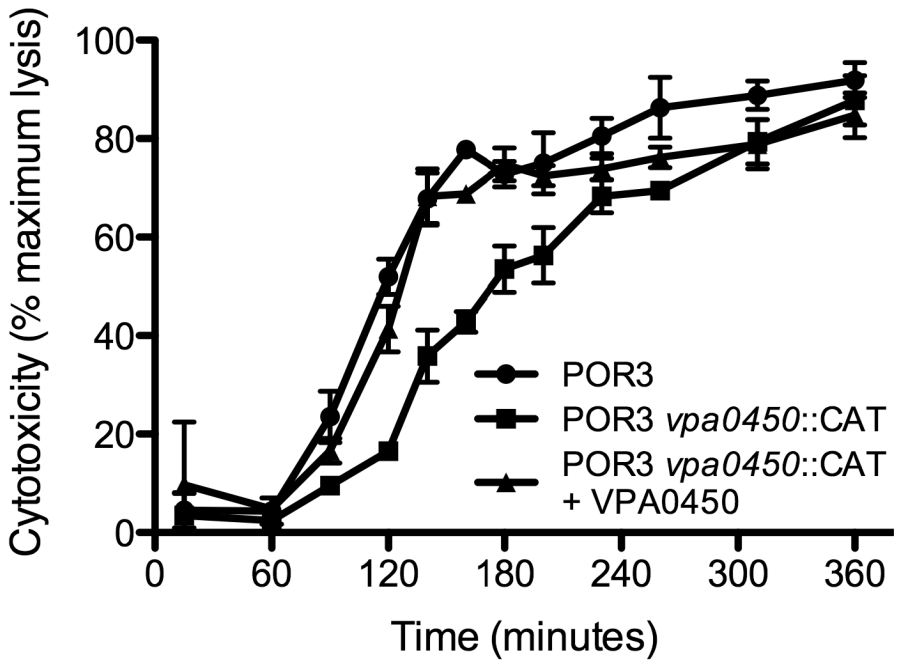

FIGURE 14. VPA0450 is required for rapid host cell lysis during infection with *V. parahaemolyticus*.
Hela cells were infected with POR3 (circles), POR3Δ*vpa0450* (squares), or POR3Δ*vpa0450* + VPA0450 (triangles), and lactate dehydrogenase (LDH) release was evaluated as a measure of cytotoxicity and host cell lysis. Data are means ± SD (n = 3 samples) from a representative experiment repeated in triplicate.

These experiments showed a correlation between VPA0450 and rapid host cell lysis. We next investigated whether VPA0450 alone was sufficient to lyse cells. Hela cells were transfected with GFP and either empty vector or VPA0450-flag. While cells transfected with the empty vector remained flat and showed a normal phenotype (Figure 15A), those transfected with VPA0450-flag did not lyse. Instead, significant portions of these cells were covered in small membrane blebs consistent with those seen during infection (Figure 15B). Blebs appeared not only on the surface of the cell, but also on other blebs (Figure 15C). Thus, VPA0450 is not sufficient to lyse cells, but does dramatically change the surface of transfected cells.

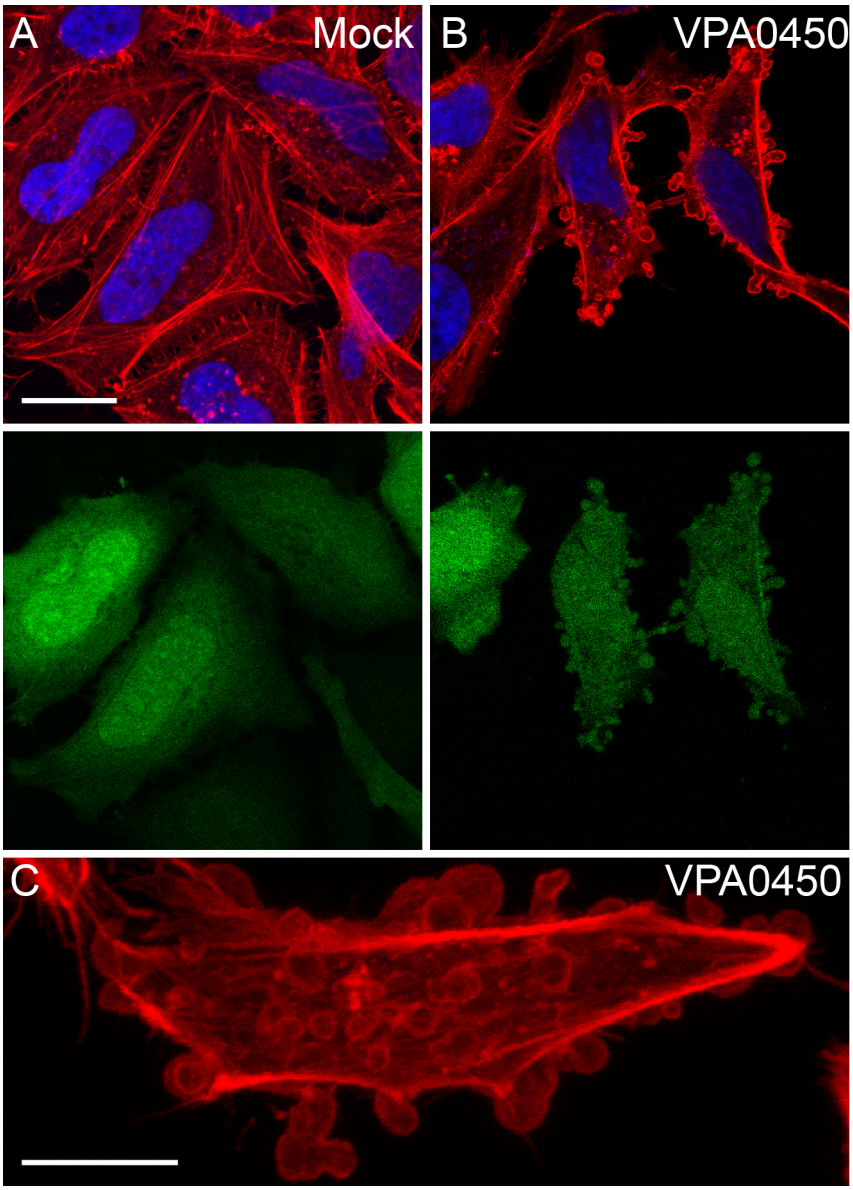

FIGURE 15. VPA0450 is sufficient to induce membrane blebbing.
Hela cells were transfected with pEGFP-N1 and empty pSFFV vector (**A**) or pSFFV-VPA0450-flag (**B**) and imaged by confocal microscopy. Scale bar 20μm. (**C**) A representative cell transfected with pSFFV-VPA0450-flag was Z-stacked and the maximun intensity projection displayed to show the extent of cellular blebbing seen during VPA0450 expression. Scale bar, 5 μm. Expression of green fluorescent protein (green) denotes transfected cells. Actin was stained with rhodamine-phalloidin (red), and nuclei were stained with Hoechst (blue).

Identification of homologous bacterial effectors and a eukaryotic domain

To identify an activity for VPA0450, the primary amino acid sequence was used in a BLAST search against the non-redundant protein sequences database, resulting in the identification of two bacterial effector homologs. VPA0450 shares 93% identity with PLU4615 from the entemopathogenic nematode commensal *Photorhabdus luminescens* TTO1, and 87% identity with Ati2 from *Aeromonas salmonicida* A449, the causative agent of furunculosis in salmonid fish which is of significant importance to the fisheries industry (Figure 16) (101). Each of these organisms also encodes a chaperone with homology to VPA0451, the predicted chaperone of VPA0450. While PLU4615 and Ati2 have been annotated as potential effectors, they are currently uncharacterized. However, all three have homology to the endonuclease/exonuclease/phosphatase family of enzymes, hinting at a potential biochemical activity.

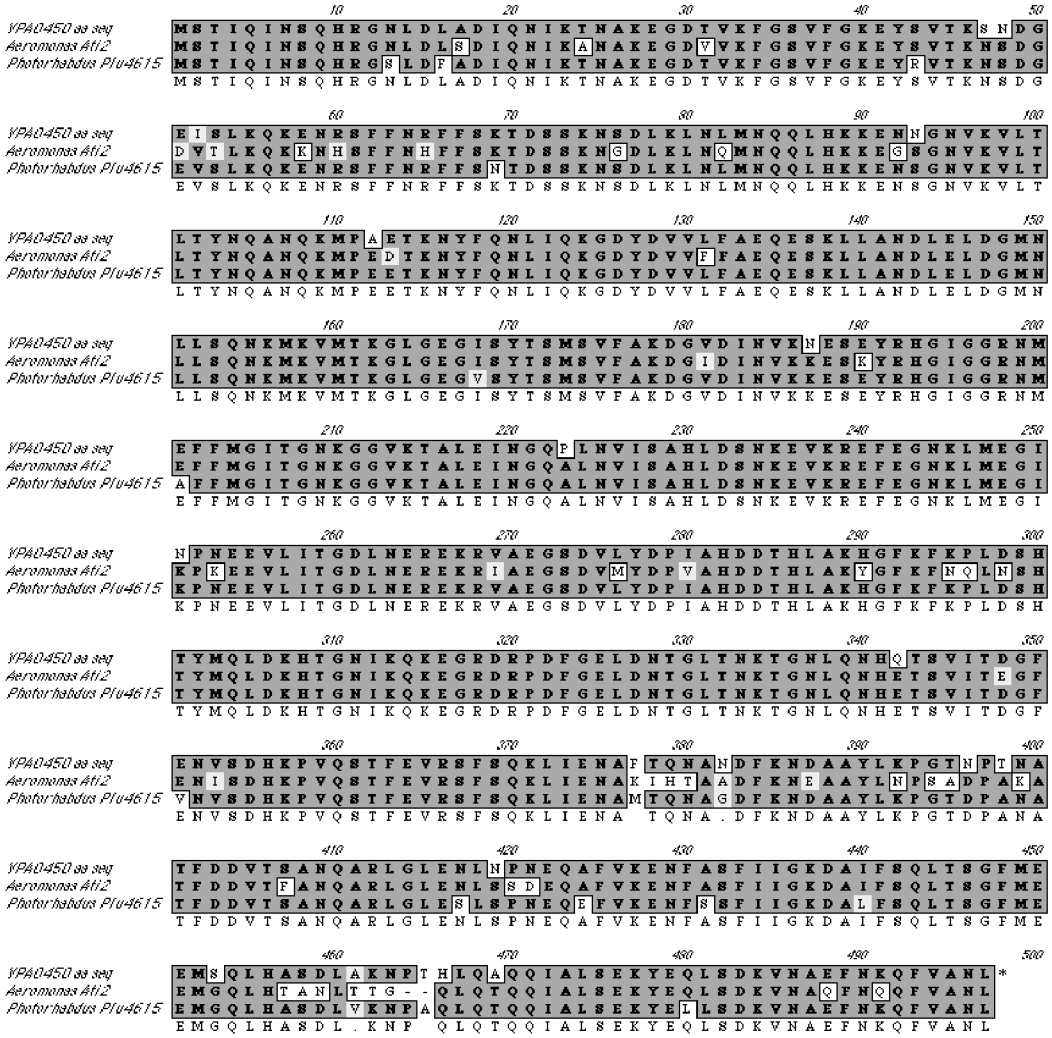

FIGURE 16. VPA0450 is homologous to other uncharacterized effectors.
The sequences of *V. parahaemolyticus* VPA0450, *Aeromonas salmonicida* Ati2, and *Photorhabdus luminescens* PLU4615 were aligned to show the high level of identity at the amino acid level.

Further bioinformatic analysis revealed that VPA0450 has homology to the eukaryotic protein synaptojanin (Figure 17A), a multi-domain enzyme that plays a role in the recycling of vesicles in neurons (11). Synaptojanin consists of a

Sac1 phosphatase domain, an inositol polyphosphate 5-phosphatase domain, and a proline rich region.

The Sac1 domain is a promiscuous inositol polyphosphate phosphatase that hydrolyses phosphate from PtdIns(3)P PtdIns(4)P, and PtdIns(3,5)P_2 to yield PtdIns, but cannot remove phosphates PtdIns(4,5)P_2 (44). The T3S effectors SigD and SopB from *Salmonella spp*. are homologous to the Sac1 domain, and are necessary for phagocytosis and maintaining the *Salmonella* containing vacuole (SCV) during intracellular infection by that pathogen (72).

The inositol polyphosphate 5-phosphatase catalytic domain (IPP5C), to which VPA0450 is homologous, specifically removes the D5 phosphate from PtdIns(4,5)P_2 (125). This domain is associated with regulation of intracellular calcium signaling, cell motility, and actin dynamics (26, 100, 125). The crystal structure has been solved for the IPP5C domain from the fission yeast *Schizosaccharomyces pombe* synaptojanin (SPSynj) (120), providing information on residues important for binding of substrate as well as catalysis of the hydrolysis reaction. Alignment of VPA0450 with this domain revealed conservation of five of the six catalytic motifs, including conservation of the putative catalytic base, His356 in VPA0450 (Figure 17B).

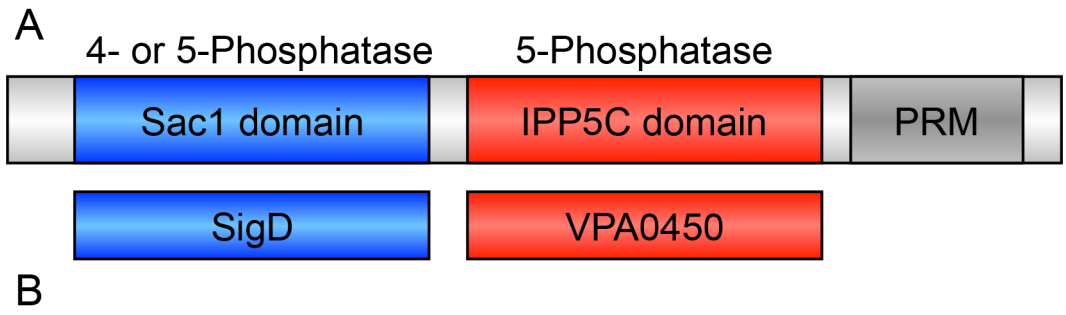

B

```
Catalytic motifs
V.para VPA0450      1  MSTIQINSQHRGNLDLADIQNIKTNAKEGDTVKFGSVFGKEYSVTKSNDGEISLKQKENRSFFNRFFSKT
SPsynj IPP5C        1  -------------YDP-----------------------------------------------IHEYV---
Consensus_ss:             eeee          hhhhhhh         eeeeehh    eeeeee     eeeee    hhhhhhhh

Catalytic motifs                                        TWN                                GxQE
V.para VPA0450     71  DSSKNSDLKLNLMNQQLHKKENNGNVKVLTLTYNQANQKMPAETKNYFQNLIQKGDYDVVLFAEQE----
SPsynj IPP5C        9  ---------NHELRKRENEFSEHKNVKIFVASYNLNGCSATTKLENWLF-PENTPLADIYVVGFQEIVQL
Consensus_ss:                 eehhhhhhhhhh     eeeeeeeeee       hhhhhhhhhhh     eeeeeee

Catalytic motifs
V.para VPA0450    137  --SKLLANDLELDGMNLLSQNKMKVMTKGLGEGISY----------TSMSVFAKDGVDINVKNESEYRHG
SPsynj IPP5C       69  TPQQVISADPAK--RREWESCVKRLLNGKCTSGPGYVQLRSGQLVGTALMIFCKE-------SCLPSIKN
Consensus_ss:           hhhhhh   hh  hhhhhhhhhhhhhhhh     eeeeeeeee  eeeeeeeeh  eeee hhhhhh

Catalytic motifs                                        NxH
V.para VPA0450    195  IGGRNMEF-FMGITGNKGGVKTALEINGQPLNVISAHLDSN--KEVKREFEGNKLMEG--------INPN
SPsynj IPP5C      130  VEGTVKKTGLGGVSGNKGAVAIRFDYEDTGLCFITSHLAAGYTNYDERDHDYRTIASGLRFRRGRSIFNH
Consensus_ss:              eeee eeee     eeeeeeee   eeeehhhh     hhhhhhhhhhhhhhhhh

Catalytic motifs           GDxNxR
V.para VPA0450    254  EEVLITGDLNER--------EKRVAEGSDVLYDPI-AHDD------THLAKHGF-----KFKPLDSHTYM
SPsynj IPP5C      200  DYVVWFGDFNYRISLTYEEVVPCIAQGK---LSYLFEYDQLNKQMLTGKVFPFFSELPITFPP----TY-
Consensus_ss:           eeeeeee  hhe   hhhhhhhhh    eehhhhhhhhhhhhhhhhhhhh              ee

Catalytic motifs                                PxWxDR                        SDHxPV
V.para VPA0450    304  QLDKHTGNIKQKEGRDRPDFGELDNTG------LTNKTGNLQNHQTSVITDGFENVSDHKPVQSTFEVRS
SPsynj IPP5C      262  ---------KFDIGTDIYDTSDKHRVPAWTDRILYRGELVPHSYQSVPLY-----YSDHRPIYATYEAN-
Consensus_ss:           ee       hhh                   eeeeeeeeeeeeeeeeee     e     ehhhhhhhh

Catalytic motifs
V.para VPA0450    368  FSQKLIENAFTQNANDFKNDAAYLKPGTNPTNATFDDVTSANQARLGLENLNPNEQAFVKENFASFIIGK
SPsynj IPP5C      317  ----------------------------------------IVKVDR----------------------------
Consensus_ss:           hhhhhhhhhhh                          hhheee  hhh         hhhhhhhhhhhhh  h

Catalytic motifs
V.para VPA0450    438  DAIFSQLTSGFMEEMSQLHASDLAKNPTHLQAQQIALSEKYEQLSDKVNAEFNKQFVA--NL-
SPsynj IPP5C      323  ---------------------------------------EKKKILFEELYNQRKQEVRDASQTS
Consensus_ss:           hhhhhhhhhhhhhhhhhhhhhhhh  hhhhhhhhhhhhhhhhhhhhhhhhhhhhhhhh
```

FIGURE 17. VPA0450 is homologous to the IPP5C domain of synaptojanin. (**A**) The architecture of synaptojanin is shown, including catalytic domains and their specific activities, as well as representative homologous bacterial effectors. (**B**) Alignment of primary sequences of VPA0450 and the IPP5C from *Schizosaccharomyces pombe* synaptojanin (SPSynj IPP5C) show the conservation of catalytic motifs (green) and predicted secondary structure (Red, alpha helix; blue, beta strand). Residues mutated for this study are highlighted in yellow.

Overexpression of Inp54, an IPP5C domain homolog from *Saccharomyces cerevisiae*, was previously shown to induce cellular blebbing (100). Expression of the SPSynj IPP5C in Hela cells results in cellular blebbing similar to, albeit at a much lower level than, that seen with VPA0450 (Figure 18) indicating they may have a shared mechanism.

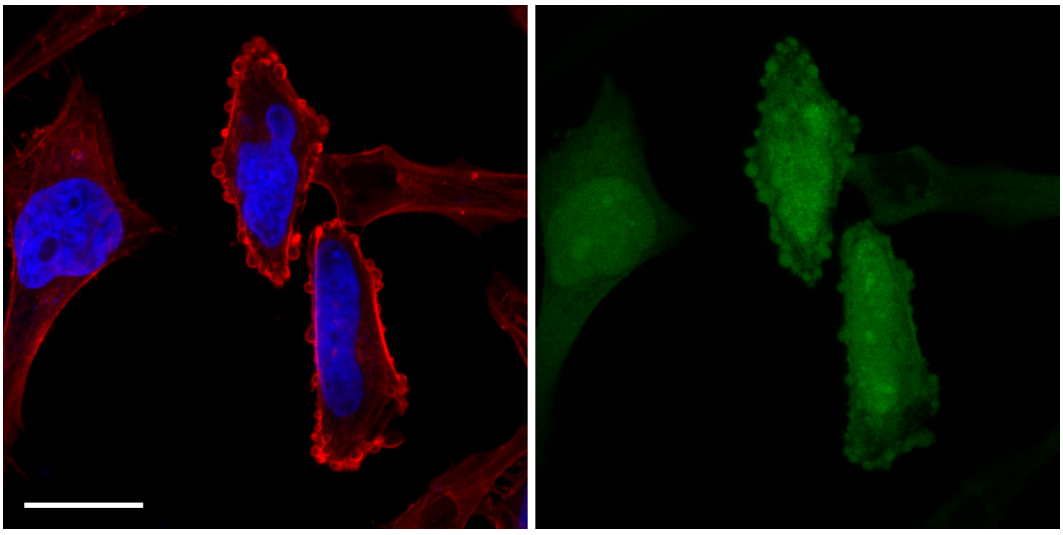

FIGURE 18. SPsynj IPP5C is sufficient to induce membrane blebbing.
Hela cells transfected with pEGFP-N1 and the IPP5C domain from SPsynj induce plasma membrane blebbing similar to that seen with VPA0450. Expression of green fluorescent protein (green) denotes transfected cells. Actin was stained with rhodamine-phalloidin (red), and nuclei were stained with Hoechst (blue). Scale bar, 20μm.

VPA0450 shares catalytic and substrate coordinating residues with SPSynj IPP5C

The similarities between VPA0450 and SPSynj IPP5C with regard to phenotype, catalytic motifs and predicted secondary structure (Figure 17) indicate VPA0450 may have an inositol polyphosphate 5-phosphatase activity. This activity is sufficient to alter membrane dynamics during infection and transfection leading to membrane blebbing. To determine the level of similarity between VPA0450 and SPSynj IPP5C, site directed mutagenesis was used to mutate the putative catalytic histidine and the substrate-coordinating residues to alanine residues. Each of these constructs was transfected into Hela cells (Figure 19A-E) and the number of transfected cells with blebs quantified (Figure 19F and G). While the wild type VPA0450 construct induced membrane blebbing in 40-45% of transfected cells, this number dropped to approximately 20% for the protein containing mutants in residues predicted to be involved in coordinating substrate binding (N104A, D261A, R261A and D355A). In stark contrast, mutation of the histidine predicted to be the catalytic base reduced blebbing to 3% of transfected cells. By comparison, blebbing was seen in 2% of cells transfected with wild type SPSynj IPP5C (Figure 19F). The dramatic contrast in activity between VPA0450 and SPsynj IPP5C is surprising but not unprecedented as T3S effectors many times are more active and unregulated enzymes compared to their endogenous homologs.

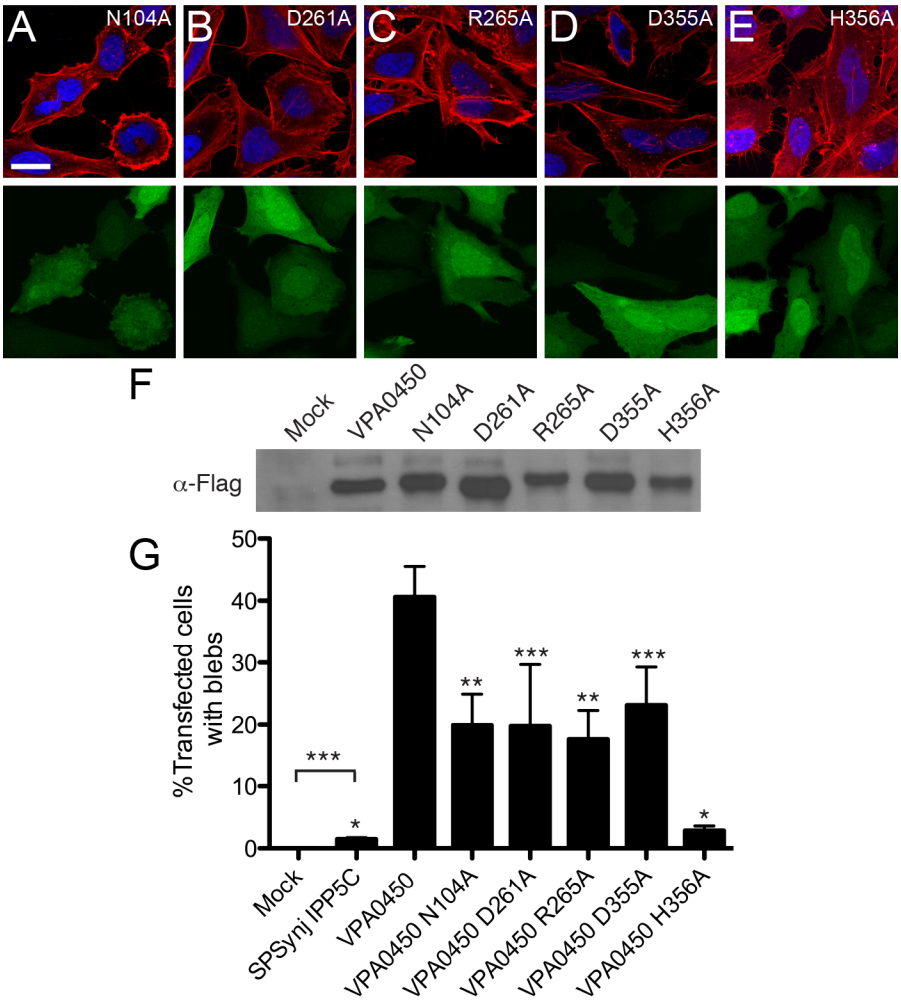

FIGURE 19. VPA0450 mutants show a diminished ability to cause blebbing. Select residues homologous to those found in SPSynj IPP5C catalytic motifs were mutated in VPA0450. Hela cells were then transfected with pEGFP-N1 and pSFFV-VPA0450-N104A-flag (**A**), pSFFV-VPA0450-D261A-flag (**B**), pSFFV-VPA0450-R265A-flag (**C**), pSFFV-VPA0450-D355A-flag (**D**), or pSFFV-VPA0450-H356A-flag (**E**), and visualized by confocal microscopy. Expression of green fluorescent protein (green) denotes transfected cells. Actin was stained with rhodamine-phalloidin (red), and nuclei were stained with Hoechst (blue). Scale bar, 20μm. (**F**) A western blot confirmed expression of each construct. (**G**) Quantification of blebbing in Hela cells transfected with empty vector, SPsynj IPP5C, VPA0450 or VPA0450 point mutants. Data are means ± SD from three independent experiments. Asterisks refer to statistically significant differences between VPA0450 transfected cells and the other constructs (*, $P<0.001$; **, $P<0.01$; ***, $P<0.05$, $N=3$) using a pair wise, two-tailed *t*-test.

These data support the hypothesis that the catalytic pocket of VPA0450 is similar to that of the SPSynj IPP5C domain. To directly test for inositol polyphosphate phosphatase activity, a malachite green assay was performed on purified recombinant VPA0450, VPA0450-H356A, and SPSynj IPP5C with synthetic phosphoinositides. We found that rVPA0450 and rSPSynj IPP5C, but not rVPA0450 H356A were able to hydrolyze PtdIns(4,5)P_2, and to a lesser extent PtdIns(3,4,5)P_3 (Figure 20A and C). None of these proteins was able to hydrolyze PtdIns(3,4)P_2 (Figure 20B). This indicates that VPA0450 is a D5-specific phosphatidylinositol phosphatase with substrate preference for PtdIns(4,5)P_2, and has an activity profile that matches that of SPSynj IPP5C (Figure 20).

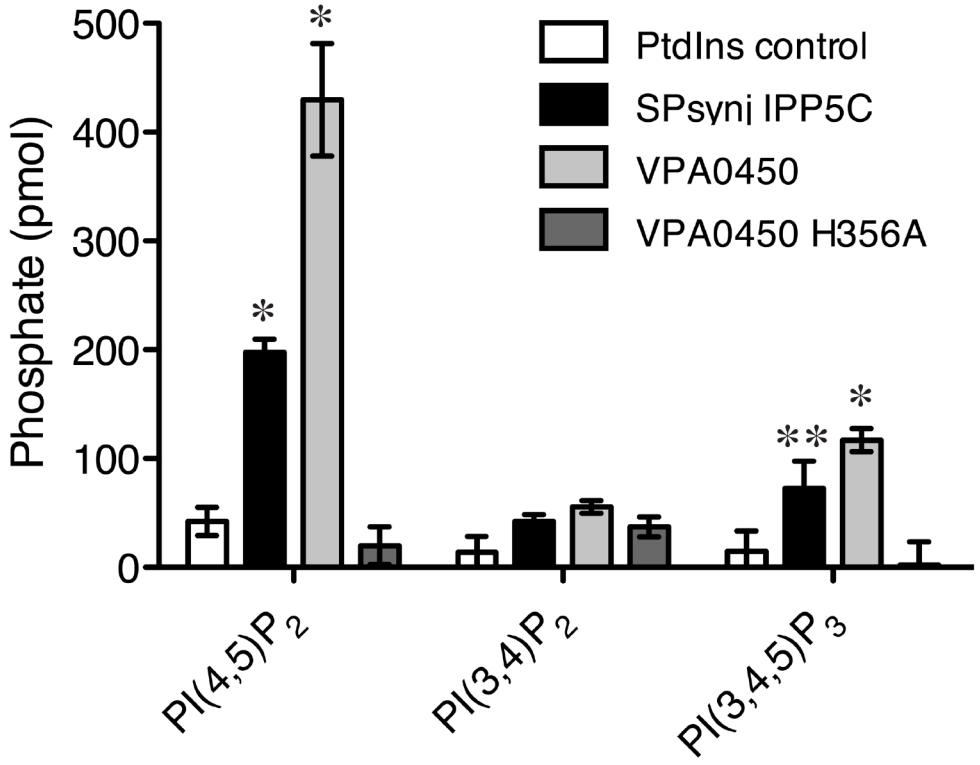

FIGURE 20. VPA0450 has inositol polyphosphate 5-phosphatase activity. Phosphatase activity was measured for rSPsynj IPP5C, rVPA0450, and rVPA0450-H356A on phosphatidylinositol (4,5) bisphosphate di-C8 ($PI(4,5)P_2$), phosphatidylinositol (3,4) bisphosphate di-C8 ($PI(3,4)P_2$), and phosphatidyl-inositol (3,4,5) triphosphate di-C8 ($PI(3,4,5)P_3$), using the malachite green assay to detect inorganic phosphate release. Asterisks refer to statistically significant differences between PtdIns control and each recombinant protein for a given substrate (*, $P<0.001$; **, $P<0.01$, $N=3$) using a pair wise, two-tailed *t*-test.

The phosphatase activity of VPA0450 disrupts the interaction between the plasma membrane and the actin cytoskeleton

There are two general mechanisms for the formation of dynamic blebs in eukaryotic cells. A disruption or tearing of the actin cortex can lead to regions of unsupported plasma membrane. As the pressure inside a cell is greater than outside, the membrane is forced outward to establish equilibrium, forming a bleb. The second mechanism leaves the actin cortex intact, but disconnects the membrane from the actin with the same final result. We hypothesized that VPA0450 forms membrane blebs by hydrolyzing PtdIns(4,5)P_2. Loss of PtdIns(4,5)P_2 can disrupt the connection of actin binding proteins that associate with PtdIns(4,5)P_2 in the membrane, allowing formation of dynamic blebs (30).

To test this hypothesis, a GFP-tagged pleckstrin homology domain from phospholipase C-δ1 (PH(PLCδ1)-GFP) was transfected into Hela cells with either empty vector, VPA0450-flag, or VPA0450-H356A-flag. PH(PLCδ1) binds specifically to PtdIns(4,5)P_2, which occurs primarily at the plasma membrane, and should therefore localize to this membrane as long as PtdIns(4,5)P_2 levels are not substantially decreased (30). In cells expressing PH(PLCδ1)-GFP and either empty vector or VPA0450-H356A-flag, a ring of GFP can be seen around the border of the cells, indicating proper association with the plasma membrane (Figure 21A, C-F). When VPA0450 is expressed, the GFP becomes localized in the cytoplasm and bleb interior, indicating PH(PLCδ1)-GFP is no longer

associated with the membrane as a direct result of the active form of VPA0450 (Figure 21B, D-F). This confirms that the catalytic activity of VPA0450 is sufficient to disrupt the binding of PtdIns(4,5)P_2 associated proteins, leading to membrane blebbing. 2x-FYVE-GFP binds specifically to PtdIns(3)P, enriched on endosomes (53). Hela cells transfected with a 2x-FYVE-GFP domain and either empty vector, VPA0450-flag, or VPA0450-H356A-flag all resulted in GFP punctae in the cytoplasm (Figure 22A-F). While this data indicates VPA0450 did not hydrolyze PtdIns(3)P on the endosomes, it is not possible to determine if this is due to a lack of activity towards this phosphoinositide, or localization to a different region of the cell.

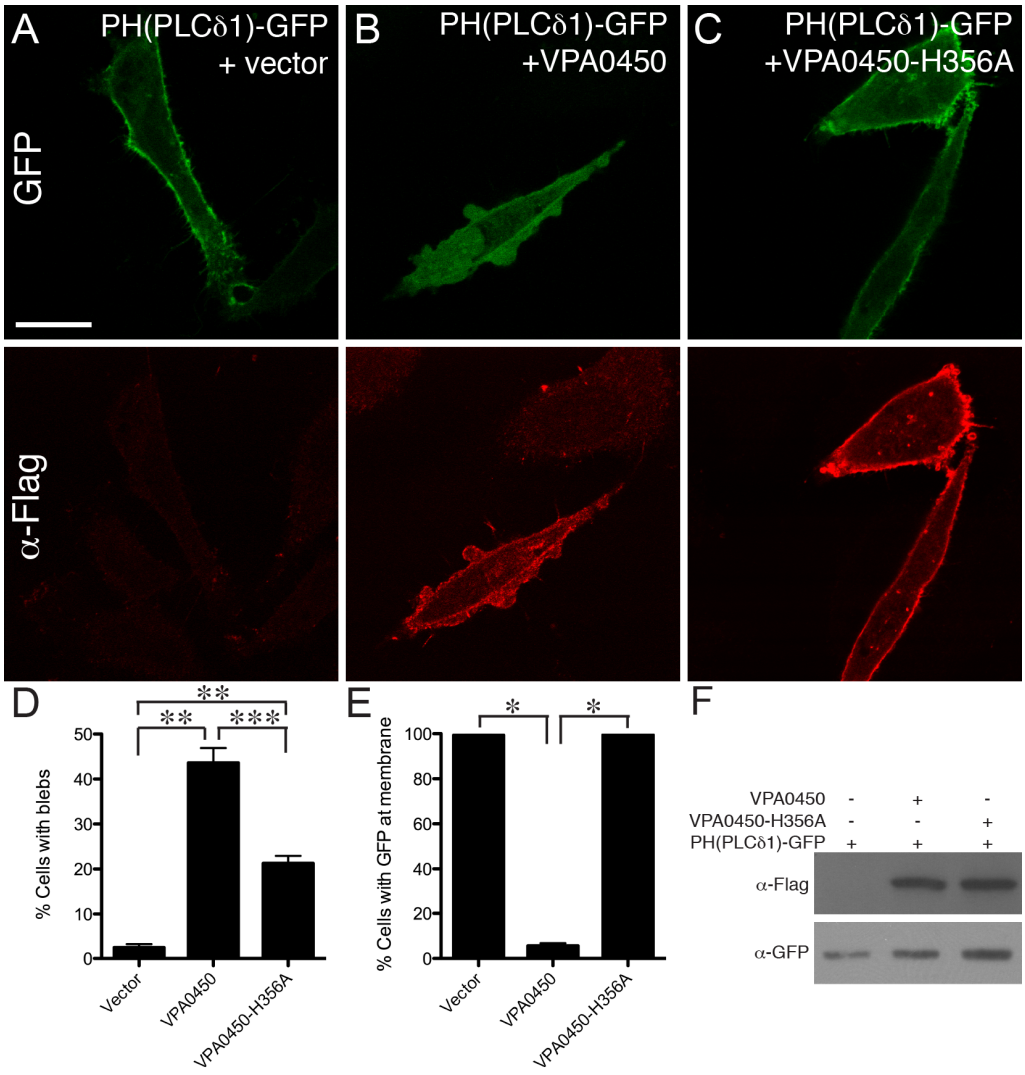

FIGURE 21. VPA0450 can delocalize a PH domain from the plasma membrane.

Hela cells were transfected with PH(PLCδ1)-GFP and either empty vector (**A**), pSFFV-VPA0450-flag (**B**) or pSFFV-VPA0450-H356A-flag (**C**) and visualized by confocal microscopy. Green denotes expression of PH(PLCδ1)-GFP and red denotes expression of VPA0450-flag. Scale bar, 20μm. These transfections were quantified for their number of blebbing cells (**D**) and cells with GFP at the membrane (**E**). Data are means ± SD from three independent experiments. Asterisks refer to statistically significant differences between cells transfected with each construct (*, $P<0.001$; **, $P<0.01$; ***, $P<0.05$, $N=3$) using a pair wise, two-tailed *t* test. (**F**) Western blot confirming expression of PH(PLCδ1)-GFP and VPA0450 constructs.

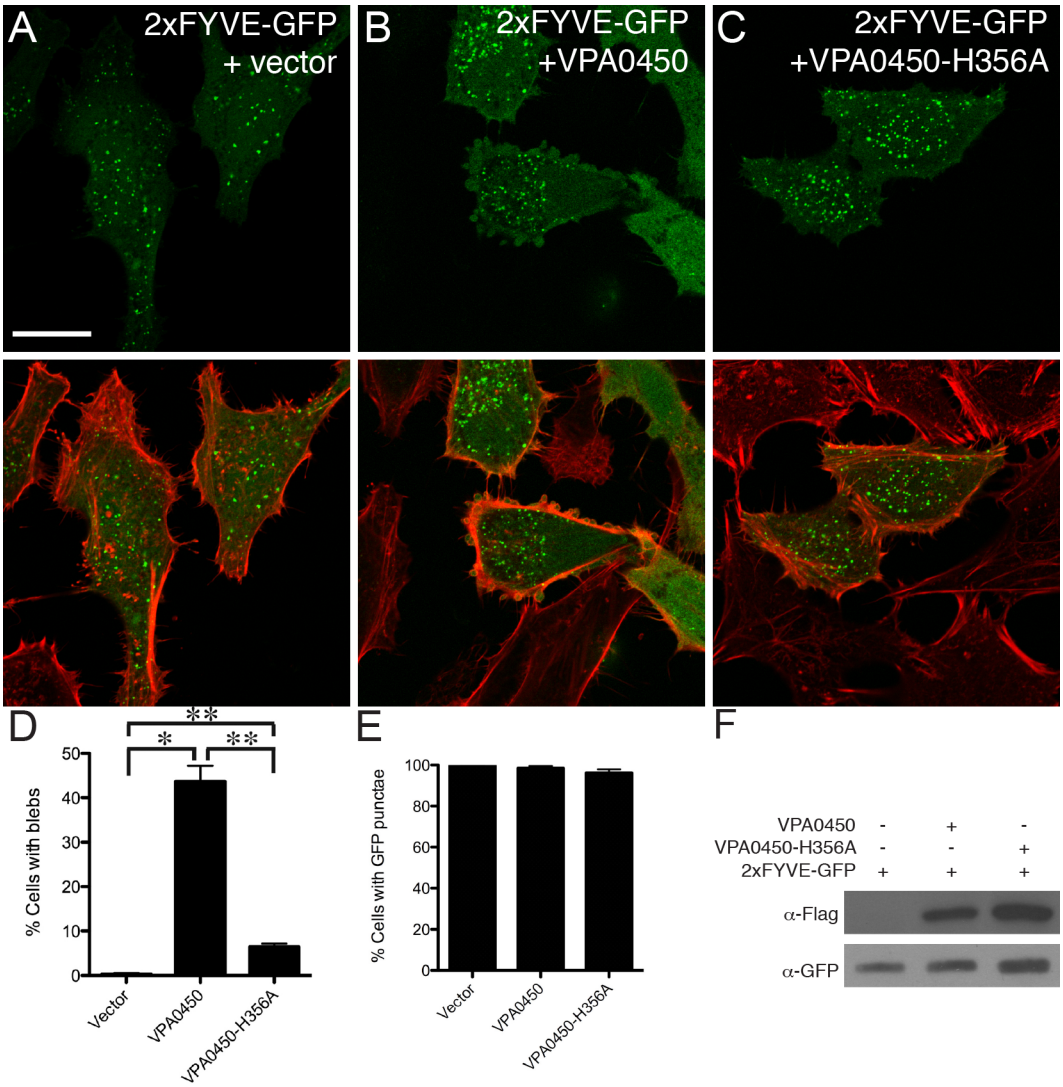

FIGURE 22. VPA0450 does not delocalize phosphatidylinositol 3-phosphate binding proteins in transfected cells.

Hela cells were transfected with 2xFYVE-GFP and either (**A**) empty vector, (**B**) pSFFV-VPA0450, or (**C**) pSFFV-VPA0450-H356A and visualized by confocal microscopy. Expression of green fluorescent protein (GFP, green) denotes localization of 2x-FYVE domain. Actin was stained with rhodamine-phalloidin (red). Scale bars, 20 μm. Transfections were quantified for the percentage of (**D**) blebbing cells and (**E**) cells with GFP punctae. Data are means ± SD from three independent experiments. Asterisks refer to statistically significant differences between cells transfected with each construct (*, $P<0.001$; **, $P<0.01$; $n = 3$) using a pairwise, two-tailed *t* test. (**F**) Western blot confirming expression of 2x-FYVE-GFP and VPA0450 constructs.

To further demonstrate that the catalytic activity of VPA0450 is that of an IPP5C, and that the activity seen in transfection experiments is relevant during infection, Hela cells were infected with POR3, POR3Δ*vpa0450*, or POR3Δ*vpa0450* + VPA0450, and the presence of PtdIns(4,5)P_2 analyzed by immunohistochemistry using a mouse anti-PtdIns(4,5)P_2 primary antibody. Cells either mock infected or infected with POR3Δ*vpa0450* had staining at the border of the cell indicating the presence of PtdIns(4,5)P_2 (Figure 23A and C), while cells infected with POR3 wild type or the complemented deletion strain showed loss of staining as a result of VPA0450-mediated PtdIns(4,5)P_2 hydrolysis (Figure 23B and D). VPA0450 is able to destroy docking sites for PtdIns(4,5)P_2-specific PH domains, disrupting the interaction between the plasma membrane and actin cortex, leading to blebbing and accelerated host cell lysis during infection.

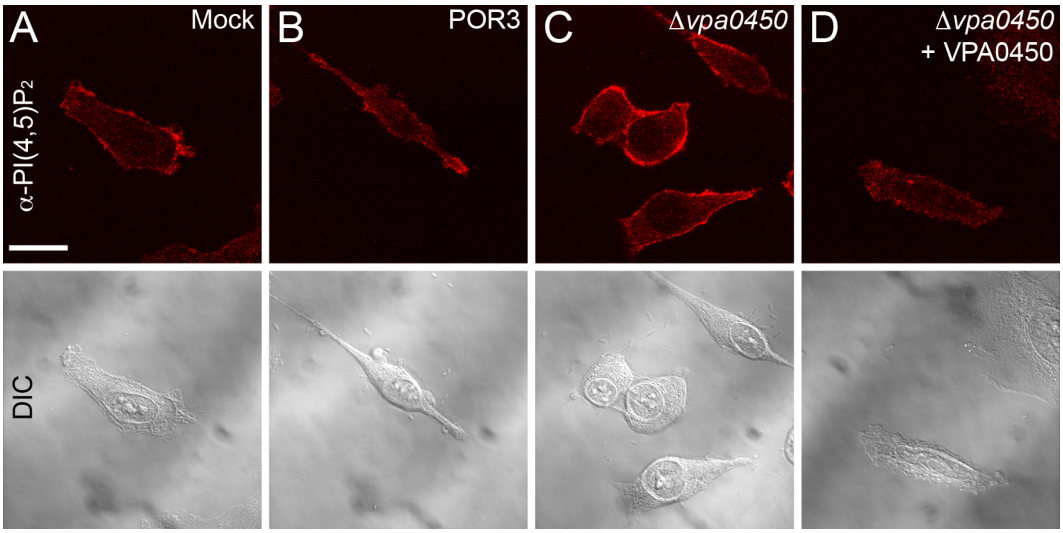

FIGURE 23. VPA0450 disrupts PtdIns(4,5)P_2 at the plasma membrane.
Hela cells were mock infected (**A**), or infected with POR3 (**B**), POR3Δ*vpa0450* (**C**), or POR3Δ*vpa0450* + VPA0450 (**D**) and analyzed for the location of PtdIns(4,5)P_2 by immunohistochemistry with a mouse anti-PtdIns(4,5)P_2 primary antibody and Alexa fluor 548-conjugated donkey anti-mouse secondary antibody (top panels). DIC images in lower panels show cell shape and location.

Discussion

There are a number of Gram-negative bacterial pathogens that use T3S to manipulate host cells to facilitate the infection process. The specific repertoire of effectors encoded by a particular pathogen determines how the disease will progress, and what the end result will be at a cellular and organismal level. To understand the disease process, the individual effectors must first be characterized. With the characterization of VPA0450, we are one step closer to fully understanding how *V. parahaemolyticus* causes disease.

T3SS1 of *V. parahaemolyticus* induces a multifaceted cell death by first inducing autophagy, followed by cell rounding, and ultimately cell lysis. This study examined the contribution of VPA0450 to this process. We have shown that this effector was not sufficient to cause cell lysis on its own but did induce membrane blebbing in about half of the transfected cells. Infection with the POR3 and complemented *vpa0450* deletion strains (POR3Δ*vpa0450* + VPA0450) resulted in a transient membrane blebbing prior to cell rounding. Blebbing was not seen in cells infected with the deletion strain (POR3Δ*vpa0450*), although they did progress more quickly to a rounded state. It is currently not understood how the activity of VPA0450 is able to delay cell rounding, although this may be related to the order of effector translocation into the infected cell. The absence of VPA0450 in the POR3Δ*vpa0450* strain may allow accelerated translocation of VopS, which has been previously shown to induce cell rounding (131). LDH release assays of cells infected with each of these strains showed that VPA0450 accelerated host cell by about 1 hour.

Bioinformatic analysis indicated that VPA0450 has homology to the IPP5C domain of synaptojanin. Transfection of SPsynj IPP5C induced membrane blebbing in Hela cells, albeit at a lower level than that seen in cells transfected with VPA0450. SPsynj IPP5C is a catalytic domain, and is lacking its endogenous localization motif. A lack of proper localization to the plasma membrane may cause the diminished activity seen with SPsynj IPP5C relative to VPA0450.

VPA0450 contains three C-terminal alpha helices that are not homologous to SPsynj IPP5C and may act as a localization domain. The ability of this domain to localize VPA0450, and the effect it has on activity in a host cell, will be examined in the next chapter.

When residues in VPA0450 that are homologous to those important for substrate binding or catalysis in SPSynj IPP5C were mutated, we observed a significant decrease in blebbing. Additionally, VPA0450 demonstrated *in vitro* phosphatase activity against synthetic inositides, specifically removing the D5 phosphate from PtdIns(4,5)P_2, and to a lesser extent PtdIns(3,4,5)P_3, which is the same catalytic activity and substrate specificity observed for SPSynj IPP5C.

We next wanted to determine how the phosphatase activity of VPA0450 could cause blebbing and contribute to the infection process. Dynamic blebs can normally occur in cells when the connection between the plasma membrane and actin cytoskeleton is disrupted. To determine how VPA0450 caused blebbing, the PH domain from PLCδ1, which binds specifically to PtdIns(4,5)P_2 (5), was tagged with GFP and transfected into Hela cells along with either empty vector, VPA0450, or VPA0450 H356A. Only wild type VPA0450 was able to delocalize PH(PLCδ1)-GFP off the membrane. This indicates that the phosphatase activity of VPA0450 is sufficient to disrupt binding of PtdIns(4,5)P_2-specific PH domains from the membrane, blocking the interaction between the membrane and the actin cytoskeleton. Immunohistochemical staining for PtdIns(4,5)P_2 during infection

confirmed that the phosphatase activity of VPA0450 was sufficient to remove this inositide from the membrane.

Host membrane integrity is maintained through the dynamic interaction of various actin nucleating and binding proteins with the plasma membrane (Figure 24A). The specific targeting of PtdIns(4,5)P_2 within the plasma membrane by VPA0450 leads to a disruption of this molecular conversation, leading to membrane blebbing (Figure 24B). This activity, along with that of other T3SS1 effectors including VopQ and VopS, destabilized the actin cytoskeleton leading to rapid host cell lysis (Figure 24C). The elucidation of the activity for VPA0450 demonstrates the importance of phosphoinositide homeostasis in eukaryotic cells, and highlights a lipid target bacterial pathogens can exploit to disrupt the integrity of the cell membrane and its interaction with the actin cytoskeleton.

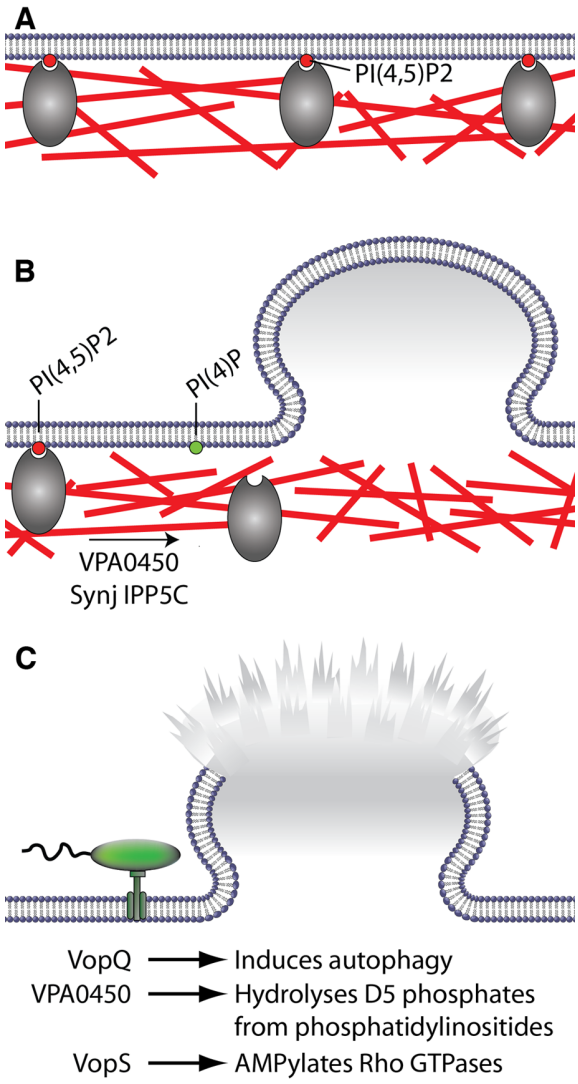

FIGURE 24. The phosphatase activity of VPA0450 causes membrane blebbing and facilitates cell lysis.
(**A**) In uninfected cells, membrane integrity is maintained by the actin cytoskeleton. Actin binding and nucleating proteins associate with PtdIns(4,5)P2 in the inner leaflet of the plasma membrane, providing a dynamic interaction that allows the cell to maintain its integrity while being able to adapt to changes in its environment. (**B**) Introduction of VPA0450, or other exogenous IPP5C domains, into the cytoplasm leads to hydrolysis of $PtdIns(4,5)_2$ to PtdIns(4)P, dissociation of actin binding proteins from the membrane, and a destabilization of the membrane leading to blebbing, or (**C**) lysis in the presence of other bacterial effectors.

CHAPTER 4

A NOVEL LOCALIZATION DOMAIN DIRECTS VPA0450 TO THE PLASMA MEMBRANE

Introduction

Localization of proteins for proper function is critical for cell homeostasis. Many proteins contain localization domains, bind to lipids or associate with other proteins to create high local concentrations of a signaling molecule that is able to efficiently transmit a signal using only a minimal amount of protein (53). Effectors are translocated into cells in small quantities (38), and must be able to overcome cellular feedback mechanisms meant to prevent perturbation of the signaling pathways they are meant to target. Effectors accomplish this by a couple different mechanisms. The effector can have a potent activity that exceeds the host cell feedback mechanisms. YopH from *Yersinia* species has an activity approximately 1000 times greater than its endogenous counterpart (133). The activity of the effector can be irreversible on the timescale of the course of the infection. YopT-mediated cleavage of the CaaX box from Rho-family GTPases delocalizes these enzymes from their substrate rendering them inactive (106, 107). To overcome this activity, the cell must synthesize new proteins. The effector can also localize specifically to its target. PipB2, a SPI-2 effector from *Salmonella enterica* has been shown to localize to microtubules (121). PipB2 binds to kinesin, a plus-end directed motor protein, and acts as a linker to the *Salmonella*

containing vacuole. The activity of PipB2 helps to maintain the vacuole and prolong survival of the bacteria (46)

The function of VPA0450 during infection is the delocalization of membrane-associated actin binding proteins leading to membrane blebbing and the facilitation of host cell lysis during infection. VPA0450 has an *in vitro* biochemical activity higher than that of SPsynj IPP5C, a homolog, but not drastically so (Figure 20). Phosphoinositides are highly dynamic in a eukaryotic cell. PI(4)P, the product formed upon VPA0450 hydrolysis of PtdIns(4,5)P_2, will not accumulate in an infected cell. This hydrolysis product will be converted either back to PtdIns(4,5)P_2, or to PI(3,4)P_2, then on to other phosphoinositide species (30, 66, 102). A sustained loss of PtdIns(4,5)P_2 within a host cell may be difficult to maintain. The target of VPA0450, PtdIns(4,5)P_2, is found primarily at the plasma membrane. As such, it is reasonable to hypothesize that VPA0450 targeted to this membrane. In a previous experiment, immunohistochemistry was used to confirm expression on cells transfected with VPA0450 and VPA0450 H356A. An unexpected result of this experiment was that VPA0450 localizes to the plasma membrane (Figure 21B-C). This led us to hypothesis that VPA0450 contains a localization domain or motif that drives it to the plasma membrane, where it can efficiently hydrolyze PtdIns(4,5)P_2.

Results

VPA0450 localizes to the plasma membrane

Comparison of the amino acid sequences for SPsynj IPP5C and VPA0450 show that VPA0450 has non-homologous sequences at both the N and C-termini (Figure 17B). The non-homologous N-terminal sequence is approximately 76 amino acids in length, which is a typical size for the secretion signal and chaperone-binding domain (1). The non-homologous C-terminal portion of VPA0450 stretches from 367 to 475, and is primarily alpha helical (Figure 17B). To determine if this portion of VPA0450 was necessary for localization to the plasma membrane, a VPA0450 mutant was made with this portion of the protein deleted. Hela cells were transfected with empty vector, full length VPA0450-flag, or the mutant VPA0450Δ367-475-flag, and cells stained by immunohisto-chemistry using a mouse anti-flag primary antibody and Alexa fluor-548 anti-mouse secondary antibody. The cells transfected with empty vector showed minimal background staining (Figure 25A). Cells transfected with full length VPA0450 displayed weak cytoplasmic staining, with the signal enhanced at the membrane (Figure 25B), while cells transfected with the VPA0450Δ367-475-flag mutant displayed only weak cytoplasmic staining (Figure 25C). This data supports the hypothesis that residues 367-475 are necessary for proper localization of VPA0450 within a host cell.

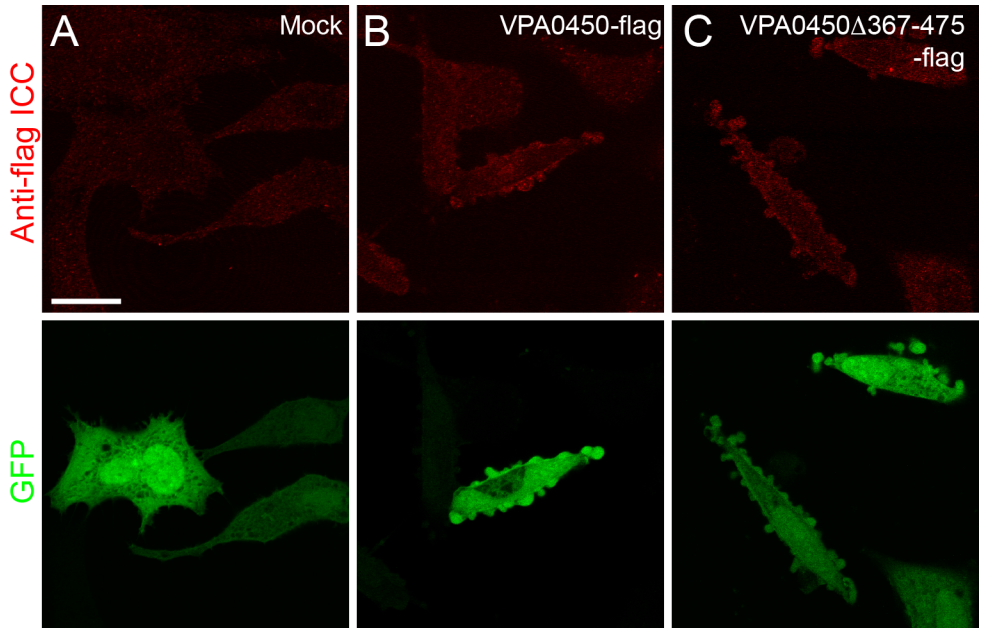

FIGURE 25. VPA0450 C-terminus is necessary for membrane localization. Hela cells were transfected with pEGFP-N1 and (**A**) empty pSFFV vector, (**B**) pSFFV-VPA0450-flag, or (**C**) pSFFV-VPA0450Δ367-475-flag, stained with mouse anti-flag primary antibody and Alex fluor 548-conjugated donkey anti-mouse secondary antibody. Slides were visualized by confocal microscopy. Green denotes transfected cells. Scale bar, 20 μm.

To confirm the localization of full length VPA0450 and VPA0450Δ367-475, N-terminal mCherry fusions of each gene were made and transfected into Hela cells. Cells transfected with empty mCherry-expressing vector showed cytoplasmic red fluorescence (Figure 26A). Cells transfected with mCherry-VPA0450 had enhanced staining of the plasma membrane (Figure 26B), while cells transfected with mCherry-VPA0450Δ367-475 had cytoplasmic red

fluorescence without membrane-specific staining. These results further support the idea that residues 367-475 of VPA0450 are required for localization.

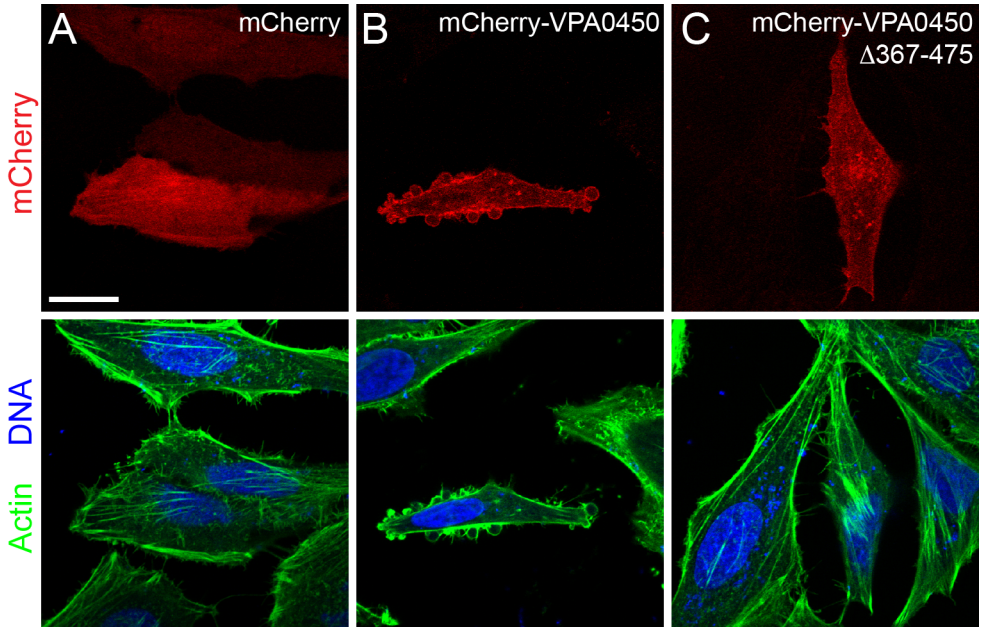

FIGURE 26. C-terminus is necessary to localize mCherry-VPA0450 to the plasma membrane.
Hela cells transfected with (**A**) pSurf-mCherry, (**B**) pSurf-mCherry-VPA0450, or (**C**) pSurf-mCherry-VPA0450Δ367-475 and imaged by confocal microscopy. Scale bar, 20 μm. Actin was stained with Alexa fluor 488-phalloidin (green), and nuclei were stained with Hoechst (blue).

We next wanted to determine if the cytoplasmic mis-localization of VPA0450 by deletion of the C-terminal helices would affect its ability to efficiently induce membrane blebbing and the delocalization of PtdIns(4,5)P_2-

associated proteins. Hela cells were transfected with PH(PLCδ1)-GFP, which specifically binds to PtdIns(4,5)P_2 creating a green fluorescent line at the membrane of tranfected cells, and either empty pSFFV vector, pSFFV-VPA0450, or pSFFV-VPA0450Δ367-475. Consistent with previous experiments, greater than 90% of cells transfected with PH(PLCδ1)-GFP alone had GFP localized to the membrane, and 7% of these cells had membrane blebs (Figure 27A and B, left columns). In cells transfected with PH(PLCδ1)-GFP and full length VPA0450, GFP localization at the membrane dropped to less than 4% (96% had cytoplasmic localization), and 48% of cells had membrane blebs (Figure 27A and B, center columns). Deletion of 367-475 did not change the number of cells with membrane blebs compared to full length (Figure 27A, right column). However, PH(PLCδ1)-GFP localization had an phenotype intermediate to the empty vector and full length VPA0450 transfected cells, with 21 % of cells showing GFP localized at the membrane. This observation supports our hypothesis that the C-terminus of VPA0450 is necessary for full activity of this effector. It is possible that the truncation of the C-terminus has altered protein folding, and that this is the reason for the decrease in ability to delocalize PH(PLCδ1)-GFP from the membrane. To test this possibility, the catalytic activity of the VPA0450Δ367-475 mutant will be compared to wild type *in vitro* by malachite green assay that measures phosphate release on purified recombinant protein.

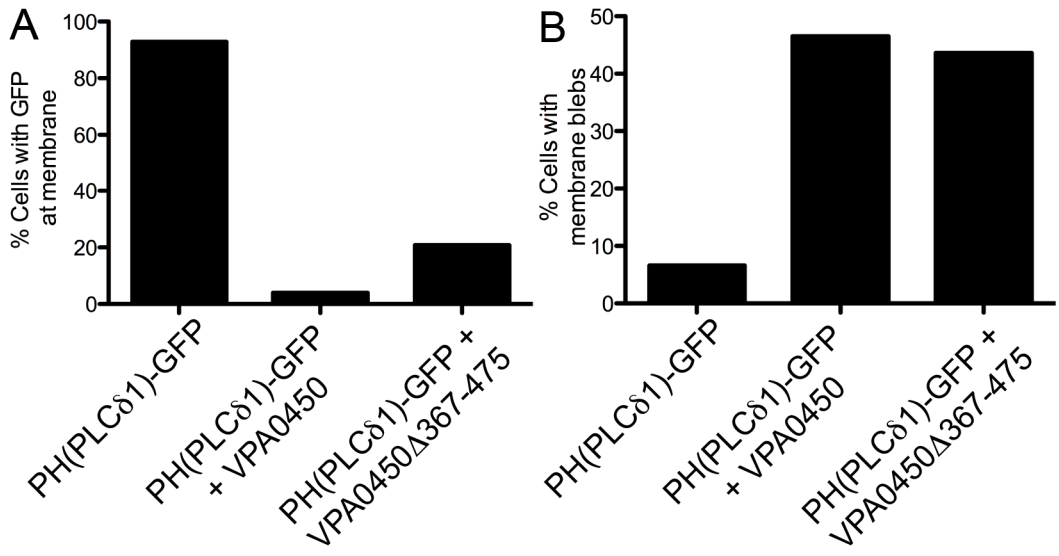

FIGURE 27. VPA0450 C-terminus is required for full delocalization of PH(PLCδ1).
Hela cells were transfected with PH(PLCδ1)-GFP and either empty vector, pSFFV-VPA0450-flag, or pSFFV-VPA0450-H356A-flag, visualized by fluorescence microscopy and quantified for the number of cells with GFP at (**A**) the membrane or (**B**) blebbing cells.

Cells with large amounts of membrane blebbing often lose adherence, and are lost during the washing steps required for staining and fixing prior to confocal visualization. Previous transfections with full length VPA0450 and VPA0450Δ367-475 had 45% and 20% of transfected cells bleb, respectively. As such, it is possible that there may be a difference in the number of cells with membrane blebs, but we are unable to consistently detect the difference by counting only adherent cells. Additional experiments, including the optimization

of transfections, will be necessary to determine if there is a statistical difference in blebbing between these two forms of VPA0450.

Sufficiency of C-terminus to localize VPA0450 to the plasma membrane

Having established that the C-terminus of VPA0450 is necessary for localization to the plasma membrane, we wanted to determine if it was also sufficient. Bioinformatic analysis of the C-terminus could not identify any known domains or motifs with homology. The alignment of VPA0450 with SPsynj IPP5C (Figure 17B) showed a lack of homology starting at residue 367 of VPA0450. As synaptojanin is localized by a proline rich motif (PRM) at the C-terminus of the IPP5C domain, we hypothesized that the region from 367 to 497 may be the localization domain for VPA0450. It is possible the reason VPA0450 did not adopt the synaptojanin PRM is due to a different binding specificity or localization requirement for maximal effector activity. To test this, a fusion protein with N-terminal GFP and C-terminal $VPA0450_{367\text{-}498}$ was made in a mammalian expression vector. Hela cells were transfected with either GFP or the translational fusion protein GFP-$VPA0450_{367\text{-}498}$ and visualized by confocal microscopy. Both GFP and GFP-$VPA0450_{367\text{-}498}$ localized to the cytoplasm, indicating residues 367-498 of VPA0450 are not sufficient for localization to the membrane (Figure 28).

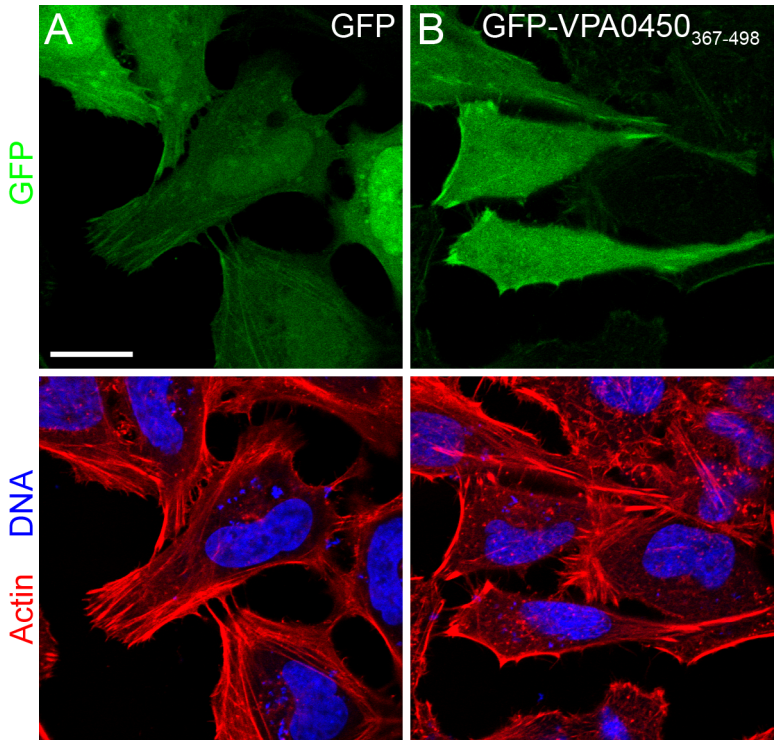

FIGURE 28. VPA0450$_{367-498}$ is not sufficient for membrane localization.
Hela cells were transfected with either (**A**) GFP or (**B**) GFP-VPA0450$_{367-498}$, a fusion of GFP to the putative VPA0450 localization domain, and visualized by confocal microscopy. Scale bar, 20μm. Actin was stained with rhodamine-phalloidin (red), and nuclei were stained with Hoechst (blue).

Reexamination of the alignment between VPA0450 and SPsynj IPP5C (Figure 17) shows the C-terminal helix (αC) of SPsynj IPP5C (residues 323-340) aligned with residues 476-494 of VPA0450. The alignment was repeated, with the VPA0450 sequence truncated to 391 residues to allow alignment of the SPsynj IPP5C αC with the eighth helix of VPA0450 (α8) (Figure 29). Both of these helices occur immediately after the sixth catalytic motif.

FIGURE 29. C-terminal helices of VPA0450 may be correct localization domain.
Alignment of VPA0450 with SPsynj IPP5C with bias for aligning C-termini removed by truncating C-terminus of VPA0450 to match length of IPP5C. Predicted alpha helices in red, predicted beta strands in blue, and catalytic motifs in green.

The remaining portion of VPA0450, residues 392-497, consists of an unstructured span followed by three closely spaced helices (Figure 30A-B). Helical wheel projections of these helices show that while α8 does not have any discernible organization (Figure 30C), both α9 and α10 are amphipathic with hydrophobic and, in the case of α10, polybasic regions (Figure 30D-E). This is a common component of proteins that bind weakly and reversibly to plasma membranes. The hydrophobic portion of some amphipathic helices can intercalate into the plasma membrane to anchor a protein. Additionally, polybasic regions are

known to bind acidic lipids, including phosphoinositides (56). It is possible that α9 acts as a general membrane anchor, and that α10 binds to phosphoinositides such as PtdIns(4,5)P_2 or PtdIns(3,4,5)P_3, providing the specificity that delivers VPA0450 to the plasma membrane and its substrate. Dot blot assays to test specific binding of the VPA0450 C-terminus, and specifically each of the different α-helices are being planned. Additional work is needed to determine if these helices are the portion of VPA0450 that is sufficient for membrane localization, as well as to identify the specific moiety that VP0450 binds.

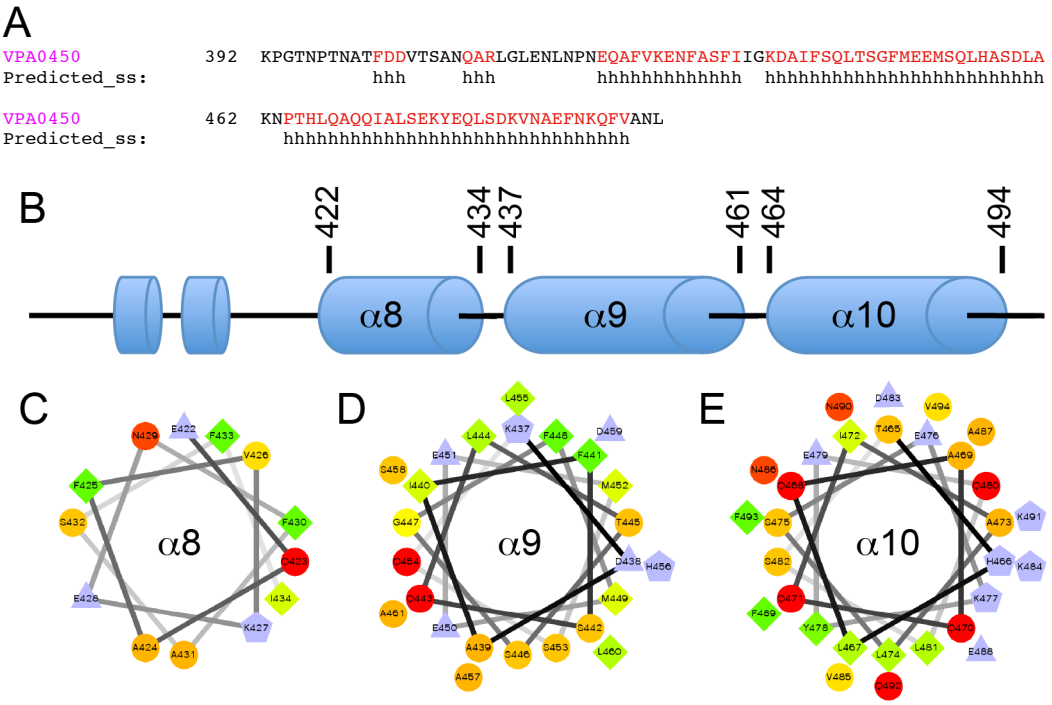

FIGURE 30. C-terminal helices of VPA0450 are amphipathic.
(**A**) C-terminus of VPA0450 not aligned with catalytic core of SPsynj IPP5C. (**B**) Secondary structure prediction of VPA0450 C-terminus. Helical wheel projections of (**C**) α8 (E422-I434), (**D**) α9 (K437-A461), and (**E**) α10 (T465-V494) of VPA0450. Hydrophilic residues are circles, with red being the most hydrophilic. Hydrophobic residues are diamonds, with green being the most hydrophobic. Potential negative charges are diamonds and potential positive residues are pentagons, with potentially charged residues in blue. Helical wheels were generated using the algorithm at rzlab.ucr.edu/scripts/wheel/

Discussion

The proper localization of an effector is critical for it to function properly. VPA0450 was shown to drive membrane blebbing at a level more than 20 times greater than that seen with SPsynj IPP5C (Figure 19G), despite only having a roughly 2-fold difference in the *in vitro* activity of these proteins (Figure 20). SPsynj IPP5C is strictly a catalytic domain, and does not carry its endogenous localization motif, while VPA0450 was shown to localize to its substrate at the plasma membrane.

Deletion of residues 367-475 in the C-terminus of VPA0450, which are not homologous to SPsynj IPP5C, resulted in the cytoplasmic localization of the VPA0450 mutant. Additionally, the VPA0450Δ367-475 mutant failed to delocalize PH(PLCδ1)-GFP from the membrane at the same level as full length VPA0450. This demonstrated that the C-terminus of VPA0450 was necessary for proper localization and full activity in host cells. Cells transfected with VPA0450Δ367-475 show membrane blebbing at levels comparable to full length VPA0450, indicating the mutant was still catalytically active. The level of over-expression may have been sufficient to overcome the lack of proper localization.

A first attempt at identifying the portion of VPA0450 sufficient to localize a protein to the membrane was not successful. Reexamination of the alignment of VPA0450 and SPsynj IPP5C identified two amphipathic helices that may localize VPA0450 to phosphatidylinositol phosphates in the plasma membrane. VPA0450

mutants deleted for α9-α10 or only α10 need to be examined for their ability to localize to the membrane, delocalize PH(PLCδ1)-GFP, and cause membrane blebbing. Additionally, these portions of VPA0450 need to be examined for sufficiency to localize proteins to the plasma membrane. The characterization of how VPA0450 is localized to the membrane will provide insight into how this effector contributes to the infection process of *V. parahaemolyticus*, and may provide a new tool for the localization of other proteins to the plasma membrane.

CHAPTER 5

STUDYING THE CONCERTED ACTION OF MULTIPLE T3SS EFFECTORS

Introduction

Out of necessity, many in the field of bacterial pathogenesis that study T3SSs have taken a reductionist approach to understanding the virulence factors secreted by this system. T3SS are complicated machines, with what is possibly an even more complicated battery of effectors. Some pathogens have a short, defined list of effectors, others are much more complicated. For example, *Yersinia pestis* has six effectors (24), while there are *Pseudomonas syringae* strains with 27 effectors characterized to date that are located in clusters throughout the genome as well as on at least one virulence plasmid (25, 63, 137).

The complexity found in *V. parahaemolyticus* stems in part from the presence of two differentially regulated T3SS, as well as the potential for chromosomal localization of effectors outside the pathogenicity islands as demonstrated by VPA0450. The presence of these effectors leads to questions about the evolution of *V. parahaemolyticus*: What was the selective pressure that gave a competitive advantage to an organism that has acquired effectors with functions new to *V. parahaemolyticus*? Where did the effectors come from? What

other effectors has *V. parahaemolyticus* acquired that are outside of the T3SS loci and have not yet been detected?

Several methods have been employed to identify new effectors in *V. parahaemolyticus* and other pathogens, including *in silico* screens for chaperones and their associated effectors (93), computational predictions (130), and mass spectrometer analysis of specific secreted proteins (91) or secreted proteins *en masse* (29). These methods all have their shortcomings, as they rely on homology to known proteins, or the ability to induce secretion *in vitro*. Another method for detection of effectors is the deletion of all known effectors followed by infection studies to determine if a novel virulence phenotype can be uncovered.

Until recently, deletion of multiple genes had not been possible in our lab due to difficulties with the Lambda red recombinase system. This system required significant time to create a single gene replacement that left an antibiotic resistance cassette in the chromosome in place of the gene of interest. The inability to resolve the antibiotic resistance cassette from the chromosome made the generation of multiple knockouts impractical. A different chromosomal gene deletion system, used successfully in the NY-4 strain of *V. parahaemolyticus* (135), has been adapted for use in RimD-derived strains of *V. parahaemolyticus*. This system uses a suicide vector with the oriR6K replication origin, a chloramphenicol resistance gene for selection of integrants, and the *sacB* gene for counterselection.

The ability to efficiently make multiple gene knockouts not only allows for the identification of additional effectors, but simplifies the study of the spatial and temporal regulation and activity of effectors. The concerted effects of two or more effectors can be studied using infections with effectors translocated at physiologically relevant levels. The system can also be used to "knock-in" effectors tagged with epitopes for antibody recognition, as well as various enzymes such as β-lactamase for the characterization of effector translocation timing or quantification of effectors under their endogenous promoters.

Results

Generation of new parent strains

The identification of the regulatory systems for T3SS1 and T3SS2 has made it possible to create strains in which only one set of virulence proteins is expressed. This has the potential to limit any cross talk that may exist between systems, and thus make the contributions of each system to pathogenesis easier to study. Previous studies have used three strains derived from the RimD 2210633 clinical isolate. The POR1 strain maintains both functional T3SSs, but has both copies of TDH deleted. POR2 and POR3 were both derived from POR1. The POR2 strain has the gene for VcrD1 deleted. This protein is an inner membrane structural ring for the T3SS apparatus, and is required for assembly of T3SS1. POR2 is able to synthesize structural proteins and effectors for both T3SSs, but

can only secrete or translocate effectors from T3SS2. The POR3 strain has the gene for VcrD2 deleted. VcrD2 is also an inner membrane structural ring, but for T3SS2. POR3 can synthesize structural proteins and effectors for both systems, but can only secrete or translocate through T3SS1. Using the POR1 genetic background, unmarked deletions were made of the positive regulators for each T3SS. Deletion of *vtrA*, the positive regulator of T3SS2, yielded a strain that can only express genes associated with T3SS1, and was designated CAB3. Likewise, deletion of *exsA*, the positive regulator of T3SS1, yielded a strain that can only express Vp-PAI genes including T3SS2, and was designated CAB2. An additional strain, CAB4, was also generated in which both *vtrA* and *exsA* were deleted (Table 7). The creation of CAB2 and CAB3 allow for the study of one secretion system without potential crosstalk from the other system. The CAB4 strain will allow for the identification of any virulence genes induced by positive regulators other than VtrA and ExsA. During studies using CAB2 or CAB3 strains and their respective inducing conditions (Table 7), CAB4 can act as a negative control.

TABLE 7. Characteristics of established and new *V. parahaemolyticus* parent strains

Strain	Genotype	Phenotypic description	Inducing condition
POR1	RimDΔ*tdhAS*	Clinical isolate, no TDH expression (KP negative)	37 °C, with growth in low Ca^{2+} media or DMEM; bile salts
POR2	POR1Δ*vcrD1*	Functional T3SS2, expresses T3SS1 proteins, but cannot form T3SS1 needle	Bile salts
CAB2	POR1Δ*exsA*	Functional T3SS2, no expression of T3SS1 genes	Bile salts
POR3	POR1Δ*vcrD2*	Functional T3SS1, expresses Vp-PAI and T3SS1 proteins, but cannot form T3SS2 needle	37 °C, with growth in low Ca^{2+} media or DMEM
CAB3	POR1Δ*vtrA*	Functional T3SS1, no expression of Vp-PAI or T3SS2 genes	37 °C, with growth in low Ca^{2+} media or DMEM
CAB4	POR1Δ*exsA* Δ*vtrA*	Does not express genes associated with T3SS1 or Vp-PAI/T3SS2	None known

To confirm that the new CAB strains were phenotypically similar to the corresponding POR strains, infections of Hela cells were performed using inducing conditions specific to each positive regulator still present in each strain (Table 7). *V. parahaemolyticus* POR2, CAB2 and CAB4 were induced with bile salts and used to infect Hela cells. We found that both POR2 and CAB2, each harboring a functional T3SS2, showed a slight induction of stress fibers at 0.5

hours (Figure 31B and G) compared to mock infected cells (Figure 31A), with the severity of the fibers increased substantially at 1 and 2 hours (Figure 31C-D and H-I). Cells became cytotoxic and began to shrink by 3 hours (Figure 31E and J), with increased cytotoxicity and apparent Hela cell lysis present at 4 hours (Figure 31F and K). The Hela cells infected with CAB4, lacking both T3SSs, did not show any change in phenotype from the mock-infected cells during the entire course of infection (Figure 31L-P). This demonstrates that T3SS2 in both POR2 and CAB2 can be induced by bile salts, and share a similar infection profile and timing during infection of cells in culture conditions. Additionally, CAB4 does not induce any morphological changes in infected cells, indicating bile salts do not induce expression of any unknown virulence factors within the time frame studied.

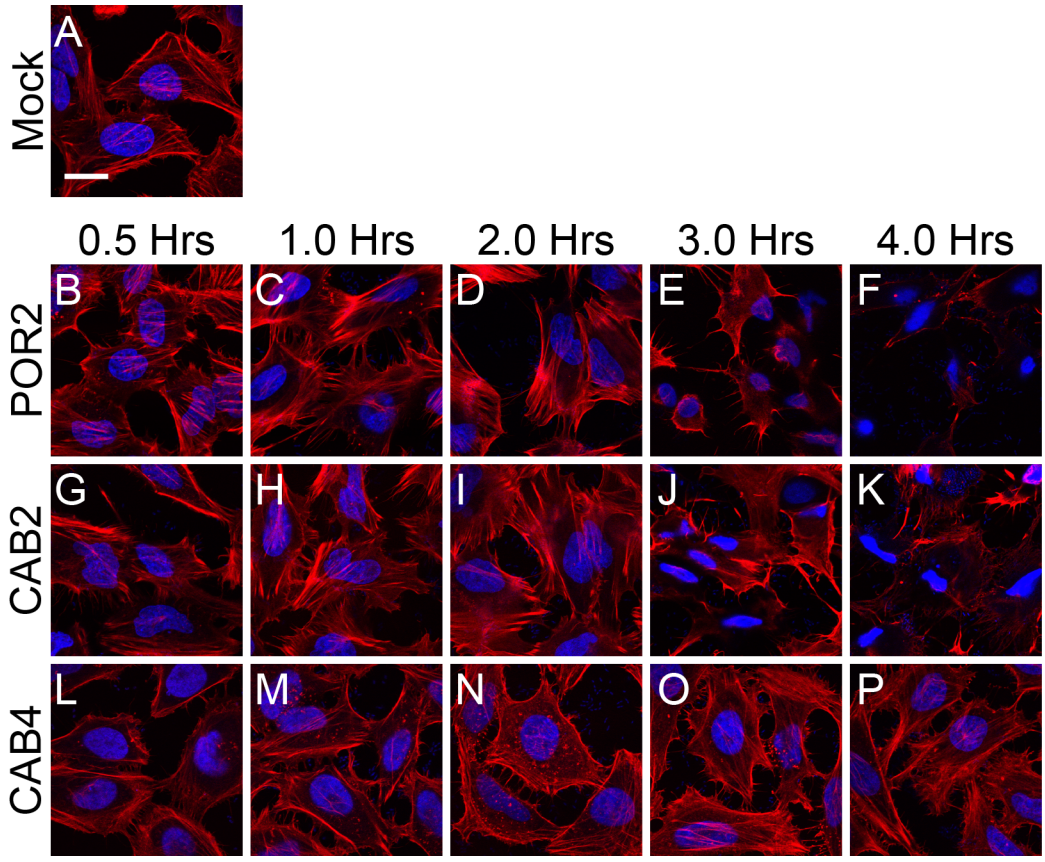

FIGURE 31. CAB2 induces stress fibers and cytotoxicity similar to POR2 while CAB4 is not cytotoxic to Hela cells.
Hela cells were (**A**) mock infected, or infected with (**B-F**) POR2, (**G-K**) CAB2, or (**L-P**) CAB4 strains of *V. parahaemolyticus* induced with bile salts. Cells were fixed at the time points indicated, stained, and visualized by confocal microscopy. Scale bar, 20 μm. Actin was stained with rhodamine-phalloidin (red), and nuclei were stained with Hoechst (blue).

Hela cells were then infected with POR3, CAB3 and CAB4 strains of *V. parahaemolyticus* that were induced by growing at 37 °C in DMEM. Compared to mock infected cells (Figure 32A), both POR3 and CAB3 showed no significant morphological changes at 0.5 hours (Figure 32B and E). At 1 hour, Hela cells

infected with POR3 and CAB3 were rounded with a cytoplasmic distribution of actin (Figure 32C and F). At 2 hours, many Hela cells were lysed, with remaining cells still showing the same rounded phenotype (Figure 32 D and G). Again, CAB4 infected cells did not cause any morphological changes (Figure 32H-K). These results demonstrate that both POR3 and CAB3 are induced by growth at 37°C in DMEM, and follow the same phenotypic progression during infection of cultured cells. These observations support the hypothesis that either all the virulence factors employed by *V. parahaemolyticus* are induced by either bile salts, or increased temperature and low environmental calcium concentrations, or that there are additional virulence factors such as the putative T6SS systems, and that the induction conditions for these proteins are not currently known. The CAB4 strain will likely prove useful for the identification of any additional virulence factors, if they exist, as well as the characterization of Bioinformatically identified *V. parahaemolyticus* T6SS1 and 2.

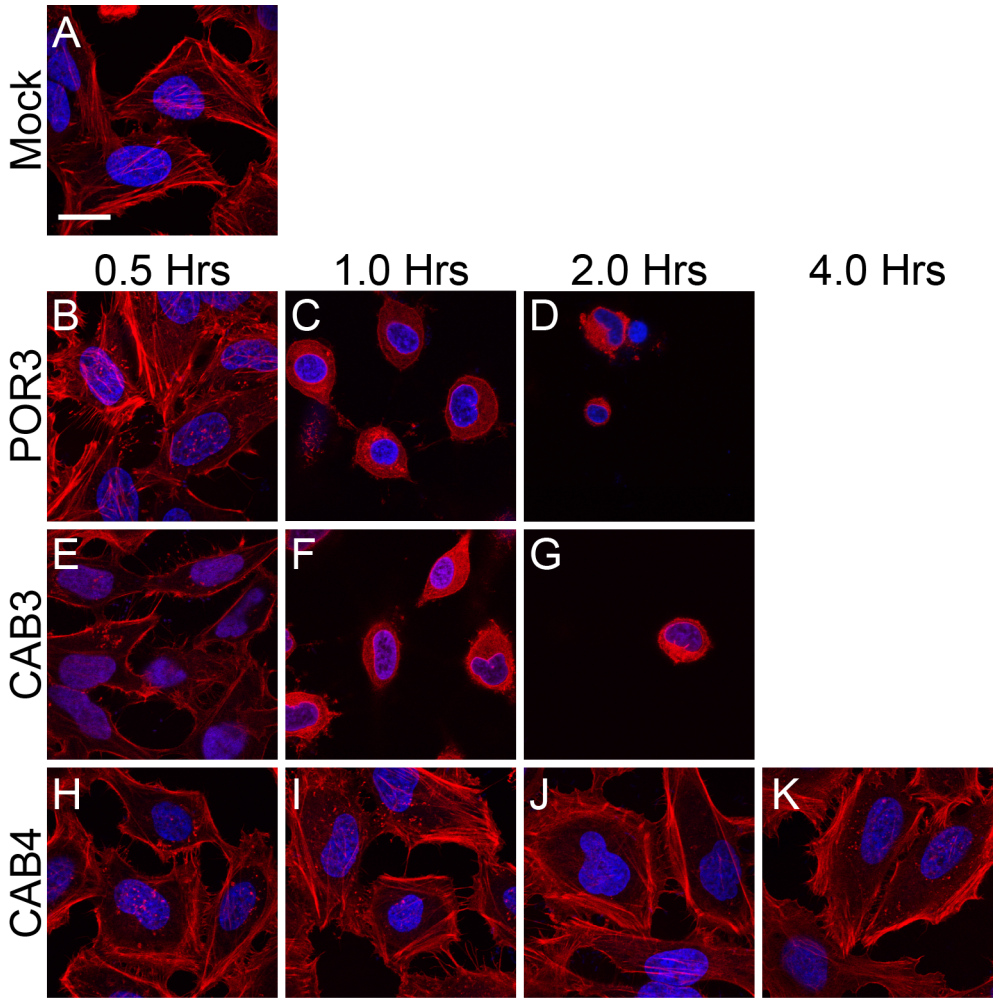

FIGURE 32. POR3 and CAB3, but not CAB4, induce cell rounding.
Hela cells were (**A**) mock infected, or infected with (**B-D**) POR3, (**E-G**) CAB3, or (**H-K**) CAB4 strains of *V. parahaemolyticus* induced by growing at 37 °C in DMEM. Cells were fixed at the time points indicated, stained, and visualized by confocal microscopy. Scale bar, 20 μm. Actin was stained with rhodamine-phalloidin (red), and nuclei were stained with Hoechst (blue).

Confirmation of VPA0450 and VopQ-induced cytotoxicity in the CAB3 strain

To further validate CAB3 as a useful strain for studying virulence in *V. parahaemolyticus*, it was prudent to create single effector knockouts to test for known infection phenotypes that had been previously observed with POR3. The gene encoding VPA0450 was deleted from the CAB3 strain, and then used to infect Hela cells. Cells infected with CAB3 followed the previously established progression of rounding by 1.5 hours, and host cell lysis after 2 hours (Figure 33B-G). CAB3Δ*vpa0450* initiated rounding by one hour, but also showed a delay in cell lysis with some cells still intact at the 3-hour time point (Figure 33H-M). CAB4 infected cells did not show a change in phenotype and, with mock infected cells, served as a negative control (Figure 33A and N-S). The infection profile for CAB3Δ*vpa0450* is consistent with infection by POR3Δ*vpa0450* (Figure 13B and E). Blebbing was not observed in Hela cells infected with CAB3 for visualization by confocal microscopy. This is not unexpected, as the blebbing is transient and was likely missed at the time points visualized for these initial experiments (10). Blebbing has been observed during infection of Hela cells with CAB3 for LDH release measurements. However, imaging of these cells was not possible. Future studies using additional time points between 0.5 and 2 hours will be performed to confirm this phenotype with CAB3, and to allow for imaging of the cells with plasma membrane blebbing.

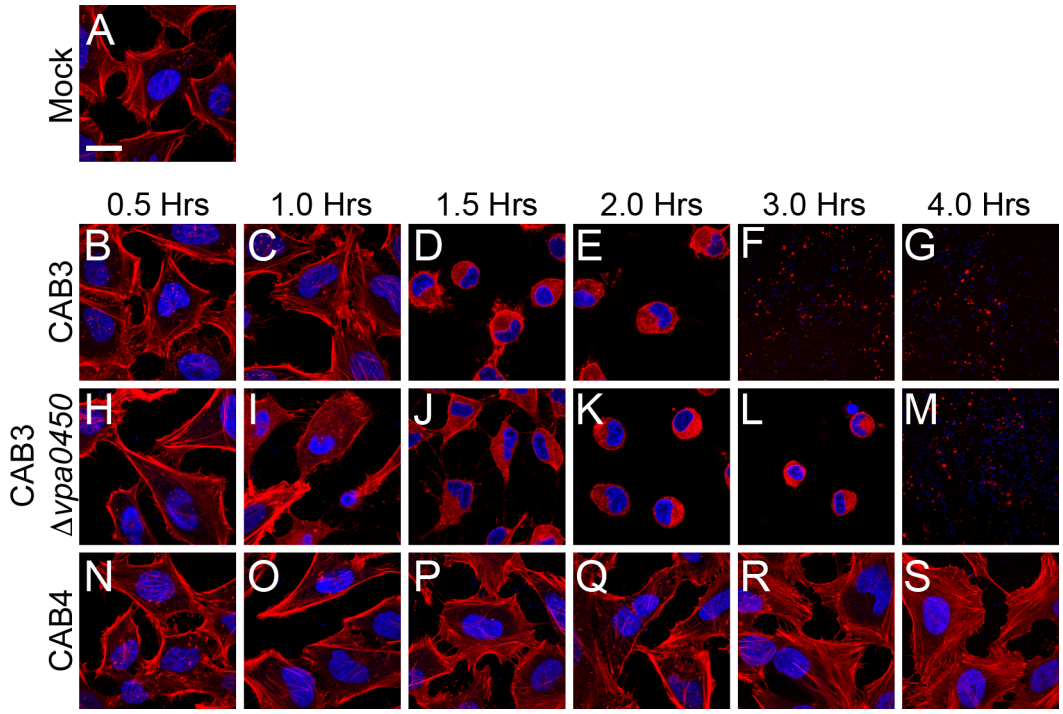

FIGURE 33. Deletion of *vpa0450* from CAB3 accelerates rounding but delays lysis upon infection of Hela cells.
Hela cells were (**A**) mock infected, or infected with (**B-G**) CAB3, (**H-M**) CAB3Δ*vpa0450*, or (**N-S**) CAB4 strains of *V. parahaemolyticus*. Cells were fixed at the time points indicated, stained, and visualized by confocal microscopy. Scale bar, 20 μm. Actin was stained with rhodamine-phalloidin (red), and nuclei were stained with Hoechst (blue).

To confirm single effector deletions in CAB3 act in a fashion similar to the POR3 strains, cytotoxicity as measured by LDH release was examined for cells infected with CAB3, CAB3Δ*vpa0450*, and CAB3Δ*vopQ* and compared to previous results done with POR3. Consistent with established profiles for cell lysis with POR3 infections, the CAB3 infected cells lysed in about 2 hours. Cells

infected with CAB3Δ*vpa0450* had a delay in cytotoxicity of 30-45 minutes, and those infected with CAB3Δ*vopQ* had a delay of about 3 hours (Figure 34). These findings are also consistent with the *vpa0450* and *vopQ* deletions made in the POR3 genetic background (Figure 14) (10, 14).

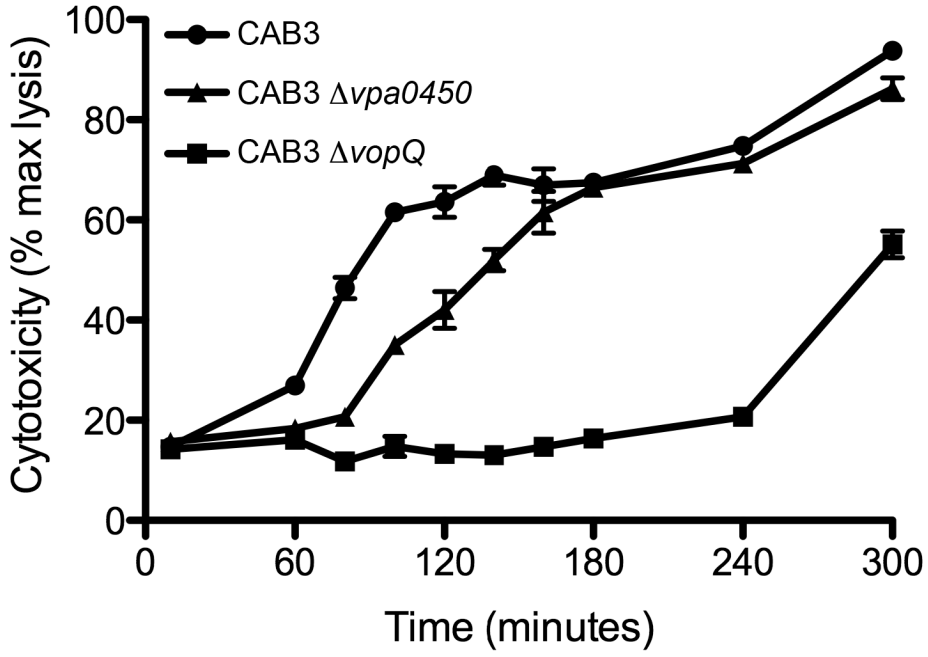

FIGURE 34. VPA0450 and VopQ are required for rapid host cell lysis during infection with CAB3.
Hela cells were infected with CAB3 (circles), CAB3Δ*vpa0450* (triangles), CAB3Δ*vopQ* (squares) strains of *V. parahaemolyticus* and lactate dehydrogenase (LDH) release evaluated as a measure of cytotoxicity and host cell lysis. Data are means ± SD (n = 2 samples) from a representative experiment repeated in duplicate.

Determination of the presence of non-T3SS1 virulence factors in CAB3

Characterization of virulence in the POR3 strain has thus far focused on T3SS1 and its known effectors. While there are still several genes encoding hypothetical proteins within the T3SS1 genomic island, they do not have homology to other know effectors or exotoxins (91). The presence of the VPA0450 gene outside of this locus indicates there may be other virulence factors under ExsA and co-expressed with T3SS1 that have yet to be identified.

To determine if ExsA induces expression of any exotoxins that may be contributing to cytotoxicity during infections, deletions of *vcrD1* and *vscN1* were made in the CAB3 strain. VcrD1 is the inner membrane structural ring for the T3SS1 needle. Deletion of this gene prevents assembly of the needle, and blocks translocation of effectors. This is the gene that was deleted to make the POR2 strain (95). VscN1 is the T3SS1 ATPase and is also required for effector translocation (95). Deletion of *vscN1* will not block assembly of the basal structure, and possibly the needle itself, but will not allow for secretion and assembly of the translocon under ExsA regulation (79). As CAB3 has VtrA deleted and cannot express proteins from Vp-PAI, including T3SS2 structural genes, effectors, or TDH, any cytotoxicity or changes in phenotype of host cells infected with CAB3Δ*vcrD1* can be attributed to secreted exotoxins. Additionally, comparison of CAB3Δ*vcrD1* and CAB3Δ*vscN1* infected cells will show if

portions of the T3SS1 apparatus can induce changes in host cells independent of effector translocation.

Hela cells infected by CAB3 had an infection profile consistent with previous studies on POR3, with cells rounding by 1.5 hours, and lysing between 2 and 3 hours (Figure 35B-F). When Hela cells were infected with CAB3Δ*vcrD1* (Figure 35G-K) or CAB3Δ*vscN1* (Figure 35L-P), no change in phenotype was seen compared to cells infected with CAB4 (Figure 35Q-U), or mock infected cells (Figure 35A). For further confirmation, LDH release was measured from Hela cells infected with these same strains. In agreement with the confocal images, cells infected with CAB3 started to lyse by 2 hours, while CAB3Δ*vcrD1*, CAB3Δ*vscN1*, and CAB4 showed nearly identical cytotoxicity profiles, with a gradual increase in LDH release from 7 to 20% between 4 and 7.5 hours (Figure 36). This increase can likely be attributed to Hela cell toxicity as a consequence of pH decrease and metabolic waste buildup from the large number of *V. parahaemolyticus* present in each sample at these later time points. While it is still possible that additional factors are present in CAB3, this data indicates the phenotypic and cytotoxic changes seen during infection with CAB3 in this model system can be attributed solely to T3SS1.

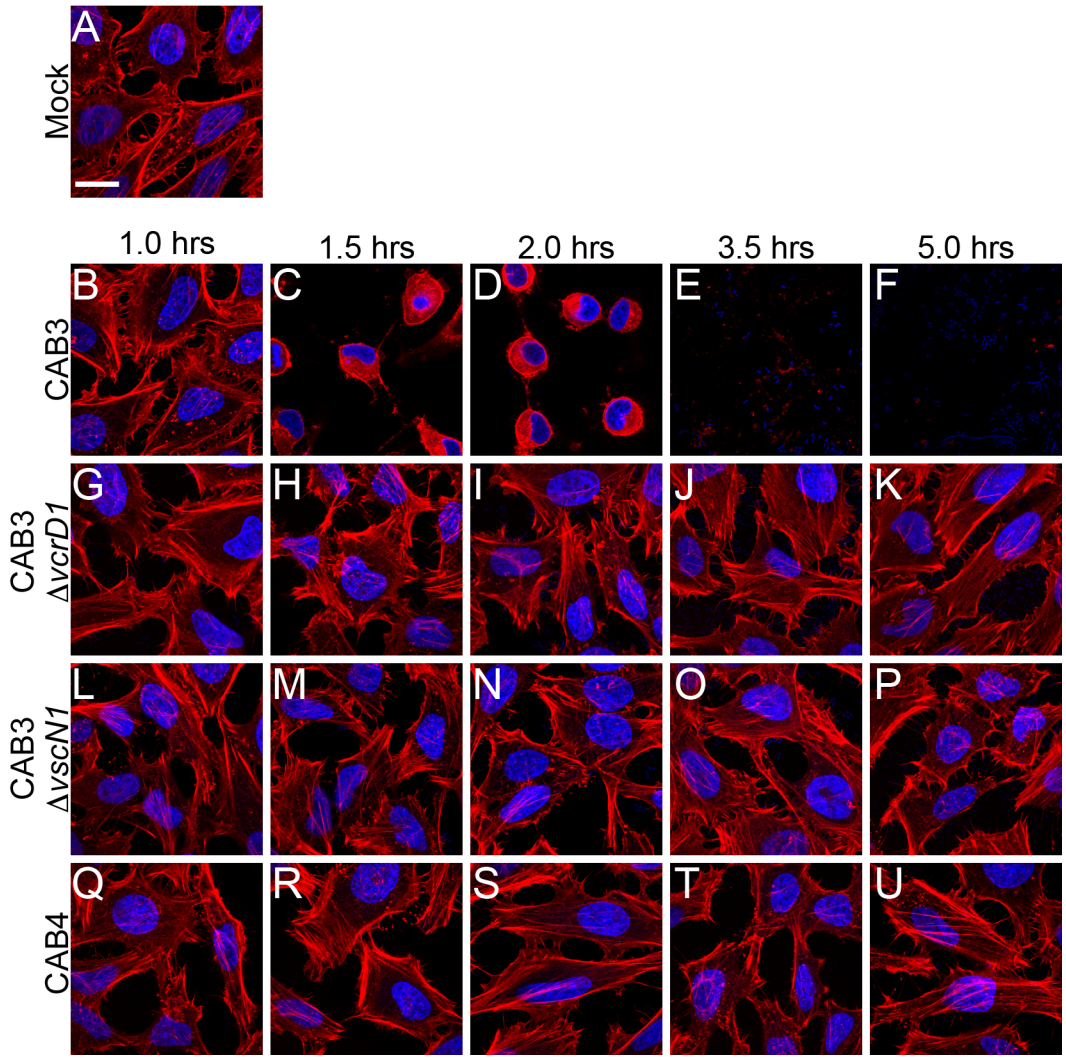

FIGURE 35. Functional T3SS1 is required for cell Hela cell rounding during infection.

Hela cells were (**A**) mock infected, or infected with (**B-F**) CAB3, (**G-K**) CAB3Δ*vcrD1*, (**L-P**) CAB3Δ*vscN1*, or (**Q-U**) CAB4 strains of *V. parahaemolyticus*. Cells were fixed at the time points indicated, stained, and visualized by confocal microscopy. Scale bar, 20 μm. Actin was stained with rhodamine-phalloidin (red), and nuclei were stained with Hoechst (blue).

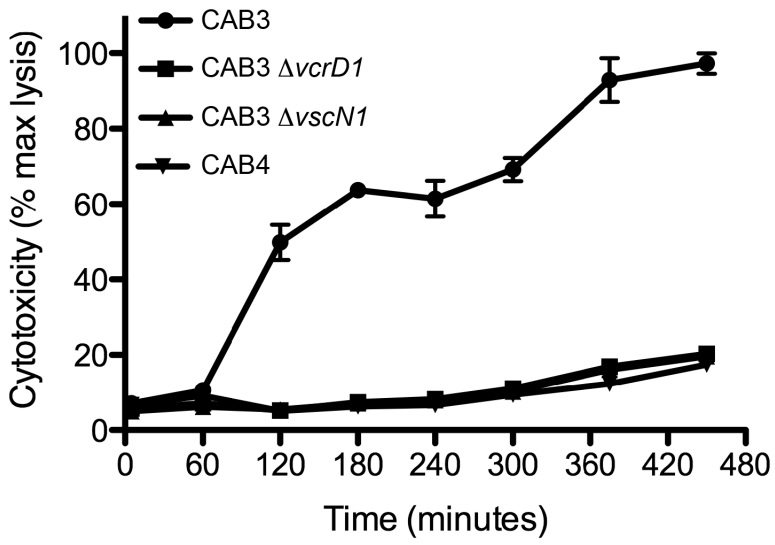

FIGURE 36. CAB3 cytotoxicity is mediated by T3SS1.
Hela cells were infected with CAB3 (circles), CAB3Δ*vcrD1* (squares), CAB3Δ*vcrN1* (triangles), or CAB4 (inverted triangles) strains of *V. parahaemolyticus* and lactate dehydrogenase (LDH) release evaluated as a measure of cytotoxicity and host cell lysis. Data are means ± SD (n = 2 samples) from a representative experiment repeated in duplicate.

Discussion

The ability to study various combinations of virulence factors will prove to be a powerful tool for studying *V. parahaemolyticus*. RimD harbors two copies of the TDH gene, a thermo labile hemolysin (TLH, VPA0226), two T3SSs, eight characterized effectors, and a number of hypothetical genes that could encode additional effectors or exotoxins. While characterizing individual virulence factors in necessary to understand *V. parahaemolyticus* pathogenesis, it is the

study of the concerted action of these proteins will yield additional clinically relevant data.

New strains of *V. parahaemolyticus* were created for this study. CAB2 and CAB3 were shown to have phenotypes similar to POR2 and POR3, respectively. Infection of Hela cells with CAB3Δ*vpa0450* and CAB3Δ*vopQ* gave phenotypic and LDH profiles of infection comparable to the POR3 equivalent strains, confirming CAB3 can be used to characterize known and potential new effectors. Infection of Hela cells performed with CAB3Δ*vcrD1* and CAB3Δ*vscN1* strains that cannot form functional T3SS1 needles. This set of experiments demonstrated that the cytotoxicity seen during these infections could be completely attributed to T3SS1.

The ability to make multiple gene deletions will aid in our understanding of interplay between effectors. VPA0450 and VopQ both contribute to cell lysis. If both of these effectors are deleted, how does the infection progress? VPA0450 and VopS both affect the structural integrity of the cell. If these effectors are deleted, are VopQ and VopR sufficient to still drive cell lysis? A library of effector deletion mutants is currently being made and will be used to answer questions like these.

The study of uncharacterized effectors can benefit from multiple gene deletions as well. While individual effectors can be studied by transfection, this method results in over-expression, and may yield results not typical of what

would be seen during an infection. This is helpful for attributing a particular phenotype to an effector. However, the ability to delete all the effectors except the one being studied may provide physiologically relevant information on how a particular effector behaves during an infection. A caveat to this interpretation is that the presence of an effector or its activity may have evolved to regulate another effector. Regardless of these exceptions, deletion mutagenesis provides a mechanism for discovering phenotypes for uncharacterized effectors, as well as the discovery of new effectors or exotoxins.

CHAPTER 6

INITIAL CHARACTERIZATION OF VOPR, A HOPX HOMOLOG

Introduction

The complement of effectors associated with a particular T3SS determines how it will manipulate a targeted host cell. T3SS1 of *V. parahaemolyticus* has four known effectors that work in concert to orchestrate an inflammatory cell death characterized by the induction of autophagy, membrane blebbing, cell rounding, and then cell lysis (10, 14, 16, 131). The changes in host cell morphology during infection with POR3 or CAB3 can be attributed to three of the four effectors. VopQ induces autophagy and accelerated cell lysis (14). VPA0450 destabilized the interaction between the membrane and actin cytoskeleton, leading to transient membrane blebbing and accelerated host cell lysis (10). VopS AMPylates Rho-family GTPases leading to a collapse of the actin cytoskeleton and cell rounding prior to lysis (131). VopQ and VopS are encoded within a genomic island with the structural genes for T3SS1, along with VopR. It is currently unknown how VopR contributes to T3SS1-mediated cell lysis.

Results

Discovery of the phenotype associated with VopR

The development of a system for making multiple effector knockouts in *V. parahaemolyticus* has enabled the study of VopR during infection without interference from the other T3SS1 effectors. To identify a phenotype for VopR, isogenic gene deletions of VopQ, VopS and VPA0450 were made in the CAB3 genetic background and used to infect Hela cells. Cells infected with CAB3 showed the normal progression of cell rounding at 1 hour, followed by lysis after 2 hours (Figure 37B-E). CAB3Δ*vopQS* Δ*vpa0450* caused shrinking of the infected cells at 1 hour, followed by irregular rounding at 2 and 3 hours (Figure 37F-I). This cell rounding differed from that observed with CAB3 infection, which had cytoplasmic staining of actin attributed to the effector VopS. By contrast, cells infected with CAB3Δ*vopQS* Δ*vpa0450* maintained a ring of actin under the plasma membrane, indicating that actin had not been depolymerized. Infection with a CAB3Δ*vopR* mutant mimicked CAB3 infection (Figure 37J-M), while infection with CAB4 did not alter cell morphology (Figure 37N-Q) and was similar to mock infected cells (Figure 37A). These data suggests that VopR contributes to cell rounding, but that its effects are masked by VopS-induced cell rounding in the CAB3 infected cells. Infection with the CAB3Δ*vopR* mutant did not appreciably change the progression of the infection from the CAB3-infected

cells. Additional time points between 0.5 and 2.0 hours may be necessary to determine if VopR accelerates or slows the rounding and lysis of cells.

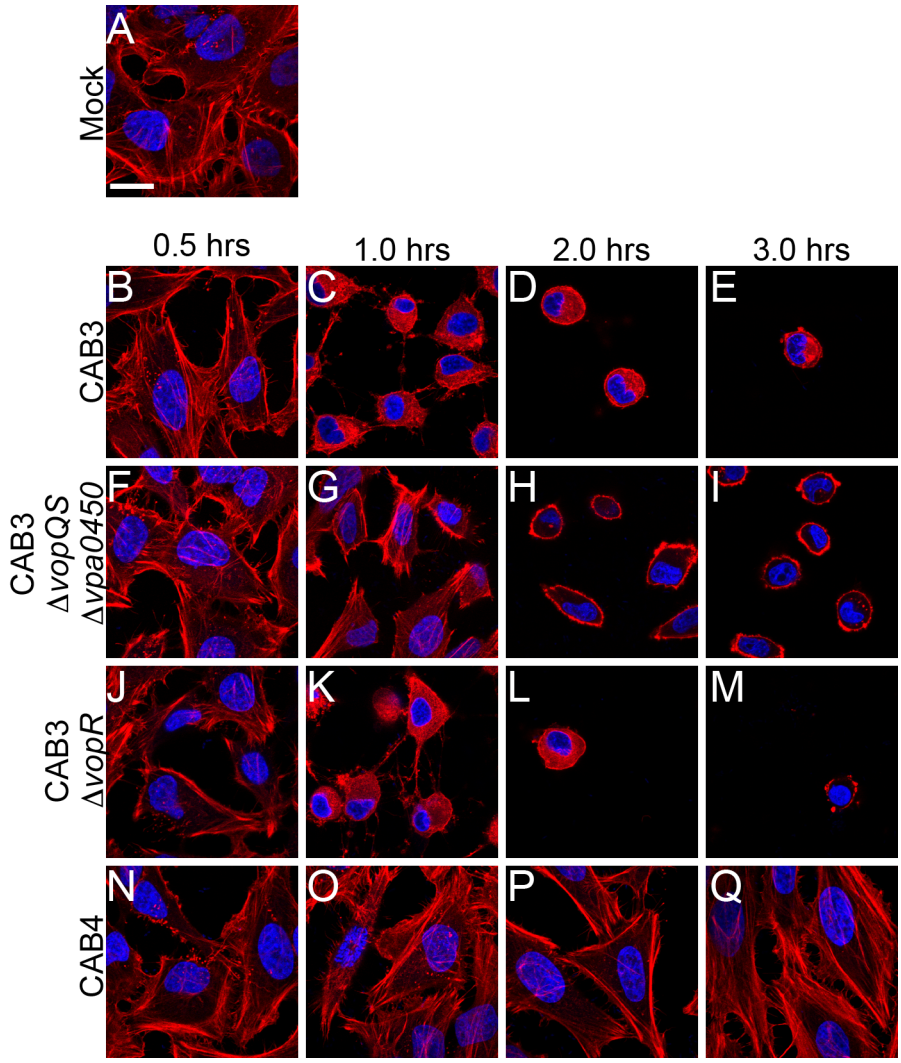

FIGURE 37. Infection with CAB3Δ*vopQS* Δ*vpa0450* uncovers the VopR phenotype.
Hela cells were (**A**) mock infected, or infected with (**B-E**) CAB3, (**F-I**) CAB3Δ*vopQS* Δ*vpa0450*, (**J-M**) CAB3Δ*vopR*, or (**N-Q**) CAB4, then fixed, stained and visualized by confocal microscopy. Scale bar, 20 μm. Actin was stained with rhodamine-phalloidin (red), and DNA stained with Hoechst (blue).

Previous work using deletion studies has shown that VopQ and VPA0450 accelerate host cell lysis. To directly test if VopR affects the rate of cell lysis, Hela cells were infected with CAB3, CAB3Δ*vopQS* Δ*vpa0450*, and CAB4, and cytotoxicity measured by release of LDH. CAB3 infected cells showed significant cytotoxicity by 2 hours. Cells infected with CAB3Δ*vopQS* Δ*vpa0450* did not show an increase in cytotoxicity over the T3SS-deficient CAB4 control until 4 hours, and only reached about 60% of the cell lysis seen with CAB3 by 7.5 hours (Figure 38). This late increase in cytotoxicity demonstrates that the activity of VopR is able to drive lysis, albeit at a much later time point. However, during infection with CAB3 harboring the other T3SS1 effectors in addition to VopR, host cells are completely lysed by the time that VopR causes any increase in cell lysis over the CAB4 mutant. This means that the cytotoxicity seen with the CAB3Δ*vopQS* Δ*vpa0450* mutant is likely not significant within the time course of infection, although it is difficult to say without knowing how VopR is targeting the host cell.

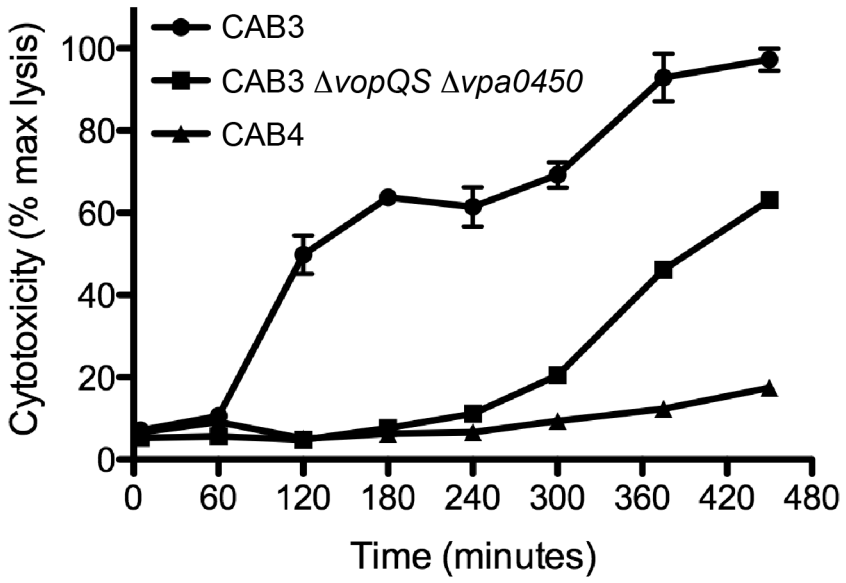

FIGURE 38. VopR does not directly contribute to cytotoxicity during infection.
Hela cells were infected with CAB3 (circles), CAB3Δ*vopQS* Δ*vpa0450* (squares), or CAB4 (triangles), and lactate dehydrogenase (LDH) release evaluated as a measure of cytotoxicity and host cell lysis. Data are means ± SD (n=2 samples) from a representative experiment repeated in duplicate.

Identification of homologs and a VopR catalytic triad

Information about an uncharacterized effector can often be uncovered through the identification of homologous effectors in other bacterial species, or homologous eukaryotic enzymes (10, 38, 67, 117). Bioinformatic analysis of VopR identified homologous T3SS effectors in *Photorhabdus luminescens* (Plu4750), an entemopathogenic commensal of nematode worms, as well as

multiple plant pathogens including *Pseudomonas* (HopX)*, Xanthomomas,* and *Ralstonia* species (Figure 39). These effectors share a conserved secondary structure and the cysteine-histidine-aspartate catalytic triad of the transglutaminase (Tgase) superfamily of eukaryotic enzymes, as well as some homology to papain-like proteases (Figure 39).

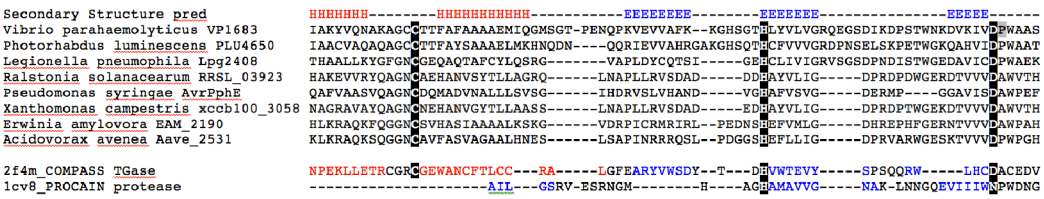

FIGURE 39. VopR has homology to multiple bacterial effectors and eukaryotic domains.
VopR aligns with T3S effectors and hypothetical proteins from several Gram-negative bacteria, as well as catalytic cores from a representative transglutaminase and protease. The catalytic core Cys-His-Asp are highlighted in black, predicted α-helices in red, and predicted β-strands in blue.

The Tgase superfamily contains the Tgases, peptide: *N*-glycanases (PNGase), and cysteine proteases, (87). Tgases catalyze the Ca^{2+}-dependent isopeptide bond formation between the ε-amino group of peptide-bound lysine, or a polyamine molecule, and γ-carboxamide of a peptide-bound glutamine. The resulting products of these reactions are often of high molecular mass, and highly resistant to proteolytic cleavage (43). PNGases remove the *N*-linked glycan

moieties from glycoproteins, and are important for the initial processing of misfolded proteins prior to proteasomal degradation (112). Cysteine proteases mediate proteolytic cleave of target proteins. VopR may catalyze a transferase or hydrolase reaction, or may use the same catalytic fold and triad of residues to mediate a completely different enzymatic process.

We next wanted to confirm that the catalytic triad residues identified in Tgases and plant effector homologs were also important for VopR activity. Hela cells were transfected with wild type VopR, or the C223A, H261A or D288A mutants. All the cells transfected with pSFFV-VopR displayed an irregular cell rounding with a ring of actin at the membrane that matches the phenotype seen during infection with CAB3Δ*vopQS* Δ*vpa0450* (Figure 40B and Figure 37H-I). Cells transfected with pSFFV-VopR-C223A, pSFFV-VopR-H261A, or pSFFV-VopR-D288A did not show any change from cells transfected with empty pSFFV vector (Figure 40A, C-E). This supports the hypothesis that this catalytic triad is important for activity. However, the conserved residues may be important for protein folding or stability.

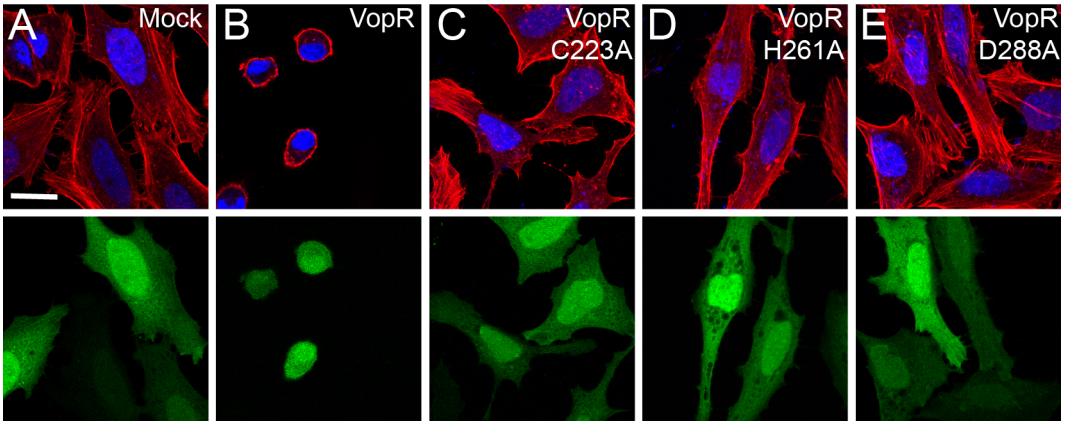

FIGURE 40. Mutation of putative catalytic residues abrogates the activity of VopR.
Hela cells were transfected with pEGFP-N1 and either (**A**) pSFFV empty vector, (**B**) pSFFV-VopR, (**C**) pSFFV-VopR-C223A, (**D**) pSFFV-VopR-H261A, or (**E**) pSFFV-VopR-D288A. Cells were then fixed, stained, and visualized by confocal microscopy. Green denotes expression of GFP and identifies transfected cells. Actin was stained with rhodamine-phalloidin (red), and DNA stained with Hoechst (blue). Scale bar, 20 μm.

Identification of this enzyme superfamily for VopR led to recognition of the catalytic triad of residues necessary for activity in mammalian cells. However, due to the varied range of activities of the Tgase family members, a substrate for VopR remains elusive. To identify a substrate, yeast genetic experiments were initiated. Yeast were transformed with a vector using a galactose-inducible promoter to express either wild type VopR, or the C223A, H261A, D288A or C222A mutants, as well as empty vector. Some Tgase family members have two adjacent cysteine residues and both were included in this experiment. Transformed yeast were first plated on yeast media with glucose to confirm viability (Figure 41A). Each strain was then plated to media with galactose and

raffinose. Galactose induces the expression of the gene of interest, but is a poor energy source for yeast. Raffinose is included to facilitate yeast growth without altering expression from the galactose promoter. Yeast expressing VopR and VopR-C222A were both growth inhibited. This indicates that VopR is toxic to yeast and inhibits growth, and that C222A is not important for growth inhibition. Those expressing the C223A, H261A or D288A mutants grew to cell densities equivalent to the empty vector control (Figure 41B), confirming these residues as important for activity attributed to growth arrest in yeast. When each strain was picked from the galactose media and replated on glucose media, only the yeast harboring C223A, H261A or D288A mutants, or the empty vector, were able to grow. This signifies that VopR and the C222A mutant were both lethal to yeast (Figure 41C).

Having confirmed that the catalytic triad mutants were viable in yeast, the C223A mutant was chosen for use in a yeast 2-hybrid screen to identify a binding substrate. Expression of the VopR-C223A bait plasmid without any prey resulted in red yeast colonies, indicating a build-up of an adenine synthesis intermediate. Adenine auxotrophy is used to select for yeast cells containing the bait plasmid. The presence of only red colonies means that the C223A mutant was still sufficiently toxic to force the yeast to kick out the plasmid, making a yeast 2-hybrid study impossible. Alternatively, a yeast multi-copy suppressor screen is currently being used to identify potential targets of VopR.

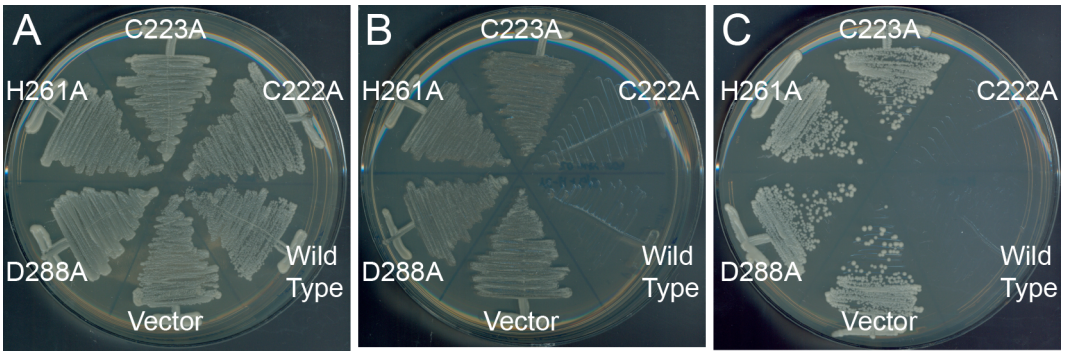

FIGURE 41. VopR is lethal to yeast.
Yeast were transformed with pRS413-P_{GAL} empty vector, pRS413-P_{GAL}-VopR, pRS413-P_{GAL}-VopR-C222A, pRS413-P_{GAL}-VopR-C223A, pRS413-P_{GAL}-VopR-H261A, or pRS413-P_{GAL}-VopR-D288A and plated to (**A**) YC-His dextrose to show viability, and (**B**) YC-His Gal/Raf media to induce effector expression and determine growth inhibition. (**C**) Streak areas for each transformant from the YC-His Gal/Raf plate were picked and replated to a new YC-His dextrose plate to identify VopR variants that were lethal to yeast.

Discussion

Perhaps one of the most interesting aspects of *V. parahaemolyticus* effectors is the diverse range of hosts that are targeted.. Based on current bioinformatic analysis, VopR has homologs in pathogens that infect mammals, insects and plants. One of the effector homologs of VopR is similar to HopX (formerly AvrPphE) from *Pseudomonas syringae*. Initial characterization of HopX confirmed the necessity for each of the putative catalytic triad residues for the lethal activity of this effector, as only wild type HopX could induce the avirulence response or tissue necrosis in plants (87). A molecular target or specific mechanism of action was not uncovered for HopX. It is interesting to

consider, however, that whatever the target is, it is likely conserved in plants, yeast, insects and humans.

A phenotype for VopR was uncovered during infection of Hela cells with a CAB3 strain with all other known effectors deleted. LDH release experiments showed that VopR has the ability to increase hydrolysis rates of infected cells, but not within a time frame that is pertinent for the current infection model. Homologs in pathogens of insects and plants were identified, as well as eukaryotic enzymes that revealed a catalytic triad of residues. Mutation of these residues abolished the activity of VopR during transfection. The ability of VopR to kill yeast was also abrogated when expressed under inducible conditions, but the C223A catalytic mutant proved too toxic for use in a yeast 2-hybrid experiment.

Much work is left to do for the characterization of VopR. Infection experiments with the CAB3Δ*vopQS* Δ*vpa0450* need to be repeated with additional time-points to determine if VopR alters the timeline for cell rounding and lysis. A CAB3Δ*vopR* + VopR complement strain needs to be constructed for use in infection studies. To this end, a new complementation vector, pMocha, has been made that is based on a pBAD-myc/his backbone, with modifications for use in *Vibrio* species. Transfection of Hela cells with GFP-tagged versions of VopR need to be performed to determine localization within the host cell. Of substantial importance for characterizing VopR will be the identification of the molecular

target and mechanism of action for this effector. Not only will this determine what other experiments need to be performed to complete our understanding of this effector, it will provide insight into the disease processes of a diverse subset of Gram-negative pathogens.

CHAPTER 7
DISCUSSION AND FUTURE DIRECTIONS

Introduction

Sixty years ago, an unknown pathogen caused an outbreak of gastroenteritis in Japan that sickened nearly 300 individuals. Study of patient samples from this outbreak identified *V. parahaemolyticus* as the etiologic agent (57). Since that time, *V. parahaemolyticus* has been shown to be a significant source of food poisoning, generally associated with the consumption of raw or undercooked seafood and shellfish (6). Concern regarding this organism as a pathogen has increased in recent years. A rise in global water temperatures and the emergence of pandemic strains have resulted in detection of *V. parahaemolyticus* in new environments, and continued outbreaks of disease (27, 122). A better understanding is needed of the virulence mechanisms employed by this organism.

Pathogenicity was initially attributed to the presence of TDH, which is found in nearly all clinical isolates (127). However, cultured cells infected with Δ*tdh* strains were still cytotoxic, indicating the presence of other virulence factors. Sequencing of the *V. parahaemolyticus* genome in 2003 identified two T3SS (71). T3SS1 has been shown cause cytotoxicity in cultured cells (16, 95). T3SS2 is

associated with pandemic strains, and induces enterotoxicity and cytotoxicity in an infection model (95).

Characterization of T3SS1 has identified four effectors to date. VopQ, VopR and VopS reside within the T3SS1 genomic island on chromosome 1, while VPA0450 is located on chromosome 2 (71, 91, 93). Study of these effectors has uncovered a paradigm of infection in which VopQ induces autophagy, blocking apoptosis in the host cell, and preventing phagocytosis of the infecting bacteria. VopS then AMPylates Rho family GTPases preventing their binding to downstream effectors, and ultimately causes the collapse of the actin cytoskeleton and cell rounding. This is followed by host cell lysis (Figure 42).

In the studies presented herein, we characterized the mechanism for VPA0450 and its contribution to T3SS1-mediated cytotoxicity. The presence of a novel localization domain was identified within VPA0450 that directs it to the plasma membrane and its substrate. A system was developed for making multiple gene deletions in *V. parahaemolyticus*. This system was used to uncover the phenotype for VopR during infection. The protein fold and catalytic residues were also identified for VopR. The characterization of T3SS1 effectors will advance our understanding of this system induces cytotoxicity, and facilitates disease progression during infection.

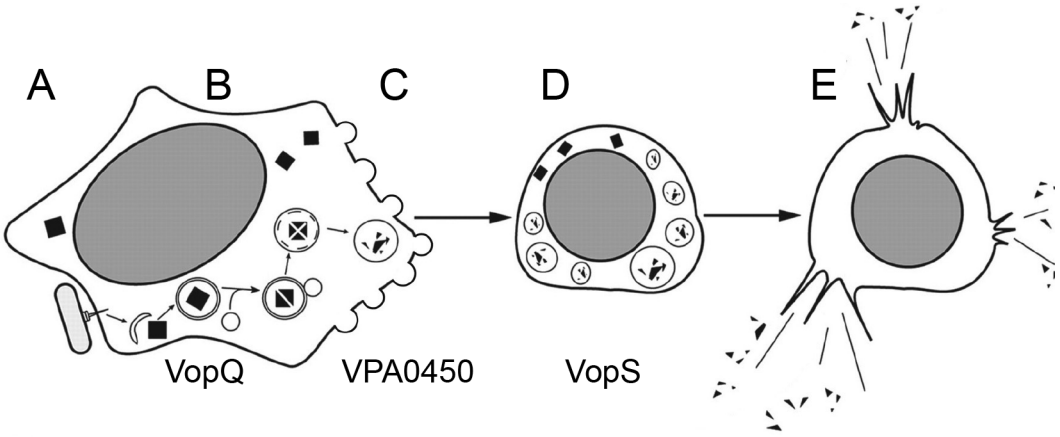

FIGURE 42. T3SS1 orchestrates a multifaceted host cell death.
(**A**) *V. parahaemolyticus* uses T3SS1 to translocate effectors into the cytoplasm of a host cell. (**B**) VopQ mediates the rapid induction of autophagy. (**C**) VPA0450 hydrolyzes the D5 phosphate from PtdIns(4,5)P_2, causing the dissociation of membrane-associated actin binding proteins. Destabilization of the membrane leads to transient blebbing. (**D**) VopS AMPylates Rho-family GTPases, causing the collapse of the actin cytoskeleton and cell rounding. (**E**) Cell rounding is followed by cell lysis and release of cytoplasmic contents. Adapted from (16).

Characterizing the multifaceted progression of T3SS1-mediated host cell death

The characterization of T3SS1-induced cytotoxicity has advanced considerably in recent years, and a multi-faceted model for infection has emerged (16). While the order of effector translocation is under investigation, phenotypes for each effector are discernible at discrete relative time points. Death of infected cells is characterized by the induction of autophagy, membrane blebbing, cell rounding, and then cell lysis (Figure 42).

Upon infection of host cells with a *V. parahaemolyticus* strain such as POR3 that has a functional T3SS1 but not T3SS2, cells undergo a rapid induction of autophagy. This is measured by conversion of LC3-I to LC3-II, which is then lipidated and inserted into autophagic vesicles. GFP-LC3 positive vesicles are readily observable in infected cells within 1 hour of infection (14). Induction of autophagy benefits *V. parahaemolyticus* by degrading cytoplasmic contents of the host cell. Upon cell lysis, nutrients and necessary cofactors such as amino acids and free iron are available for uptake by the bacteria. The ability to gain nutrients rapidly is important for a pathogen that will be expelled within a short time from the host.

Autophagy requires cytoplasmic localization of membranes. By driving membrane to the interior of the cell, there may not be sufficient lipid remaining in the plasma membrane for phagocytosis of infecting bacteria. *V. parahaemolyticus* is normally an extracellular pathogen. However, cells infected with a Δ*vopQ* strain had bacteria localized to vesicles in the cytoplasm (14). The induction of autophagy may be a mechanism to prevent phagocytosis and subsequent immune clearance of the bacteria during infection. VopQ has also been shown to block induction of apoptosis (16). It is unknown if autophagy is the intended consequence of VopQ translocation, or an effect secondary to blocking apoptosis. Induction of apoptosis in EPC fish cells infected with a *V. alginlyticus* strain that contains the VopQ homolog Va1680 implies induction of autophagy is not the

primary function of VopQ. However, it is still possible that both blocking apoptosis, and preventing phagocytosis are intended effects of VopQ during infection of mammalian cells, or a human host. Maintaining an inflammatory cell death provides nutrients to the bacteria upon cell lysis. Autophagy induction prevents phagocytosis by immune cells responding to the infection. Identification of a target and mechanism of action for VopQ is necessary for a definitive answer as to the intended consequence of VopQ translocation during infection.

Induction of autophagy is followed by a severe but transient blebbing of the plasma membrane caused by VPA0450 mediated hydrolysis of PtdIns(4,5)P_2 (10). This work has shown VPA0450 to be an inositol polyphosphate 5-phosphatase (IPP5C) with homology to the IPP5C domain of the eukaryotic enzyme synaptojanin. The specific hydrolysis of the D5 phosphate from PtdIns(4,5)P_2 disrupted association of membrane-associated proteins, leading to blebbing. Blebbing is a normal phenomenon in eukaryotic cells. Localized disruption of the actin cytoskeleton, or disconnection of actin from the plasma membrane allows the hydrostatic pressure of the cytoplasm to force the membrane outward (21). Normally, reformation of the actin cortex halts bleb expansion. Then, the attachment of myosin, and actomyosin contractility retracts the bleb (34). The increased activity over endogenous IPP5C domains, coupled with localization of VPA0450 to the membrane, may prevent sufficient PtdIns(4,5)P_2 reformation. This could prevent sufficient binding of actin to the

interior of the bleb for bleb retraction. The hydrolysis of PtdIns(4,5)P_2 induced by VPA0450 was necessary for rapid cell lysis seen during infection.

Preliminary data indicate that the localization of VPA0450 is mediated by the C-terminus of the effector. Bioinformatic analysis identified the presence of two amphipathic helices. One of these contains a polybasic patch, and may bind phosphoinositides thereby providing substrate specificity and driving VPA0450 to the plasma membrane. The exact domain sufficient to localize proteins to the plasma membrane has not been elucidated. Full-length synaptojanin contains a Sac1 phosphatase domain, the IPP5C domain homologous to VPA0450, in addition to a proline rich region. It is localized to endocytic vesicles through interaction of its C-terminal proline rich region with SH3-containing proteins including endophilin and amphiphysin (19). Without a localization domain, SPsynj IPP5C has a diminished ability to induce blebbing compared to full length VPA0450. The presence of this novel localization domain with the IPP5C catalytic core of VPA0450 substantially increases its activity *in vivo* over the IPP5C of SPsynj (10).

Host cell rounding immediately follows host cell membrane blebbing. VopS was previously shown to AMPylate the switch 1 region of Rho-family GTPases. This prevents GTPase binding to downstream effectors and blocks this signaling cascade. The end result is the collapse of the actin cytoskeleton and cell rounding.

Within this infection process, VopR is also expressed. Infection of Hela cells with CAB3Δ*vopQS* Δ*vpa0450* resulted in irregular rounded cells with a ring of actin at the membrane. This phenotype was confirmed by transfection of VopR into Hela cells. This phenotype is seen during infection with POR3Δ*vopS*, indicating that VopR is present and active in infected cells at the same time as VopS, but is masked by the effects of VopS (data not shown). The target and mechanism of VopR have not yet been identified. VopR homologs were identified in insect and plant pathogens as well as eukaryotic enzyme domains. Secondary structure prediction and alignment with homologs predicts VopR has a cysteine protease-like fold, is a member of the transglutaminase superfamily, and has a cysteine-histidine-aspartate catalytic triad.

While it is not currently known how VopR contributes to this process, the presence of VopR homologs in a large number of other pathogens, including HopX in *P. syringae* and Plu4750 in *P. luminescens*, indicate its function is important for the disease process. It is interesting to note that *P. luminescens*, an entemopathogenic commensal of nematode worms, also has a VPA0450 homolog (Plu4615), and five hypothetical proteins with fic domains (Plu4880, Plu3214, Plu3930, Plu2421 and Plu4284). This domain is indispensible for AMPylation activity by VopS. While there is not a VopQ homolog, *P.luminescens* does contain a homolog to *Yersinia* YopT (LopT), and *P. aeruginosa* ExoU (LopU) (12, 13). ExoU and other cytosolic phospholipase A_2 ($cPLA_2$) proteins require a

catalytic dyad of glycine rich sequences with a serine residue (GxSxG), and aspartate residue (DxG), for enzymatic activity (126). While VopQ has both of these motifs, mutation of the serine and aspartate residues followed by transfection to Hela cells was inconclusive. Infection of Hela cells with POR3 in the presence of phospholipase inhibitors indicated that VopQ is not a phospholipase (data not shown). It is possible that *P. luminescens* and *V. parahaemolyticus* share a paradigm of host cell death using homologous effectors.

Improved methods for studying T3SS effector interplay

Many studies of *V. parahaemolyticus* pathogenicity have taken a reductionist approach. Individual toxins or effectors have been characterized, providing insight into the various mechanisms by which *V. parahaemolyticus* can cause disease. This approach was taken in our lab out of necessity. Deletion of a single chromosomal gene from *V. parahaemolyticus* took 2 to 6 months, and left an unresolvable antibiotic resistance cassette in place of the deleted gene. This prevented deletion of multiple genes, and hampered our ability to study various effector combinations during infection.

While the use oriR6K suicide vectors is not new, it had not previously been attempted in our lab. Adaptation of a protocol used on the NY-4 strain of *V. parahaemolyticus* yielded a system that allows for unmarked deletions of chromosomal genes in two weeks time. This study used several products of this

new system, including the new CAB2, CAB3 and CAB4 parent strains, as well as the Δ*vcrD1*, Δ*vscN1*, and Δ*vopQS* Δ*vpa0450* strains made in the CAB3 background. In addition, a library of T3SS1 effector knockouts is being constructed. In short time, every possible combination of T3SS1 effector knockouts will be available for infection studies. Additionally, T3SS2 effector knockouts are being created in the CAB2 background. Confocal imaging and LDH release assay analysis of each strain will yield valuable data regarding synergistic and antagonistic relationships between effectors. Additionally, various deletion strains can be complemented *in cis* using the same knockout vector system to allow for endogenous expression of tagged effectors, as well as studies to determine timing of effector translocation. The use of these strains will greatly increase our knowledge of *V. parahaemolyticus* mediated infection.

Future work

Identify minimum domain necessary and sufficient for proper VPA0450 localization

The work presented herein provides an improved understanding of T3SS1 mediated virulence, but does not complete the picture. There are several aspects of VPA0450 activity that remain to be characterized. The C-terminus of VPA0450 was shown to be necessary for proper localization to the plasma membrane (Figure 26Band C), as well as efficient delocalization of a

PtdIns(4,5)P_2-specific PH domain from the membrane (Figure 27). The minimum portion of VPA0450 that is necessary and sufficient for this localization is not currently known. A fusion protein of GFP attached in frame to the N-terminus of VPA0450, similar to the mCherry construct used herein (Figure 26B), will need to be constructed for improved visualization of VPA0450 localization. Truncated proteins will then be made from the GFP-VPA0450 fusion, including the Δ367-475 construct, as well as Δα8-α10, Δα9-α10, Δα9, and Δα10 constructs. These constructs will be used in transfection experiments to identify the portion of VPA0450 necessary for proper localization to the plasma membrane. The induction of membrane blebbing and delocalize PH(PLCδ1)-GFP from the membrane will be measured for each construct. The malachite green assay for phosphate release will be used to confirm activity of constructs that fail to localize properly or induce blebbing to ensure that any decrease in activity *in vivo* is not a result of improper folding.

Portions of the effector identified as necessary for localization will then be fused directly to GFP and transfected into Hela cells. Fusion proteins containing a portion of the VPA0450 C-terminus sufficient for proper localization will form a ring of GFP around the transfected cell, similar to cells transfected with PH(PLCδ1)-GFP (Figure 21A). Constructs that localize to the plasma membrane will then have the VPA0450 domain serially truncated to determine the minimum portion of this effector that is sufficient for localization. If α9 and/or α10 are part

of the localization domain, site directed mutagenesis will be used to alter the hydrophobic and polybasic regions to incorporate hydrophilic and acidic residues, respectively. This will determine the contribution of these properties to localization.

We will next determine the binding specificity of the VPA0450 localization domain. Full length VPA0450, and a truncation mutant that does not localize to the membrane, will be expressed in *E. coli* and purified. Dot blot analysis using phosphoinositides and individual membrane lipids will be used to identify potential binding moieties in the plasma membrane.

Proper localization and VPA0450 activity

Once the VPA0450 localization domain is identified, the contribution of this domain and proper localization to overall activity will be assessed. The 2xFYVE domain will be fused to VPA0450 deleted for the endogenous localization domain to drive VPA0450 to early endosomes (5). This construct will then be transfected into Hela cells, and membrane blebbing and PH(PLCδ1)-GFP delocalization measured. Other domains that localize to the plasma membrane, including PH(PLCδ1), ARNO-PH, and TAPP1 will be fused to the truncated VPA0450. These domains bind to PtdIns(4,5)P_2, PtdIns(3,4,5)P_3, and PtdIns(3,4)P_2, respectively (5). Additionally, an N-terminal palmitoylation site, and a C-terminal CaaX box, will each be fused to localization domain-deficient

VPA0450 to drive phosphoinositide-independent localization to membranes. This will determine if binding to a specific moiety at the membrane, or just general localization, is required for activity as determined by blebbing and PH(PLCδ1)-GFP delocalization.

During characterization of VPA0450, it was found that the biochemical activity of VPA0450 was two-fold higher than SPsynj IPP5C, but caused a 20-25 fold increase in the number of blebbing cells during transfection (Figure 19G and Figure 20). We will determine if this is due to the lack of a localization domain on the SPsynj IPP5C. The VPA0450 localization domain will be fused to SPsynj IPP5C, and this construct transfected into Hela cells to measure blebbing. The number of transfected cells with membrane blebs will be determined and compared to the IPP5C domain alone. Additionally, the ability of each construct ot delocalize PH(PLCδ1)-GFP will be determined. Finally, residues 1-76 of VPA0450, comprising the N-terminal secretion signal and chaperone-binding region will be fused to the SPsynj IPP5C-VPA0450 localization domain hybrid. This construct will be cloned into a *V. parahaemolyticus* complementation vector containing the endogenous VPA0450 promoter region. This vector will be mated into CAB3Δ*vopQRS* Δ*vpa0450* to determine if the SPsynj IPP5C domain can act as a bacterial effector in place of the VPA0450 IPP5C domain. This construct will also be mated into the CAB3Δ*vpa0450* strain to determine if the SPsynj IPP5C is sufficient to complement the *vpa0450* deletion in LDH release assays. If the

hybrid construct is translocated and active, the hybrid gene will be knocked into CAB3Δ*vopQRS* Δ*vpa0450*, and compared to the CAB3Δ*vopQRS* strain for its ability to induce blebbing.

Interaction between effectors during infection

The ability to make multiple unmarked chromosomal gene deletions in V. parahaemolyticus has opened up several lines of research. The work herein has demonstrated the use of a multiple effector knockout, CAB3Δ*vopQS* Δ*vpa0450*, to elucidate the phenotype for an uncharacterized effector. We are in the process of making the CAB3Δ*vopQRS* Δ*vpa0450* strain, which will be used to detect additional effectors by infecting Hela cells and comparing to CAB4-infected cells.

Various effectors may work synergistically or antagonistically to alter the level or timing of activity of other effectors during infection. To determine if this occurs in *V. parahaemolyticus*, each possible pair of T3SS1 effectors will be deleted in the CAB3 strain and used in infection studies. Most of the T3SS1 effector deletion combinations have been constructed in CAB3 and are currently being verified. Confocal imaging and LDH release assays will determine changes in infection profiles.

The timing of effector translocation into a host cell is not well understood, and the mechanisms that control delivery of effectors are just now being elucidated (64). Beta-lactamase fusions of each T3SS1 effector are currently

being constructed, and will be knocked in to each respective single gene deletion. These reporter strains will then be used to infect Hela cells pretreated with CCF2-AM. This is a binary fluorescent FRET dye that will change from green to blue upon cleavage by the β-lactamase domain of each reporter fusion. Development of blue fluorescence occurs upon effector translocation, and allows for determination of effector translocation timing (78).

In addition to the library of T3SS1 effector deletion strains being constructed in CAB3, a comparable library is under construction for T3SS2 effectors in the CAB2 background. Each combination of the T3SS2 effectors, VopA/P, VopC, VopL, and VopT will be deleted and subjected to assays similar to those described above for T3SS1 effectors in the CAB3 strain. There are a number of hypothetical genes within the Vp-PAI that are upregulated upon bile induction and may be effector proteins (42). Use of the β-lactamase fusion system described above can be used to confirm translocation of any of these proteins that are effectors.

Identification of target and mechanism of action for VopR

The use of the CAB3 Δ*vopQS* Δ*vpa0450* strain was able to identify a phenotype for VopR (Figure 37H and I). While some progress has been made on the characterization of this effector, there are many experiments needed to characterize the contribution VopR makes during infection by *V.*

parahaemolyticus. The data presented herein are preliminary and need to be repeated. Infection studies need additional time points to determine if VopR changes the timing of cell lysis or lysis.

During infection with the CAB3 Δ*vopQS* Δ*vpa0450* strain, or transfection with VopR, cells have an irregular rounded shape with actin at the membrane (Figure 37H and I; and Figure 40B). Under the microscope, these cells look as though the membrane has regions of small blebs (1-2 μm). These appear much smaller than those induced by VPA0450, or during apoptosis. Additional confocal microscopy, and possibly electron microscopy, will be required to fully characterize the membrane morphology of cells in which VopR has been translocated or transfected.

Many of the experiments to fully characterize VopR will be determined by its target and mechanism of action. As these are not currently known, the identification of the molecular target of VopR is a priority. Attempts at using a yeast 2-hybrid screen were unsuccessful. Currently, a yeast multi-copy suppressor screen is being used to identify possible targets for VopR. Any proteins identified will need to be verified. The characterization of VopR, as well as VPA0450 localization and effector interplay, will greatly improve our understanding of T3SS1-mediated virulence, and the pathogenesis of *V. parahaemolyticus*.

BIBLIOGRAPHY

1. **Akeda, Y., and J. E. Galan.** 2005. Chaperone release and unfolding of substrates in type III secretion. Nature **437:**911-5.
2. **Alam, M. J., K. I. Tomochika, S. I. Miyoshi, and S. Shinoda.** 2002. Environmental investigation of potentially pathogenic Vibrio parahaemolyticus in the Seto-Inland Sea, Japan. FEMS Microbiol Lett **208:**83-7.
3. **Arnold, R., A. Jehl, and T. Rattei.** 2010. Targeting effectors: the molecular recognition of Type III secreted proteins. Microbes Infect **12:**346-58.
4. **Baffone, W., R. Tarsi, L. Pane, R. Campana, B. Repetto, G. L. Mariottini, and C. Pruzzo.** 2006. Detection of free-living and plankton-bound vibrios in coastal waters of the Adriatic Sea (Italy) and study of their pathogenicity-associated properties. Environ Microbiol **8:**1299-305.
5. **Balla, T., and P. Varnai.** 2009. Visualization of cellular phosphoinositide pools with GFP-fused protein-domains. Curr Protoc Cell Biol **Chapter 24:**Unit 24 4.
6. **Barker, W. H., Jr., and E. J. Gangarosa.** 1974. Food poisoning due to Vibrio parahaemolyticus. Annu Rev Med **25:**75-81.
7. **Belas, M. R., and R. R. Colwell.** 1982. Adsorption kinetics of laterally and polarly flagellated Vibrio. J Bacteriol **151:**1568-80.
8. **Belas, M. R., and R. R. Colwell.** 1982. Scanning electron microscope observation of the swarming phenomenon of Vibrio parahaemolyticus. J Bacteriol **150:**956-9.
9. **Blake, P. A., M. H. Merson, R. E. Weaver, D. G. Hollis, and P. C. Heublein.** 1979. Disease caused by a marine Vibrio. Clinical characteristics and epidemiology. N Engl J Med **300:**1-5.
10. **Broberg, C. A., L. Zhang, H. Gonzalez, M. A. Laskowski-Arce, and K. Orth.** 2010. A Vibrio Effector Protein is an Inositol Phosphatase and Disrupts Host Cell Membrane Integrity. Science **329:**1660-62.
11. **Brodin, L., P. Low, and O. Shupliakov.** 2000. Sequential steps in clathrin-mediated synaptic vesicle endocytosis. Curr Opin Neurobiol **10:**312-20.
12. **Brugirard-Ricaud, K., E. Duchaud, A. Givaudan, P. A. Girard, F. Kunst, N. Boemare, M. Brehelin, and R. Zumbihl.** 2005. Site-specific antiphagocytic function of the Photorhabdus luminescens type III secretion system during insect colonization. Cell Microbiol **7:**363-71.
13. **Brugirard-Ricaud, K., A. Givaudan, J. Parkhill, N. Boemare, F. Kunst, R. Zumbihl, and E. Duchaud.** 2004. Variation in the effectors of

the type III secretion system among Photorhabdus species as revealed by genomic analysis. J Bacteriol **186:**4376-81.

14. **Burdette, D. L., J. Seemann, and K. Orth.** 2009. Vibrio VopQ induces PI3-kinase-independent autophagy and antagonizes phagocytosis. Mol Microbiol **73:**639-49.
15. **Burdette, D. L., M. L. Yarbrough, and K. Orth.** 2009. Not without cause: Vibrio parahaemolyticus induces acute autophagy and cell death. Autophagy **5:**100-2.
16. **Burdette, D. L., M. L. Yarbrough, A. Orvedahl, C. J. Gilpin, and K. Orth.** 2008. Vibrio parahaemolyticus orchestrates a multifaceted host cell infection by induction of autophagy, cell rounding, and then cell lysis. Proc Natl Acad Sci U S A **105:**12497-502.
17. **Caburlotto, G., M. M. Lleo, T. Hilton, A. Huq, R. R. Colwell, and J. B. Kaper.** 2010. Effect on human cells of environmental Vibrio parahaemolyticus strains carrying type III secretion system 2. Infect Immun **78:**3280-7.
18. **Carter, S. G., and D. W. Karl.** 1982. Inorganic phosphate assay with malachite green: an improvement and evaluation. J Biochem Biophys Methods **7:**7-13.
19. **Cestra, G., L. Castagnoli, L. Dente, O. Minenkova, A. Petrelli, N. Migone, U. Hoffmuller, J. Schneider-Mergener, and G. Cesareni.** 1999. The SH3 domains of endophilin and amphiphysin bind to the proline-rich region of synaptojanin 1 at distinct sites that display an unconventional binding specificity. J Biol Chem **274:**32001-7.
20. **Chao, G., X. Jiao, X. Zhou, F. Wang, Z. Yang, J. Huang, Z. Pan, L. Zhou, and X. Qian.** 2010. Distribution of genes encoding four pathogenicity islands (VPaIs), T6SS, biofilm, and type I pilus in food and clinical strains of Vibrio parahaemolyticus in China. Foodborne Pathog Dis **7:**649-58.
21. **Charras, G., and E. Paluch.** 2008. Blebs lead the way: how to migrate without lamellipodia. Nat Rev Mol Cell Biol **9:**730-6.
22. **Charras, G. T.** 2008. A short history of blebbing. J Microsc **231:**466-78.
23. **Cornelis, G. R.** 2006. The type III secretion injectisome. Nat Rev Microbiol **4:**811-25.
24. **Cornelis, G. R., A. Boland, A. P. Boyd, C. Geuijen, M. Iriarte, C. Neyt, M. P. Sory, and I. Stainier.** 1998. The virulence plasmid of Yersinia, an antihost genome. Microbiol Mol Biol Rev **62:**1315-52.
25. **Cunnac, S., M. Lindeberg, and A. Collmer.** 2009. Pseudomonas syringae type III secretion system effectors: repertoires in search of functions. Curr Opin Microbiol **12:**53-60.

26. **Czech, M. P.** 2000. PIP2 and PIP3: complex roles at the cell surface. Cell **100:**603-6.
27. **Daniels, N. A., L. MacKinnon, R. Bishop, S. Altekruse, B. Ray, R. M. Hammond, S. Thompson, S. Wilson, N. H. Bean, P. M. Griffin, and L. Slutsker.** 2000. Vibrio parahaemolyticus infections in the United States, 1973-1998. J Infect Dis **181:**1661-6.
28. **Datsenko, K. A., and B. L. Wanner.** 2000. One-step inactivation of chromosomal genes in Escherichia coli K-12 using PCR products. Proc Natl Acad Sci U S A **97:**6640-5.
29. **Deng, W., C. L. de Hoog, H. B. Yu, Y. Li, M. A. Croxen, N. A. Thomas, J. L. Puente, L. J. Foster, and B. B. Finlay.** 2010. A comprehensive proteomic analysis of the type III secretome of Citrobacter rodentium. J Biol Chem **285:**6790-800.
30. **Di Paolo, G., and P. De Camilli.** 2006. Phosphoinositides in cell regulation and membrane dynamics. Nature **443:**651-7.
31. **Ditta, G., S. Stanfield, D. Corbin, and D. R. Helinski.** 1980. Broad host range DNA cloning system for gram-negative bacteria: construction of a gene bank of Rhizobium meliloti. Proc Natl Acad Sci U S A **77:**7347-51.
32. **Dorman, C. J.** 2004. H-NS: a universal regulator for a dynamic genome. Nat Rev Microbiol **2:**391-400.
33. **Enninga, J., and I. Rosenshine.** 2009. Imaging the assembly, structure and activity of type III secretion systems. Cell Microbiol **11:**1462-70.
34. **Fackler, O. T., and R. Grosse.** 2008. Cell motility through plasma membrane blebbing. J Cell Biol **181:**879-84.
35. **Ferreira, R. B., L. C. Antunes, E. P. Greenberg, and L. L. McCarter.** 2008. Vibrio parahaemolyticus ScrC modulates cyclic dimeric GMP regulation of gene expression relevant to growth on surfaces. J Bacteriol **190:**851-60.
36. **Friedman, A. M., S. R. Long, S. E. Brown, W. J. Buikema, and F. M. Ausubel.** 1982. Construction of a broad host range cosmid cloning vector and its use in the genetic analysis of Rhizobium mutants. Gene **18:**289-96.
37. **Fukui, T., K. Shiraki, D. Hamada, K. Hara, T. Miyata, S. Fujiwara, K. Mayanagi, K. Yanagihara, T. Iida, E. Fukusaki, T. Imanaka, T. Honda, and I. Yanagihara.** 2005. Thermostable direct hemolysin of Vibrio parahaemolyticus is a bacterial reversible amyloid toxin. Biochemistry **44:**9825-32.
38. **Galan, J. E.** 2009. Common themes in the design and function of bacterial effectors. Cell Host Microbe **5:**571-9.
39. **Galan, J. E., and H. Wolf-Watz.** 2006. Protein delivery into eukaryotic cells by type III secretion machines. Nature **444:**567-73.

40. **Ghosh, P.** 2004. Process of protein transport by the type III secretion system. Microbiol Mol Biol Rev **68:**771-95.
41. **Gode-Potratz, C. J., R. J. Kustusch, P. J. Breheny, D. S. Weiss, and L. L. McCarter.** 2011. Surface sensing in Vibrio parahaemolyticus triggers a programme of gene expression that promotes colonization and virulence. Mol Microbiol **79:**240-63.
42. **Gotoh, K., T. Kodama, H. Hiyoshi, K. Izutsu, K. S. Park, R. Dryselius, Y. Akeda, T. Honda, and T. Iida.** 2010. Bile acid-induced virulence gene expression of Vibrio parahaemolyticus reveals a novel therapeutic potential for bile acid sequestrants. PLoS One **5:**e13365.
43. **Griffin, M., R. Casadio, and C. M. Bergamini.** 2002. Transglutaminases: nature's biological glues. Biochem J **368:**377-96.
44. **Guo, S., L. E. Stolz, S. M. Lemrow, and J. D. York.** 1999. SAC1-like domains of yeast SAC1, INP52, and INP53 and of human synaptojanin encode polyphosphoinositide phosphatases. J Biol Chem **274:**12990-5.
45. **Harder, K. W., P. Owen, L. K. Wong, R. Aebersold, I. Clark-Lewis, and F. R. Jirik.** 1994. Characterization and kinetic analysis of the intracellular domain of human protein tyrosine phosphatase beta (HPTP beta) using synthetic phosphopeptides. Biochem J **298 (Pt 2):**395-401.
46. **Henry, T., C. Couillault, P. Rockenfeller, E. Boucrot, A. Dumont, N. Schroeder, A. Hermant, L. A. Knodler, P. Lecine, O. Steele-Mortimer, J. P. Borg, J. P. Gorvel, and S. Meresse.** 2006. The Salmonella effector protein PipB2 is a linker for kinesin-1. Proc Natl Acad Sci U S A **103:**13497-502.
47. **Hirsch, P. R., and J. E. Beringer.** 1984. A physical map of pPH1JI and pJB4JI. Plasmid **12:**139-41.
48. **Hiyoshi, H., T. Kodama, T. Iida, and T. Honda.** 2010. Contribution of Vibrio parahaemolyticus virulence factors to cytotoxicity, enterotoxicity, and lethality in mice. Infect Immun **78:**1772-80.
49. **Hlady, W. G., and K. C. Klontz.** 1996. The epidemiology of Vibrio infections in Florida, 1981-1993. J Infect Dis **173:**1176-83.
50. **Honda, T., T. Iida, Y. Akeda, and T. Kodama.** 2008. Sixty years of Vibrio parahaemolyticus. Microbe **3:**462-466.
51. **Honda, T., Y. Ni, T. Miwatani, T. Adachi, and J. Kim.** 1992. The thermostable direct hemolysin of Vibrio parahaemolyticus is a pore-forming toxin. Can J Microbiol **38:**1175-80.
52. **Hongping, W., Z. Jilun, J. Ting, B. Yixi, and Z. Xiaoming.** 2011. Insufficiency of the Kanagawa hemolytic test for detecting pathogenic Vibrio parahaemolyticus in Shanghai, China. Diagn Microbiol Infect Dis **69:**7-11.

53. **Hurley, J. H., and S. Misra.** 2000. Signaling and subcellular targeting by membrane-binding domains. Annu Rev Biophys Biomol Struct **29:**49-79.
54. **Jaques, S., and L. L. McCarter.** 2006. Three new regulators of swarming in Vibrio parahaemolyticus. J Bacteriol **188:**2625-35.
55. **Johnson, C. N., A. R. Flowers, N. F. Noriea, 3rd, A. M. Zimmerman, J. C. Bowers, A. DePaola, and D. J. Grimes.** 2010. Relationships between environmental factors and pathogenic vibrios in the Northern Gulf of Mexico. Appl Environ Microbiol **76:**7076-84.
56. **Johnson, J. E., and R. B. Cornell.** 1999. Amphitropic proteins: regulation by reversible membrane interactions (review). Mol Membr Biol **16:**217-35.
57. **Joseph, S. W., R. R. Colwell, and J. B. Kaper.** 1982. Vibrio parahaemolyticus and related halophilic Vibrios. Crit Rev Microbiol **10:**77-124.
58. **Kim, Y. K., and L. L. McCarter.** 2000. Analysis of the polar flagellar gene system of Vibrio parahaemolyticus. J Bacteriol **182:**3693-704.
59. **Kim, Y. K., and L. L. McCarter.** 2007. ScrG, a GGDEF-EAL protein, participates in regulating swarming and sticking in Vibrio parahaemolyticus. J Bacteriol **189:**4094-107.
60. **Kodama, T., K. Gotoh, H. Hiyoshi, M. Morita, K. Izutsu, Y. Akeda, K. S. Park, V. V. Cantarelli, R. Dryselius, T. Iida, and T. Honda.** 2010. Two regulators of Vibrio parahaemolyticus play important roles in enterotoxicity by controlling the expression of genes in the Vp-PAI region. PLoS One **5:**e8678.
61. **Kodama, T., M. Rokuda, K. S. Park, V. V. Cantarelli, S. Matsuda, T. Iida, and T. Honda.** 2007. Identification and characterization of VopT, a novel ADP-ribosyltransferase effector protein secreted via the Vibrio parahaemolyticus type III secretion system 2. Cell Microbiol **9:**2598-609.
62. **Kodama, T., C. Yamazaki, K. S. Park, Y. Akeda, T. Iida, and T. Honda.** 2010. Transcription of Vibrio parahaemolyticus T3SS1 genes is regulated by a dual regulation system consisting of the ExsACDE regulatory cascade and H-NS. FEMS Microbiol Lett.
63. **Kvitko, B. H., D. H. Park, A. C. Velasquez, C. F. Wei, A. B. Russell, G. B. Martin, D. J. Schneider, and A. Collmer.** 2009. Deletions in the repertoire of Pseudomonas syringae pv. tomato DC3000 type III secretion effector genes reveal functional overlap among effectors. PLoS Pathog **5:**e1000388.
64. **Lara-Tejero, M., J. Kato, S. Wagner, X. Liu, and J. E. Galan.** 2011. A Sorting Platform Determines the Order of Protein Secretion in Bacterial Type III Systems. Science.

65. **Levine, W. C., and P. M. Griffin.** 1993. Vibrio infections on the Gulf Coast: results of first year of regional surveillance. Gulf Coast Vibrio Working Group. J Infect Dis **167:**479-83.
66. **Liu, Y., and V. A. Bankaitis.** 2010. Phosphoinositide phosphatases in cell biology and disease. Prog Lipid Res **49:**201-17.
67. **Liverman, A. D., H. C. Cheng, J. E. Trosky, D. W. Leung, M. L. Yarbrough, D. L. Burdette, M. K. Rosen, and K. Orth.** 2007. Arp2/3-independent assembly of actin by Vibrio type III effector VopL. Proc Natl Acad Sci U S A **104:**17117-22.
68. **Lloyd, S. A., M. Norman, R. Rosqvist, and H. Wolf-Watz.** 2001. Yersinia YopE is targeted for type III secretion by N-terminal, not mRNA, signals. Mol Microbiol **39:**520-31.
69. **Luong, P., L. N. Kinch, C. A. Brautigam, N. V. Grishin, D. R. Tomchick, and K. Orth.** 2010. Kinetic and structural insights into the mechanism of AMPylation by VopS Fic domain. J Biol Chem **285:**20155-63.
70. **Lynch, T., S. Livingstone, E. Buenaventura, E. Lutter, J. Fedwick, A. G. Buret, D. Graham, and R. DeVinney.** 2005. Vibrio parahaemolyticus disruption of epithelial cell tight junctions occurs independently of toxin production. Infect Immun **73:**1275-83.
71. **Makino, K., K. Oshima, K. Kurokawa, K. Yokoyama, T. Uda, K. Tagomori, Y. Iijima, M. Najima, M. Nakano, A. Yamashita, Y. Kubota, S. Kimura, T. Yasunaga, T. Honda, H. Shinagawa, M. Hattori, and T. Iida.** 2003. Genome sequence of Vibrio parahaemolyticus: a pathogenic mechanism distinct from that of V cholerae. Lancet **361:**743-9.
72. **Mallo, G. V., M. Espina, A. C. Smith, M. R. Terebiznik, A. Aleman, B. B. Finlay, L. E. Rameh, S. Grinstein, and J. H. Brumell.** 2008. SopB promotes phosphatidylinositol 3-phosphate formation on Salmonella vacuoles by recruiting Rab5 and Vps34. J Cell Biol **182:**741-52.
73. **Marlovits, T. C., and C. E. Stebbins.** 2010. Type III secretion systems shape up as they ship out. Curr Opin Microbiol **13:**47-52.
74. **Matlawska-Wasowska, K., R. Finn, A. Mustel, C. P. O'Byrne, A. W. Baird, E. T. Coffey, and A. Boyd.** 2010. The Vibrio parahaemolyticus Type III Secretion Systems manipulate host cell MAPK for critical steps in pathogenesis. BMC Microbiol **10:**329.
75. **Matsuda, S., T. Kodama, N. Okada, K. Okayama, T. Honda, and T. Iida.** 2010. Association of Vibrio parahaemolyticus thermostable direct hemolysin with lipid rafts is essential for cytotoxicity but not hemolytic activity. Infect Immun **78:**603-10.

76. **McCarter, L.** 1999. The multiple identities of Vibrio parahaemolyticus. J Mol Microbiol Biotechnol **1:**51-7.
77. **McLaughlin, J. B., A. DePaola, C. A. Bopp, K. A. Martinek, N. P. Napolilli, C. G. Allison, S. L. Murray, E. C. Thompson, M. M. Bird, and J. P. Middaugh.** 2005. Outbreak of Vibrio parahaemolyticus gastroenteritis associated with Alaskan oysters. N Engl J Med **353:**1463-70.
78. **Mills, E., K. Baruch, X. Charpentier, S. Kobi, and I. Rosenshine.** 2008. Real-time analysis of effector translocation by the type III secretion system of enteropathogenic Escherichia coli. Cell Host Microbe **3:**104-13.
79. **Minamino, T., and R. M. Macnab.** 1999. Components of the Salmonella flagellar export apparatus and classification of export substrates. J Bacteriol **181:**1388-94.
80. **Miraglia, A. G., S. Travaglione, S. Meschini, L. Falzano, P. Matarrese, M. G. Quaranta, M. Viora, C. Fiorentini, and A. Fabbri.** 2007. Cytotoxic necrotizing factor 1 prevents apoptosis via the Akt/IkappaB kinase pathway: role of nuclear factor-kappaB and Bcl-2. Mol Biol Cell **18:**2735-44.
81. **Molenda, J. R., W. G. Johnson, M. Fishbein, B. Wentz, I. J. Mehlman, and T. A. Dadisman, Jr.** 1972. Vibrio parahaemolyticus gastroenteritis in Maryland: laboratory aspects. Appl Microbiol **24:**444-8.
82. **Monack, D. M., J. Mecsas, N. Ghori, and S. Falkow.** 1997. Yersinia signals macrophages to undergo apoptosis and YopJ is necessary for this cell death. Proc Natl Acad Sci U S A **94:**10385-90.
83. **Morris, J. G., Jr.** 2003. Cholera and other types of vibriosis: a story of human pandemics and oysters on the half shell. Clin Infect Dis **37:**272-80.
84. **Morris, J. G., Jr., R. Wilson, B. R. Davis, I. K. Wachsmuth, C. F. Riddle, H. G. Wathen, R. A. Pollard, and P. A. Blake.** 1981. Non-O group 1 Vibrio cholerae gastroenteritis in the United States: clinical, epidemiologic, and laboratory characteristics of sporadic cases. Ann Intern Med **94:**656-8.
85. **Mukherjee, S., G. Keitany, Y. Li, Y. Wang, H. L. Ball, E. J. Goldsmith, and K. Orth.** 2006. Yersinia YopJ acetylates and inhibits kinase activation by blocking phosphorylation. Science **312:**1211-4.
86. **Nair, G. B., T. Ramamurthy, S. K. Bhattacharya, B. Dutta, Y. Takeda, and D. A. Sack.** 2007. Global dissemination of Vibrio parahaemolyticus serotype O3:K6 and its serovariants. Clin Microbiol Rev **20:**39-48.
87. **Nimchuk, Z. L., E. J. Fisher, D. Desveaux, J. H. Chang, and J. L. Dangl.** 2007. The HopX (AvrPphE) family of Pseudomonas syringae type

III effectors require a catalytic triad and a novel N-terminal domain for function. Mol Plant Microbe Interact **20:**346-57.

88. **Nishibuchi, M., and J. B. Kaper.** 1995. Thermostable direct hemolysin gene of Vibrio parahaemolyticus: a virulence gene acquired by a marine bacterium. Infect Immun **63:**2093-9.
89. **Ogawa, M., T. Yoshimori, T. Suzuki, H. Sagara, N. Mizushima, and C. Sasakawa.** 2005. Escape of intracellular Shigella from autophagy. Science **307:**727-31.
90. **Okada, N., S. Matsuda, J. Matsuyama, K. S. Park, C. de los Reyes, K. Kogure, T. Honda, and T. Iida.** 2010. Presence of genes for type III secretion system 2 in Vibrio mimicus strains. BMC Microbiol **10:**302.
91. **Ono, T., K. S. Park, M. Ueta, T. Iida, and T. Honda.** 2006. Identification of proteins secreted via Vibrio parahaemolyticus type III secretion system 1. Infect Immun **74:**1032-42.
92. **Palmer, L. E., A. R. Pancetti, S. Greenberg, and J. B. Bliska.** 1999. YopJ of Yersinia spp. is sufficient to cause downregulation of multiple mitogen-activated protein kinases in eukaryotic cells. Infect Immun **67:**708-16.
93. **Panina, E. M., S. Mattoo, N. Griffith, N. A. Kozak, M. H. Yuk, and J. F. Miller.** 2005. A genome-wide screen identifies a Bordetella type III secretion effector and candidate effectors in other species. Mol Microbiol **58:**267-79.
94. **Park, K. S., T. Ono, M. Rokuda, M. H. Jang, T. Iida, and T. Honda.** 2004. Cytotoxicity and enterotoxicity of the thermostable direct hemolysin-deletion mutants of Vibrio parahaemolyticus. Microbiol Immunol **48:**313-8.
95. **Park, K. S., T. Ono, M. Rokuda, M. H. Jang, K. Okada, T. Iida, and T. Honda.** 2004. Functional characterization of two type III secretion systems of Vibrio parahaemolyticus. Infect Immun **72:**6659-65.
96. **Pei, J., and N. V. Grishin.** 2007. PROMALS: towards accurate multiple sequence alignments of distantly related proteins. Bioinformatics **23:**802-8.
97. **Pineyro, P., X. Zhou, L. H. Orfe, P. J. Friel, K. Lahmers, and D. R. Call.** 2010. Development of two animal models to study the function of Vibrio parahaemolyticus type III secretion systems. Infect Immun **78:**4551-9.
98. **Quenee, L. E., and O. Schneewind.** 2007. Ubiquitin-Yop hybrids as probes for post-translational transport by the Yersinia type III secretion pathway. Mol Microbiol **65:**386-400.

99. **Ralph, A., and B. J. Currie.** 2007. Vibrio vulnificus and V. parahaemolyticus necrotising fasciitis in fishermen visiting an estuarine tropical northern Australian location. J Infect **54:**e111-4.
100. **Raucher, D., T. Stauffer, W. Chen, K. Shen, S. Guo, J. D. York, M. P. Sheetz, and T. Meyer.** 2000. Phosphatidylinositol 4,5-bisphosphate functions as a second messenger that regulates cytoskeleton-plasma membrane adhesion. Cell **100:**221-8.
101. **Reith, M. E., R. K. Singh, B. Curtis, J. M. Boyd, A. Bouevitch, J. Kimball, J. Munholland, C. Murphy, D. Sarty, J. Williams, J. H. Nash, S. C. Johnson, and L. L. Brown.** 2008. The genome of Aeromonas salmonicida subsp. salmonicida A449: insights into the evolution of a fish pathogen. BMC Genomics **9:**427.
102. **Saarikangas, J., H. Zhao, and P. Lappalainen.** 2010. Regulation of the actin cytoskeleton-plasma membrane interplay by phosphoinositides. Physiol Rev **90:**259-89.
103. **Sambrook, J., and D. J. Russell.** 2001. Molecular Cloning, 3rd ed. CSHL Press, Cold Spring Harbor, NY.
104. **Samudrala, R., F. Heffron, and J. E. McDermott.** 2009. Accurate prediction of secreted substrates and identification of a conserved putative secretion signal for type III secretion systems. PLoS Pathog **5:**e1000375.
105. **Schlumberger, M. C., and W. D. Hardt.** 2006. Salmonella type III secretion effectors: pulling the host cell's strings. Curr Opin Microbiol **9:**46-54.
106. **Shao, F., P. M. Merritt, Z. Bao, R. W. Innes, and J. E. Dixon.** 2002. A Yersinia effector and a Pseudomonas avirulence protein define a family of cysteine proteases functioning in bacterial pathogenesis. Cell **109:**575-88.
107. **Shao, F., P. O. Vacratsis, Z. Bao, K. E. Bowers, C. A. Fierke, and J. E. Dixon.** 2003. Biochemical characterization of the Yersinia YopT protease: cleavage site and recognition elements in Rho GTPases. Proc Natl Acad Sci U S A **100:**904-9.
108. **Shimohata, T., M. Nakano, X. Lian, T. Shigeyama, H. Iba, A. Hamamoto, M. Yoshida, N. Harada, H. Yamamoto, M. Yamato, K. Mawatari, T. Tamaki, Y. Nakaya, and A. Takahashi.** 2011. Vibrio parahaemolyticus Infection Induces Modulation of IL-8 Secretion Through Dual Pathway via VP1680 in Caco-2 Cells. J Infect Dis **203:**537-44.
109. **Shinoda, S., and K. Okamoto.** 1977. Formation and function of Vibrio parahaemolyticus lateral flagella. J Bacteriol **129:**1266-71.
110. **Sorg, J. A., N. C. Miller, and O. Schneewind.** 2005. Substrate recognition of type III secretion machines--testing the RNA signal hypothesis. Cell Microbiol **7:**1217-25.

111. **Su, Y. C., and C. Liu.** 2007. Vibrio parahaemolyticus: a concern of seafood safety. Food Microbiol **24:**549-58.
112. **Suzuki, T., H. Park, and W. J. Lennarz.** 2002. Cytoplasmic peptide:N-glycanase (PNGase) in eukaryotic cells: occurrence, primary structure, and potential functions. FASEB J **16:**635-41.
113. **Taber, C. W.** 2005. Taber's Cyclopedic Medical Dictionary, Indexed, p. 2788. *In* D. Venes (ed.), 20th ed. F. A. Davis Company.
114. **Tam, V. C., M. Suzuki, M. Coughlin, D. Saslowsky, K. Biswas, W. I. Lencer, S. M. Faruque, and J. J. Mekalanos.** 2010. Functional Analysis of VopF Activity Required for Colonization in Vibrio cholerae. MBio **1**.
115. **Taylor, G. S., and J. E. Dixon.** 2004. Assaying phosphoinositide phosphatases. Methods Mol Biol **284:**217-27.
116. **Tena, D., M. Arias, B. T. Alvarez, C. Mauleon, M. P. Jimenez, and J. Bisquert.** 2009. Fulminant necrotizing fasciitis due to Vibrio parahaemolyticus. J Med Microbiol.
117. **Trosky, J. E., Y. Li, S. Mukherjee, G. Keitany, H. Ball, and K. Orth.** 2007. VopA inhibits ATP binding by acetylating the catalytic loop of MAPK kinases. J Biol Chem **282:**34299-305.
118. **Trosky, J. E., S. Mukherjee, D. L. Burdette, M. Roberts, L. McCarter, R. M. Siegel, and K. Orth.** 2004. Inhibition of MAPK signaling pathways by VopA from Vibrio parahaemolyticus. J Biol Chem **279:**51953-7.
119. **Tseng, T. T., B. M. Tyler, and J. C. Setubal.** 2009. Protein secretion systems in bacterial-host associations, and their description in the Gene Ontology. BMC Microbiol **9 Suppl 1:**S2.
120. **Tsujishita, Y., S. Guo, L. E. Stolz, J. D. York, and J. H. Hurley.** 2001. Specificity determinants in phosphoinositide dephosphorylation: crystal structure of an archetypal inositol polyphosphate 5-phosphatase. Cell **105:**379-89.
121. **Van Engelenburg, S. B., and A. E. Palmer.** 2010. Imaging type-III secretion reveals dynamics and spatial segregation of Salmonella effectors. Nat Methods **7:**325-30.
122. **Vasconcelos, G. J., W. J. Stang, and R. H. Laidlaw.** 1975. Isolation of Vibrio parahaemolyticus and Vibrio alginolyticus from estuarine areas of Southeastern Alaska. Appl Microbiol **29:**557-9.
123. **Viboud, G. I., and J. B. Bliska.** 2005. Yersinia outer proteins: role in modulation of host cell signaling responses and pathogenesis. Annu Rev Microbiol **59:**69-89.
124. **Von Pawel-Rammingen, U., M. V. Telepnev, G. Schmidt, K. Aktories, H. Wolf-Watz, and R. Rosqvist.** 2000. GAP activity of the Yersinia

YopE cytotoxin specifically targets the Rho pathway: a mechanism for disruption of actin microfilament structure. Mol Microbiol **36:**737-48.

125. **Whisstock, J. C., F. Wiradjaja, J. E. Waters, and R. Gurung.** 2002. The structure and function of catalytic domains within inositol polyphosphate 5-phosphatases. IUBMB Life **53:**15-23.
126. **Winstead, M. V., J. Balsinde, and E. A. Dennis.** 2000. Calcium-independent phospholipase A(2): structure and function. Biochim Biophys Acta **1488:**28-39.
127. **Wong, S., D. Street, S. I. Delgado, and K. C. Klontz.** 2000. Recalls of foods and cosmetics due to microbial contamination reported to the U.S. Food and Drug Administration. J Food Prot **63:**1113-6.
128. **Woolery, A. R., P. Luong, C. A. Broberg, and K. Orth.** 2010. AMPylation: something old is new again. Front Microbiol **1:**1-6.
129. **Yanagihara, I., K. Nakahira, T. Yamane, S. Kaieda, K. Mayanagi, D. Hamada, T. Fukui, K. Ohnishi, S. Kajiyama, T. Shimizu, M. Sato, T. Ikegami, M. Ikeguchi, T. Honda, and H. Hashimoto.** 2010. Structure and functional characterization of Vibrio parahaemolyticus thermostable direct hemolysin. J Biol Chem **285:**16267-74.
130. **Yang, Y., J. Zhao, R. L. Morgan, W. Ma, and T. Jiang.** 2010. Computational prediction of type III secreted proteins from gram-negative bacteria. BMC Bioinformatics **11 Suppl 1:**S47.
131. **Yarbrough, M. L., Y. Li, L. N. Kinch, N. V. Grishin, H. L. Ball, and K. Orth.** 2009. AMPylation of Rho GTPases by Vibrio VopS disrupts effector binding and downstream signaling. Science **323:**269-72.
132. **Yeung, P. S., and K. J. Boor.** 2004. Epidemiology, pathogenesis, and prevention of foodborne Vibrio parahaemolyticus infections. Foodborne Pathog Dis **1:**74-88.
133. **Zhang, Z. Y., J. C. Clemens, H. L. Schubert, J. A. Stuckey, M. W. Fischer, D. M. Hume, M. A. Saper, and J. E. Dixon.** 1992. Expression, purification, and physicochemical characterization of a recombinant Yersinia protein tyrosine phosphatase. J Biol Chem **267:**23759-66.
134. **Zhao, Z., C. Chen, C. Q. Hu, C. H. Ren, J. J. Zhao, L. P. Zhang, X. Jiang, P. Luo, and Q. B. Wang.** 2010. The type III secretion system of Vibrio alginolyticus induces rapid apoptosis, cell rounding and osmotic lysis of fish cells. Microbiology **156:**2864-72.
135. **Zhou, X., M. E. Konkel, and D. R. Call.** 2009. Type III secretion system 1 of Vibrio parahaemolyticus induces oncosis in both epithelial and monocytic cell lines. Microbiology **155:**837-51.
136. **Zhou, X., D. H. Shah, M. E. Konkel, and D. R. Call.** 2008. Type III secretion system 1 genes in Vibrio parahaemolyticus are positively

regulated by ExsA and negatively regulated by ExsD. Mol Microbiol **69:**747-64.

137. **Zumaquero, A., A. P. Macho, J. S. Rufian, and C. R. Beuzon.** 2010. Analysis of the role of the type III effector inventory of Pseudomonas syringae pv. phaseolicola 1448a in interaction with the plant. J Bacteriol **192:**4474-88.